TGF-β mediates alveolar fluid balance by regulating the cell-surface stability of the epithelial sodium channel in the lung

Inaugural Dissertation
submitted to the
Faculty of Medicine
in partial fulfillment of the requirements
for the PhD-degree
of the faculties of Veterinary Medicine and Medicine
of the Justus-Liebig-University Giessen

by Dorothea Maren Peters
of
Darmstadt

Giessen 2011

From the Department of Medicine
Director/Chairman: Prof. Dr. Werner Seeger
of the Faculty of Medicine of the Justus-Liebig-University Giessen

Prof. Dr. Werner Seeger (supervisor)
Prof. Dr. Wolfgang Kübler
Prof. Dr. Ernst Petzinger
Prof. Dr. Wolfgang Clauss

Date of Doctoral Defense: 24th of June 2011

I Table of contents

II List of figures and tables

III List of abbreviations

3NPA	3-nitroproprionic acid
AFC	alveolar fluid clearance
AFU	arbitrary fluorescence units
ALI	acute lung injury
Amil	amiloride
AntiA	antimycinA
Apocy	apocynin
APS	ammonium persulfate
ARDS	acute respiratory distress syndrome
ATI	alveolar type I
ATII	alveolar type II
ATP	adenosine triphosphate
BABTA-AM	1,2-*bis*-(*o*-aminophenoxy)-ethane-N,N,N′,N′-tetraacetic acid, tetraacetoxymethyl ester
BAL	broncho-alveolar lavage
BFA	brefeldin A
Bis	bisindolylmaleimide I hydrochloride
BMP	bone morphogenetic protein
BMPR	bone morphogenetic protein receptor
BSA	bovine serum albumin
C	Celsius
cm	centimeter(s)
Ctrl	control
DCF	5-chloromethyl-2′-7′-dichloro-fluorescein
DMSO	dimethylsulfoxide
dn	dominant-negative
DNA	deoxyribosenucleic acid
DTT	dithiothreitol
ECM	extracellular matrix
EDTA	ethylene dinitril *o*-N,N,*N*′,*N*′-tetraacetic acid

EGTA	ethylene glycol-bis (2-aminoethylether)-N,N,*N′*,*N′*-tetraacetic acid
ELF	epithelial lining fluid
ELISA	enzyme-linked immunosorbent assay
EMT	epithelial mesenchymal transition
ENaC	epithelial sodium channel
ER	endoplasmic reticulum
EV	empty vector-transfected
FCS	fetal calf serum
FiO_2	fraction of inspired oxygen
FSB	frozen storage buffer
g	gram(s)
GDF	growth and differentiation factor
h	hour(s)
H_2DCFDA	2′,7′dichlorodihydrofluorescein diacetate
HEPES	2-(-4-2-hydroxyethyl)-piperazinyl-1-ethansulfonate
i	single channel conductance
IB	immunoblot
ICU	intensive care unit
IgG	immunoglobulin G
kDa	kilodalton
l	liter(s)
LAP	left atrial pressure
LB	Luria broth
L-NAME	L-nitro-arginine methyl ester
LTBP	latent TGF-β-binding protein
LVP	left ventricular pressure
m	mouse
mg	milligram(s)
min	minute(s)
MIS	Muellerian inhibiting substance
ml	milliliter(s)

mM	millimolar
mm	millimeter(s)
mmHg	millimeter mercury
mV	millivolt(s)
N	number of functional channels at the cell-surface
Na,K-ATPase	ATPase, Na^+/K^+-transporting
nAb	neutralizing antibody
NADPH	nicotinamide adenine dinucleotide phosphate
ND	not detectable
ng	nanogram(s)
nm	nanometer(s)
nM	nanomolar
nmol	nanomol(s)
NS	not significant
PA	phosphatidic acid
PAGE	polyacrylamide electrophoresis
PaO_2	partial pressure of arterial oxygen
PAP	pulmonary arterial pressure
PAR	plasminogen activator receptor
PBS	phosphate-buffered saline
PBST	phosphate-buffered saline + Tween® 20
PBut	phosphatidylbutanol
PC	phosphatidylcholine
PEEP	positive end-expiratory pressure
PEG	polyethylene glycol
pg	picogram(s)
PI4P	phosphatidylinositol-4-monophosphate
PIPK Iα	phosphatidylinositol-4-phosphate 5-kinase 1α
PLD	phospholipase D
P_o	open probability
PO	phalloidin oleate
PtdIns(4,5)P_2	phosphatidylinositol (4,5)-bisphosphate

ROS	reactive oxygen species
Roten	rotenone
rpm	revolutions per minute
RT	room temperature
s	second(s)
S.D.	standard deviation
S2/3	Smad2 and Smad3
SB	SB431542
scr	scrambled
si	small interfering
SOD	superoxide dismutase
Sol-Endo	soluble endoglin
TEMED	N,N,*N´*,*N´*-tetramethylethane-1,2-diamine
TF	transfected
TGF	transforming growth factor
TGFBR	transforming growth factor-β receptor
TTFA	thenoyltrifluoroacetone
µg	microgram(s)
µl	microliter(s)
µM	micromolar
UT	untransfected
Veh	vehicle
VP	ventilation pressure
w/v	weight per unit volume
wt	wild-type
x	*Xenopus*

1 Introduction

1.1 The acute respiratory distress syndrome

The acute respiratory distress syndrome (ARDS) is a devastating syndrome, characterized by severe alveolar flooding with a protein-rich exudate that impairs alveolar gas exchange and which ultimately leads to respiratory failure (1). Current epidemiological analyses indicate that approximately 190,000 cases of acute lung injury (ALI) occur per year in the United States of America, mortality rates being 38.5% for ALI and 41.1% for ARDS (2). The acute respiratory distress syndrome was first described in 1967, when Dr. David G. Ashbaugh described a group of 12 adult patients suffering from a respiratory syndrome which did not respond to the usual methods of therapy. He had made the observation that "the pathophysiology of the illness closely resembled the infantile respiratory distress syndrome." Although the patients originally had experienced several different underlying illnesses and traumata, the outcome of the respiratory distress syndrome was similar. Initially this condition was termed "adult respiratory distress syndrome" (3, 4), but as it occurs in infants as well as in adults, it is now called "acute respiratory distress syndrome". In 1994 the American-European Consensus Conference committee suggested a new definition of the syndrome, categorizing patients into those having "acute lung injury" with less severe hypoxemia, and in patients with "acute respiratory distress syndrome" which describes more severe cases. According to the definition, ALI is considered to be present if $PaO_2/FiO_2 < 300$ and ARDS if $PaO_2/FiO_2 < 200$ (5). The initial trigger for ALI/ARDS is always a systemic or direct injury to the alveolar epithelium. The most common systemic causes are sepsis or acute pancreatitis; direct injuries can be trauma, aspiration or pneumonia, to name the most common. In the acute, exsudative phase inflammation is observed, in conjunction with atelectasis, congestion and alveolar flooding, leading to respiratory failure. If pulmonary edema persists, a fibroproliferative phase has been described, leading to the onset of pulmonary fibrosis. Other consequences include multiple organ failure or pulmonary hypertension. Impaired alveolar fluid clearance (AFC), caused by epithelial injury, is the underlying pathomechanism of persistent pulmonary

edema. There is a positive statistical correlation between patient mortality and the persistence of pulmonary edema due to an inability to clear edema (6-8). The key features of the alveolar pathology associated with ARDS are illustrated in Figure 1 [adapted from (9)].

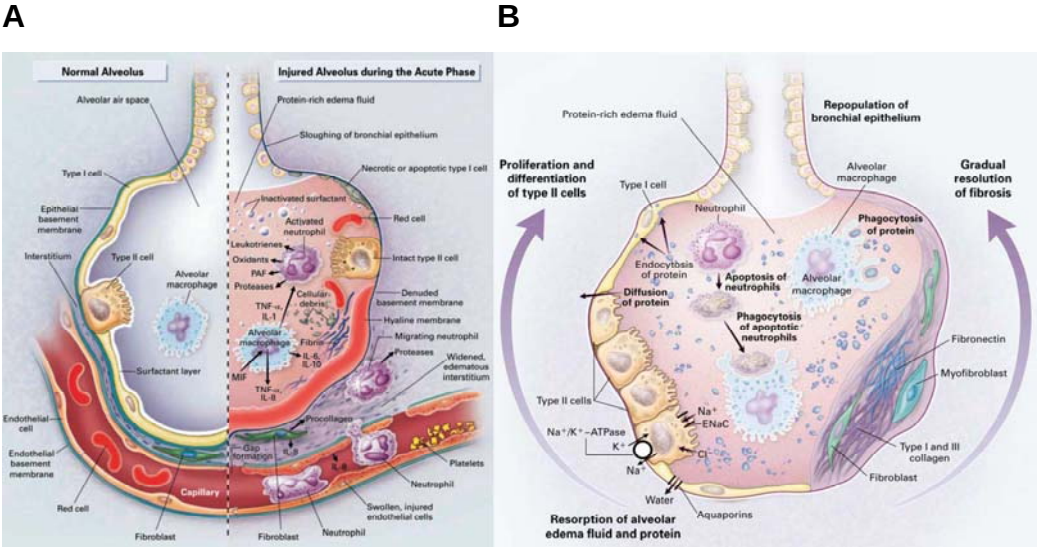

Figure 1. A healthy alveolus in comparison to an alveolus in the acute exsudative phase of the acute respiratory distress syndrome and in the phase of edema resolution.

(**A**) On the left side a healthy alveolus with an intact epithelial cell layer, consisting of alveolar type I and type II cells, is illustrated. In an injured alveolus depicted on the right side, the epithelial cell layer is disrupted and permeable, with infiltration of inflammatory and blood cells, and the alveolus is filled with protein-rich edema fluid. (**B**) An alveolus in recovery: resolution of the edema fluid proceeds, where protein is resorbed and phagocytosed, and type II cells proliferate to restore tissue integrity. If the patient survives the exsudative phase of ARDS, fibrosis can occur, characterized by differentiation of fibroblasts to myofibroblasts and accumulation of extracellular matrix [from (9)].

1.2 Alveolar fluid clearance

When ARDS was first described in 1967, little was known about the mechanisms by which the epithelium regulates fluid transport. In healthy humans, AFC is an essential mechanism to keep the amount of epithelial lining fluid (ELF) constant, and thereby prevent pulmonary edema. During fetal development, prior to birth, the lungs are filled with a protein-free and isoosmolar fluid. This fluid is secreted by the lung during ontogenesis, and gas exchange is a function of the placenta.

The presence of this fluid in the lungs of the fetus is essential for the proper development of the respiratory system. During birth and soon thereafter, the lungs must be rapidly cleared of fluid and switched from placental to pulmonary gas exchange (10). It is now widely accepted that the epithelial barrier plays an essential role in the regulation of fluid balance in the healthy as well as the diseased lung. Alveolar fluid clearance is known to be a complex process that comprises the well-regulated vectorial transport of sodium, chloride and water, amongst other molecules, across the epithelial barrier (11). A significant fraction of the transepithelial water transport is driven by active Na^+ transport across the alveolar epithelium, creating an osmotic force which constitutes the mechanism that clears the fetal fluid from the lung during birth, and helps the adult alveolus to stay clear from excessive fluid (12-15). Through this mechanism, alveolar edema fluid can be transported into the interstitium and cleared by the lymphatic drainage or, if transported into the vasculature, by the circulation (16). Therefore, it is no surprise that fluid absorption in the lungs of newborns, as well as the clearance of pulmonary edema, is dependent upon the presence of the epithelial sodium channel, ENaC (17, 18).

1.3 The epithelial sodium channel

Active transepithelial Na^+ transport is performed in two steps: the Na,K-ATPase (official full name: ATPase, Na^+/K^+-transporting) at the basolateral membrane of the epithelial cell actively transports Na^+ out of the cell, thereby producing an electrochemical gradient. This gradient provides the driving force for Na^+ influx into the cell through ENaC, hence, ENaC mediates the vectorial transport of sodium ions across the epithelium through epithelial cells (19). As the net salt movement drives the flow of water through tight epithelia, the active transepithelial sodium transport is crucial to keep the volume and the composition of fluid on both sides of an epithelial cell layer constant. In tissues responsive to aldosterone, ENaC plays an important role in the electrolyte balance and blood pressure regulation (20). The ENaC channel was first characterized as a single channel in 1986 by Lawrence G. Palmer and Gustavo Frindt, who studied single-channel activity in the apical membrane of cortical collecting duct cells from rat kidneys, using the patch-clamp technique (21). In 1993 Canessa *et al.*

provided a more molecular definition of ENaC after cloning the genes encoding the α, β and γ ENaC subunits, *scnn1a*, *scnn1b* and *scnn1g*, respectively, from the rat colon (22, 23). It was thus demonstrated that ENaC consists of three homologous subunits: the α, β and γ subunits (24). In humans, an additional subunit (δENaC) has also been reported (25). In *Xenopus*, six different subunits are known, where, in addition to the α, β, and γ subunits, a γ_2xENaC subunit has been identified, as well as an εxENaC subunit (26). Each subunit has two membrane-spanning domains and a large extracellular loop. The N- and C-termini are both located intracellularly (27). The ENaC complex is expressed in different epithelia, including those located in the colon, kidney and the lung, where it is present on the apical membrane of polarized epithelial cells. Structurally, ENaC is a heteromultimeric channel, and all three ENaC subunits are required for maximal expression of channel activity. Expression of αENaC alone in *Xenopus* oocytes leads to a retention of this subunit in the endoplasmic reticulum (ER) and thus to low expression at the cell surface, probably due to the absence of a molecular signal for targeting to the cell surface (19). Although the α subunit of ENaC can form a functional channel alone, the preferred subunit stoichiometry of ENaC has been found to be two α subunits together with one β and one γ subunit, to form a tetrameric ion channel at the cell surface (28). Other subunit stoichiometries have been suggested, for example a nine-subunit channel, each composed of three each of the α, the β and the γ subunits (29, 30), or an eight-or-nine subunit channel with a minimum of two γ subunits (31). Activity of ENaC can be blocked by amiloride, at concentrations in the submicromolar range (19, 32). The activity of ENaC can be regulated by three different mechanisms, namely the open probability of the channel (P_o), the single channel conductance (i) – although there is no known regulatory change in ENaC function due to (i) – and by the number of functional channels at the cell surface (N) (32, 33).

1.4 ENaC in the lung

In the lung active Na^+ absorption is important for keeping the amount and the composition of the ELF constant. The osmotic gradient generated by the net Na^+ flow across the epithelium leads to the absorption of fluid out of the alveolus into the interstitium (12-15). In the human lung α, β and γENaC are highly expressed

in the small and medium-sized airways. The smallest gas exchange unit of the lung is the alveolus, and the human lung contains approximately 500 million alveoli, generating a surface area of *circa* 130 m^2 for gas exchange and fluid reabsorption (34). The alveolar epithelium consists of two cell-types, namely type I (ATI) and type II (ATII) alveolar epithelial cells. Type I cells cover up to 95% of the internal surface area of the lung, although ATI cells constitute only one third of the total number of alveolar epithelial cells (35). The ATI cells mediate gas exchange, being 50-100 μm in diameter and very thin, minimizing the diffusion distance between the air space and the pulmonary capillary blood. Until recently, the accepted paradigm was that ATI cells do not participate in ion transport through the alveolar epithelium and thus do not contribute to AFC. Since (rat) ATI cells have been demonstrated to express functional ENaC (36, 37), a new model has been suggested in which ion transport occurs across the entire alveolar surface. Still, little is known about the ability of ATI cells to specifically contribute to ion transport and fluid clearance in the lung. Type II cells, in contrast to ATI cells, are cuboidal cells which serve as precursor cells for both types of alveolar epithelial cells. Type II cells cover up to 5% of the internal surface of the human lung. Alveolar epithelial type II cells produce surfactant proteins, regulate fluid and ion transport in the alveolus, have innate immune functions and contribute to epithelial repair by removing apoptotic cells (38, 39).

1.5 ENaC in disease

Mutations in ENaC have been associated with several disorders, namely Liddle's Syndrome, pseudohyperaldosteronism and hypertension. Liddle's Syndrome, also called pseudoaldosteronism, was first described in 1963 by Grant Winder Liddle who died in 1989 (40). Liddle's Syndrome is characterized by excessive Na^+-absorption in the distal nephron and K^+ secretion in conjunction with low aldosterone levels, which leads to early onset hypertension. This inherited disease is linked to stop, point or frameshift mutations or deletions in the genes encoding the intracellular COOH termini of the β or the γ subunit. Coexpression of a β subunit that carries the mutations which are characteristic of Liddle's syndrome together with wild-type α and γ subunits in *Xenopus laevis* oocytes increases the amiloride-sensitive Na^+-current approximately three-fold in comparison to the

wild-type channel, demonstrating that a larger number of open channels is the underlying mechanism for the abnormal regulation of ENaC in this salt-sensitive hypertension disorder (41). Furthermore, ENaC mutations have been suggested to play a role in cystic fibrosis (42, 43). Resolution of pulmonary edema in ARDS patients is critically dependent on AFC, which occurs via sodium transport through ENaC. The ENaC channel was implicated in AFC, since amiloride, an inhibitor of ENaC, inhibited a vast proportion of fluid clearance in the lungs of several animal models, and in the human lung (16). In addition, application of amiloride to the lungs of newborn guinea pigs caused respiratory distress (44), and targeted deletion of both ENaCα alleles in mice inhibited AFC (18). Furthermore, transgenic overexpression of *scnn1a* (encoding αENaC) in *scnn1a*-deficient mice rescued AFC in those mice (45), whereas airway-specific overexpression of ENaC in wild-type mice lead to a depletion of ELF trough accelerated sodium absorbtion (46). Taken together, these data implicate ENaC and active epithelial sodium transport in AFC. Various factors have been described which can impair epithelial sodium transport by downregulating the activity of either the Na,K-ATPase or ENaC, as schematically depicted in Figure 2 [adapted from (16)].

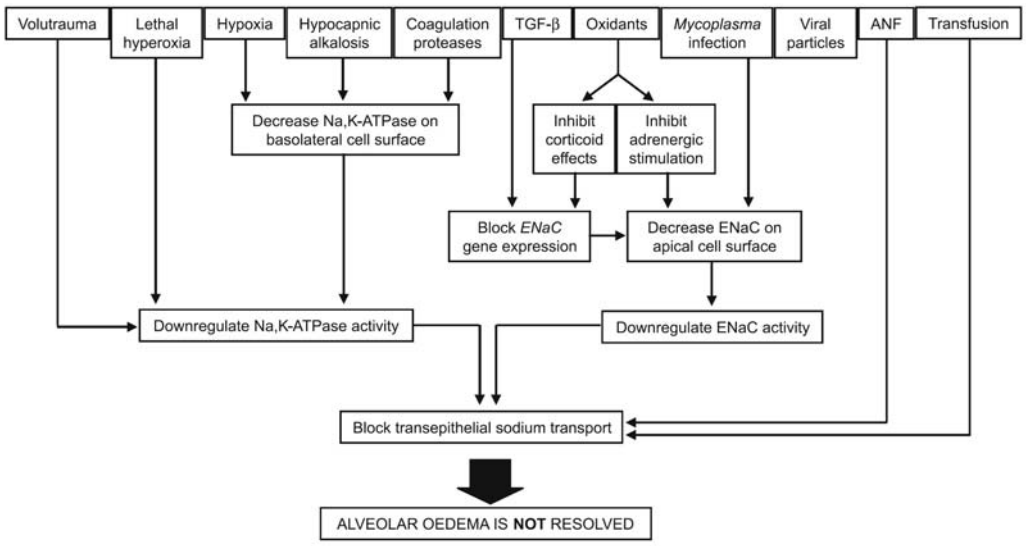

Figure 2. Factors that cause impaired alveolar fluid clearance.

ANF, atrial natriuretic factor; ENaC, epithelial sodium channel; Na,K-ATPase, sodium, potassium transporting ATPase [from (16)].

Inflammation and inflammatory mechanisms lead to an increase in the capacity of the lung epithelium to remove excess alveolar fluid as a protective mechanism to overcome pulmonary edema in a rat model of septic shock (47). However, lung infections can impair AFC due to a variety of underlying causes. For instance, an experimental infection of live mice with *Mycoplasma pneumoniae* reduced cell surface expression of ENaC and impaired AFC through the production of reactive oxygen nitrogen intermediates (48). Glucocorticoids increase *scnn1a* mRNA levels and ENaC expression at the apical membrane (49). Beta-adrenergic stimulation leads to an increased P_o for ENaC (50), enhanced the expression of αENaC in ATII cells (51), and lead to alveolar edema resolution in hypoxia-induced ALI and ventilator-induced lung injury (52). Oxidants such as hydrogen peroxide suppress glucocorticoid-induced ENaC expression, and antioxidant administration seems to restore catecholamine-induced upregulation of AFC. Proinflammatory factors, including transforming growth factor (TGF)-β, are elevated in broncho-alveolar lavage (BAL) fluids from ARDS patients (16). Transforming growth factor-β, a multifunctional cytokine that regulates the immune and inflammatory systems, impaired transepithelial sodium transport and AFC in live rats and downregulates ENaC expression (53). Transforming growth factor-β-inducible genes are upregulated in the lungs of ARDS patients (54), as well as in the lungs of nickel- (55) and bleomycin-treated (56) mice. Pharmacological inhibition of TGF-β protected mice from bleomycin-induced lung injury (1). Altogether, these data suggest a critical role for TGF-β in ARDS, and it seems likely that TGF-β influences ENaC, given the role of ENaC in AFC.

1.6 Transforming growth factor-β

The first isoform of TGF-β was purified and described in 1983 (57). Richard K. Assoian and his colleagues chemically and biologically characterized a 25 kDa homodimer consisting of two 12.5 kDa subunits which are held together by disulfide bonds (57). This growth factor from human platelets, at that time termed "platelet derived TGF-β" is now known as TGF-β1. Almost three decades later, several related isoforms have been discovered and TGF-β is now considered as a multifunctional cytokine. To date, the TGF-β superfamily of ligand proteins is a group of more than 60 structurally-related polypeptide growth factors, and up to

42 of which are encoded by the human genome. In this group there are three TGF-β isoforms, named TGF-β1, TGF-β2 and TGF-β3 (58). The TGF-β superfamily of proteins is divided into two subfamilies: the TGF-β/activin/nodal subfamily and the bone morphogenetic protein (BMP)/growth/differentiation factor (GDF)/Muellerian inhibiting substance (MIS) subfamily. These subfamilies, which are defined by sequence similarity and the signaling pathways they activate in a cell-specific manner, regulate a variety of cellular functions in development, tissue homeostasis and repair, as well as disease pathogenesis (59, 60). In the healthy human lung TGF-β is expressed mainly in the airway epithelium and alveolar macrophages (61) as well as in endothelial and mesenchymal cells (62). The TGF-β polypeptide is synthesized as a latent complex containing three components: dimeric mature TGF-β, noncovalently associated with its latency-associated peptide, which in turn is bound through disulfide bonds to the latent TGF-β binding protein (LTBP) (63). Upon activation this complex is deposited in – and associated with – the extracellular matrix (ECM) which serves as a storage structure and regulator of activity of TGF-β (64). For activation, mature TGF-β is cleaved from the latent form by proteases, or by nonproteolytic dissociation from latency associated peptide (65). The TGF-β ligand regulates various cellular functions by binding three receptors located at the cell surface, namely TGF-β receptor types I, II and III (66). The TGF-β receptor type I and TGF-β receptor type II contain intracellular serine/threonine kinases in their C-terminal domain. To date, twelve members of the receptor serine/threonine kinase family have been identified, five of which are type II receptors and seven of which are type I receptors (59, 67). Two TGF-β type III receptors, betaglycan and endoglin, are accessory receptors with no known intracellular signaling capacity. These type III receptors play an important role in the regulation of the TGF-β signaling pathway, and play inhibiting or potentiating roles, depending on the respective ligand to which the cell is exposed (68, 69). Endoglin only binds TGF-β1 and TGF-β3, whereas betaglycan and TGF-β receptors I and II bind all three mammalian TGF-β isoforms (69).

1.7 TGF-β signaling and Smads

In the absence of TGF-β, the TGF-β receptors exist at the cell surface as homodimers. In general, signal transduction by TGF-β occurs by binding of TGF-β at the cell surface to the three receptors described above. Transforming growth factor-β either binds to the type III receptor betaglycan, which then presents the ligand to the type II receptor, alternatively TGF-β binds to the type II receptor directly. Endoglin, a homodimeric membrane glycoprotein has been shown to bind TGF-β1 and TGF-β3, as well as the type I and type II receptors (70). Together with betaglycan, endoglin is regarded as an accessory receptor which regulates TGF-β access to the type I and type II receptors (70). Upon TGF-β binding, the type II receptors recruit type I receptors and transactivate them by phosphorylation (71). The activated type I receptor transduces the signal within the cell by activating receptor-regulated Smad proteins at two C-terminal serine residues. There are five receptor-regulated Smads, also called R-Smads: Smad1, Smad2, Smad3, Smad5 and Smad8, which form a heterotrimeric complex with Smad4, also called common-partner Smad, and translocate into the nucleus where gene transcription is regulated in a cell-type-specific manner, together with transcription factors, coactivators and repressors (67, 72, 73). These DNA-binding cofactors have the ability to bind to R-Smads and to specific DNA sequences simultaneously, and are differentially expressed in different cell types, thereby providing a basis for cell-type-specific TGF-β signaling (74). Smad6 and Smad7 act as inhibitory Smads and thus form a distinct subgroup called I-Smads. Using different mechanisms, Smad6 and Smad7 oppose R-Smad signaling (75). In some cell types TGF-β additionally activates several types of non-Smad-signaling pathways (76). A schematic overview of TGF-β signaling is presented in Figure 3 [adapted from (77)].

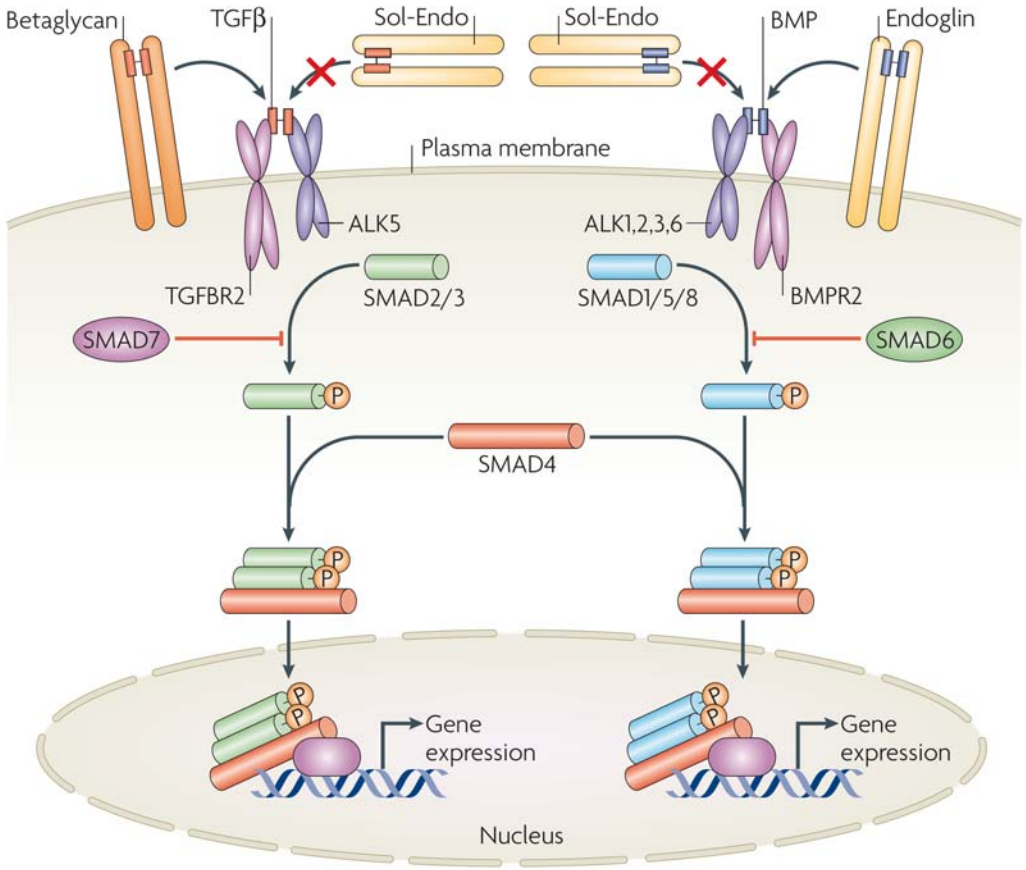

Figure 3. The TGF-β signaling pathway.

Active TGF-β either binds to the type III receptor which then presents it to the type II receptor, alternatively, TGF-β binds to the type II receptor directly. Soluble endoglin (Sol-Endo) is thought to inhibit receptor binding by sequestering the ligand (77). Upon TGF-β binding, type II receptors recruit type I receptors, which are activated by phosphorylation (71). The activated type I receptor transduces the signal through the cell by activating receptor-regulated Smads at two C-terminal serine residues, which form a heterotrimeric complex with Smad4, also called common-partner Smad, and translocate into the nucleus where transcription is regulated in a cell-type-specific manner, together with transcription factors, coactivators and repressors [from (77)].

As mentioned above, there is much evidence to suggest that TGF-β plays a role in the pathogenesis of ARDS, with malfunction of AFC being a key mechanism in the development of the disease, which might be affected by TGF-β. Little is known, however, about the mechanism by which TGF-β might impair transepithelial sodium transport and AFC. The present study aimed to address this issue.

2 Aim of this study

Impaired AFC, caused by epithelial injury, is the underlying pathomechanism of persistent pulmonary edema. There is a positive statistical correlation between patient mortality [38.5% for ALI and 41.1% for ARDS (2)] and the persistence of pulmonary edema and the inability to clear fluid (6-8). In order to prevent pulmonary edema, active transepithelial sodium – and thereby fluid – transport by ENaC is crucial to keep the volume of fluid on both sides of an epithelial cell layer constant. Patients who suffer from ARDS demonstrate significantly elevated concentrations of TGF-β in their ELF (54) and in these patients, lower TGF-β levels correlate with more ventilator-free and intensive care unit (ICU)-free days (78). Therefore, **it was hypothesized that a mechanism exists, by which TGF-β blocks AFC in the lungs of ARDS patients.**

In detail our specific aims were

a) to determine the possible impact of TGF-β on AFC and ENaC function;

b) if TGF-β does indeed impact ENaC activity, to assess the mechanism at a cellular and molecular level.

3 Materials and methods

3.1 Materials

3.1.1 Technical devices

Autoclave; Systec, Germany

Benchtop Incubator-Shaker; Sartorius AG, Germany

Biofuge Fresco; Heraeus, Germany

Cat/rabbit ventilator; Hugo Sachs Elektronik, Germany

Cell culture incubator Cytoperm2; Heraeus, Germany

Cell culture sterile working bench; Heraeus, Germany

Developing machine X Omat 2000; Kodak, USA

Electromechanical pressure converter Combitrans; Braun, Germany

Electrophoresis chambers; Bio-Rad, USA

Film cassette; Sigma-Aldrich, Germany

Freezer -20 ºC; Bosch, Germany

Freezer -40 ºC; Kryotec, Germany

Freezer -80 ºC; Heraeus, Germany

Fridge 4 ºC; Bosch, Germany

Fume hood; Köttermann, Germany

Fusion A153601 Reader; Packard Bioscience, Germany

Glass beakers 50, 100, 200, 500, 1000 ml; Schott, Germany

Glass bottles: 250, 500, 1000 ml; Fischer, Germany

Incubator (*E. coli*); Heraeus, Germany

Light microscope; Leica, Germany

Magnetic stirrer; Heidolph, Germany

Microplate reader; MDS Analytical Technologies, Germany, software: SoftMax Pro 5.3; Molecular Devices, USA

Mini spin centrifuge; Eppendorf, Germany

Mini-Protean® 3 Cell; Bio-Rad, USA

Multifuge centrifuge 3 s-R; Heraeus, Germany

Nanodrop® Spectrophotometer; PeqLab Biotechnologie GmbH, Germany

pH Meter; inoLab® WTW Laboratory Products, Germany

Pipetboy; Eppendorf, Germany

Pipetmans: P10, P20, P100, P200, P1000; Gilson, France

PlotIT 3.1 software; Scientific Programming Enterprises SPE, USA

Power supply Power PAC 300; Bio-Rad, USA

Pump Masterflex 7518-10; Cole Parmer, USA

Quantity One software; Bio-Rad, USA

Rocking platform; Heidolph, Germany

Sequence Detection System StepOnePlus; Applied Biosystems, USA

Tank for liquid nitrogen; Airliquide, Germany

Ultrasonic nebulizer Optineb; NEBU-TEC, Germany

Vacuum centrifuge; Eppendorf, Germany

Vortex mixer; Eppendorf, Germany

Water bath Thermo-Frigomix; Braun, Germany

Western blot chambers: Mini Trans-Blot®; Bio-Rad, USA

3.1.2 Consumables

Cryotubes vials; Greiner Bio-One, Germany

Durapore™ surgical tape; 3M Germany

Film; Agfa Gevaert, Belgium

Film; Amersham GE Healthcare, Germany

Filter 0.2 µm Pall Cardioplegia; Terumo, Germany

Filter Iso-Gard Filter S; Hudson RCI, USA

Filter Tip FT: 10, 20, 100, 200, 1000; Greiner Bio-One, Germany

Filter units 0.22 µm syringe-driven; Millipore, USA

Gel blotting paper 70×100 mm; Bioscience, Germany

Optics plates, 96-well; Corning®, Sigma-Aldrich, Germany

Pasteur pipettes; VWR International, Germany

Petri dishes for bacteria; Greiner Bio-One, Germany

Pipette tip 10 µl; Gilson, USA

Pipette tip 200, 1000 µl; Sarstedt, Germany

Platinum® SYBR® Green qPCR SuperMix UDG kit; Invitrogen, UK

PureYield™ Plasmid Midiprep System; Promega, Germany

QIAprep Spin Miniprep Kit; Qiagen, Germany

QuikChange II Site-directed mutagenesis kit; Stratagene, Germany

Scalpel, disposable; Feather, Japan

Serological pipettes: 2, 5, 10, 25, 50 ml; Falcon, USA

Streptavidin Agarose and UltraLink Resins; Thermo Fisher Scientific Inc., USA

Suture material; Mersilene Ethicon, Belgium

Syringe 50 ECOJECT® Plus; DispoMed, Germany

Test tubes: 15, 50 ml; Greiner Bio-One, Germany

Tissue cell scraper; Greiner Bio-One, Germany

Tissue culture dish 60/100 mm; Greiner Bio-One, Germany

Tissue culture flask 250 ml; Greiner Bio-One, Germany

Tissue culture plates: 6-well; Greiner Bio-One, Germany

Transfer membrane nitrocellulose; Bio-Rad, USA

3.1.3 Chemicals and reagents

2-Propanol; Merck, Germany

2-Thenoyltrifluoroacetone; Sigma-Aldrich, Germany

3-Nitropropionic acid; Sigma-Aldrich, Germany

Acrylamide solution Rotiphorese Gel 30; Roth, Germany

Agarose; Promega, Germany

Albumine, bovine serum; Sigma-Aldrich, Germany

Amiloride; Sigma-Aldrich, Germany

Ammonium persulfate; Promega, Germany

Ammonium sulfate; Sigma-Aldrich, Germany

Ampicillin sodium salt; Sigma-Aldrich, Germany

Antimycin A; Sigma-Aldrich, Germany

Apocynin; Sigma-Aldrich, Germany

BABTA-AM; Sigma-Aldrich, Germany

Bisindolylmaleimide I hydrochloride; Sigma-Aldrich, Germany

Brefeldin A; Calbiochem, Germany

Bromophenol blue; Sigma-Aldrich, Germany

Calcium chloride; Sigma-Aldrich, Germany

Complete™ Protease inhibitor; Roche, Germany

D-MEM medium; Gibco BRL, Germany

D-MEM medium, phenol red-free; Gibco BRL Germany

DMSO; Sigma-Aldrich, Germany

Dry milk powder; Carl Roth, Germany

DTT; Promega, USA

Dulbecco's phosphate buffered saline 10×; PAA Laboratories, Austria

Dulbecco's phosphate buffered saline with/without Ca & Mg 1×; PAA Laboratories, Austria

ECL Plus Western Blotting Detection System; Amersham Biosciences, UK

EDTA; Promega, USA

EGTA; Sigma-Aldrich, Germany

Elektrolytlösung IIN; Serag-Wiessner, Germany

Ethanol 70%; SAV-LP, Germany

Ethanol 99%; J.T. Baker Mallinckrodt Baker B.V., Netherlands

Ethanol absolute; Riedel-de Haën, Germany

Ethidium bromide; Carl Roth, Germany

EUK-134; Cayman Chemical, USA

EZ-Link Sulfo-NHS-LC-Biotin; Thermo Fisher Scientific Inc., USA

Fetal calf serum (FCS); Gibco BRL, Germany

Glycerol; Carl Roth, Germany

Glycine; Carl Roth, Germany

H_2DCFDA; Invitrogen, UK

Heparin-Natrium-25 000-ratiopharm®; Ratiopharm, Germany

HEPES; Sigma-Aldrich, Germany

Hexamine cobalt chloride; Sigma-Aldrich, Germany

Hydrochloric acid; Sigma-Aldrich, Germany

Hydrocortisone; Sigma-Aldrich, Germany

Hydrogen peroxide; Sigma-Aldrich, Germany

Igepal CA-630; Sigma-Aldrich, Germany

Insulin-Transferrin-Sodium-Selenite supplement; Gibco BRL, Germany

Isotetrandrine; Calbiochem USA

Ketavet; Pfizer, Germany

LipofectamineTM 2000; Invitrogen, UK

L-NAME; Sigma-Aldrich, Germany

Luria Broth Base powder; Invitrogen, UK

Magnesium chloride; Sigma-Aldrich, Germany

Magnesium sulfate; Sigma-Aldrich, Germany

Manganese tetrachloride; Sigma-Aldrich, Germany

Mannit-15%; Serag-Wiessner, Germany

Methanol; Fluka, Germany

N-(*p*-Amylcinnamoyl)anthranilic acid; Calbiochem USA

n/*t*-Butanol; Sigma-Aldrich, Germany

Opti-MEM medium; Gibco BRL, Germany

Phalloidin oleate; Calbiochem USA

Potassium acetate; Sigma-Aldrich, Germany

Potassium borate; Grom-chromatography, Germany

Potassium chloride; Merck, Germany

Potassium phosphate; Sigma-Aldrich, Germany

Precision Plus ProteinTM Standards; Bio-Rad, USA

Quick StartTM Bradford Dye Reagent; Bio-Rad, USA

Rompun®; Bayer, Germany

Rotenone; Sigma-Aldrich, Germany

SB431542; Calbiochem USA

Sodium acetate; Sigma-Aldrich, Germany

Sodium azide; Merck, Germany

Sodium chloride; Merck, Germany

Sodium dodecyl sulfate 10% (SDS); Promega, USA

Sodium hydrogen carbonate NaBic8.4 %; Braun, Germany

Sodium hydroxide solution; Merck, Germany

Sodium ortho vanadate; Sigma-Aldrich, Germany

Sodium phosphate; Sigma-Aldrich, Germany

Sodium sulfate; Merck, Germany

STO-609; Sigma-Aldrich, Germany

Superoxide dismutase - polyethylene glycol; Sigma-Aldrich, Germany

SuperSignal® West Pico Chemiluminescent Substrate; Pierce, USA

TEMED; Bio-Rad, USA

Transforming growth factor (TGF)-β1; R&D Systems, USA

Tris; Carl Roth, Germany

Tris-Cl; USB, USA

Trypsin/EDTA; Gibco BRL, Germany

Tryptone yeast extract; Sigma-Aldrich, Germany

Tween® 20: Sigma-Aldrich, Germany

Xylocain 2 % 20 mg/ml: AstraZeneca, Germany

β-glycerophosphate: Sigma-Aldrich, Germany

β-mercaptoethanol: Sigma-Aldrich, Germany

3.1.4 Plasmids

Name	Source
pcDNA 3.1 mαENaC, FLAG-tagged,	Dr. Thomas R. Kleyman
pcDNA 6.0 V5/His A (+) mβENaC	Dr. Thomas R. Kleyman
pcDNA 3.0 mγENaC, FLAG-tagged	Dr. Thomas R. Kleyman
pcDNA 3.1 hαENaC, FLAG-tagged	this study
pcDNA 6.0 V5/His A (+) hβENaC	this study
pcDNA 3.0 hγENaC, FLAG-tagged	this study
pcDNA 6.0 V5/His A (+) mβENaC C10A	this study
pcDNA 6.0 V5/His A (+) mβENaC C10S	this study
pcDNA 6.0 V5/His A (+) h and mβENaC C30A	this study
pcDNA 6.0 V5/His A (+) h and mβENaC C30S	this study
pcDNA 6.0 V5/His A (+) h and mβENaC C43A	this study
pcDNA 6.0 V5/His A (+) h and mβENaC C43S	this study
pcDNA 6.0 V5/His A (+) mβENaC C557A	this study
pcDNA 6.0 V5/His A (+) mβENaC C557S	this study
pcDNA 6.0 V5/His A (+) mβENaC C595A	this study
pcDNA 6.0 V5/His A (+) mβENaC C595S	this study
pCGN hPLD1	Dr. Michael A. Frohman
pCGN hPLD1-K898R	Dr. Michael A. Frohman
pcDNA3 mPIP5KIβ	Dr. Kyota Aoyagi
pcDNA3 mPIP5KIβ K178A	Dr. Kyota Aoyagi
pcDNA 3.1 NOX4	Dr. Karl-Heinz Krause

In the abbreviations, a lower-case “h” denotes a human gene while a lower-case “m” denotes a mouse gene.

3.1.5 Cell lines

A549 epithelial cell line, human lung carcinoma; ATCC-LGC, Germany

MLE-12 cell line; ATCC-LGC, Germany

3.1.6 Primers for expression analysis

Table 1. Primers for expression analysis

gene	forward primer	reverse primer
scnn1a (αENaC)	5´-GTGTGCATTCACTCCTGC-3´	5´-CTGCACGGCTTCCTGCAC-3´
scnn1b (βENaC)	5´-GACAAGCTGCAACGCAAG-3´	5´-GGAAGTCCCTGTTGTTGC-3´
scnn1g (γENaC)	5´-CCACCAGCTTGGCACAGT-3´	5´-ACTGTTGGCTGGGCTCTC-3´
SCNN1A (αENaC)	5´-GGTGGACTGGAAGGACTGGAAGATCG-3´	5´-ATGAAGTTGCCCAGCGTGTCCTCCTC-3´
SCNN1B (βENaC)	5´-TTCATCAGGACCTACTTGAGCTGG-3´	5´-GGCATTGGCATGGCTTAGCTCAGGAG-3´
SCNN1G (γENaC)	5´-CTGGAGCTAAGGTGATCATCCATCG-3´	5´-GCAGCGTTGTAGATGTTCCTGATTG-3´
hprt	5´-GATGATCTCTCAACTTTA-3´	5´- AGTCTGGCCTGTATCCAA-3´
HPRT	5´-AAGGACCCCACGAAGTGTTG-3´	5´-GGCTTTGTATTTTGCTTTTCCA-3´

Mouse genes are indicated in lower case, and human genes in upper case.

3.1.7 Primers for site-directed mutagenesis

Table 2. Primers for site-directed mutagenesis

Gene	forward primer	reverse primer
pCMV-Tag4B (vector)	5´-GATACCGTCGACACCGGTTAATACAAGGATGAC-3´	5´-GTCATCCTTGTATTAACCGGTGTCGACGGTATC-3´
scnn1b (βENaC C10A)	5´-AAGTACCTCCTGAAGGCCCTGCACCGGCTGCAG-3´	5´-CTGCAGCCGGTGCAGGGCCTTCAGGAGGTACTT-3´
scnn1b (βENaC C10S)	5´-AAGTACCTCCTGAAGAGCCTGCACCGGCTGCAG-3´	5´-CTGCAGCCGGTGCAGGCTCTTCAGGAGGTACTT-3´
scnn1b (βENaC C30A)	5´-CTGCTAGTGTGGTACGCCAATAACACCAACACC-3´	5´-GGTGTTGGTGTTATTGGCGTACCACACTAGCAG-3´
scnn1b (βENaC C30S)	5´-CTGCTAGTGTGGTACAGCAATAACACCAACACC-3´	5´-GGTGTTGGTGTTATTGCTGTACCACACTAGCAG-3´
scnn1b (βENaC C43A)	5´-CCCAAACGCATCATCGCTGAGGGGCCCAAGAAG-3´	5´-CTTCTTGGGCCCCTCAGCGATGATGCGTTTCCC-3´
scnn1b (βENaC C43S)	5´-CCCAAACGCATCATCAGTGAGGGGCCCAAGAAG-3´	5´-CTTCTTGGGCCCCTCACTGATGATGCGTTTCCC-3´
scnn1b (βENaC C557A)	5´-AAGCTGGTGGCCTCCGCCAAAGGCCTGCGCAGG-3´	5´-CCTGCGCAGGCCTTTGGCGGAGGCCACCAGCTT-3´
scnn1b (βENaC C557S)	5´-AAGCTGGTGGCCTCCAGCAAAGGCCTGCGCAGG-3´	5´-CCTGCGCAGGCCTTTGCTGGAGGCCACCAGCTT-3´
scnn1b (βENaC C595A)	5´-CCTGACACAACCAGCGCCAGGCCCCACGGCGAG-3´	5´-CTCGCCGTGGGGCCTGGCGCTGGTTGTGTCAGG-3´
scnn1b (βENaC C595S)	5´-CCTGACACAACCAGCAGCAGGCCCCACGGCGAG-3´	5´-CTCGCCGTGGGGCCTGCTGCTGGTTGTGTCAGG-3´
SCNN1B (βENaC C30S)	5´-CTGCTGGTGTGGTACTCCGACAACACCAACACC-3´	5´-GGTGTTGGTGTTGTCGGAGTACCACACCAGCAG -3´
SCNN1B (βENaC C43S)	5´-CCCAAGCGCATCATCTCTGAGGGGCCCAAGAAG-3´	5´- CTTCTTGGGCCCCTCAGAGATGATGCGCTTGGG-3´

Mouse genes are indicated in lower case, and human genes in upper case. Engineered restriction sites are indicated in bold type, while engineered stop-codons are underlined.

3.1.8 Antibodies

FLAG antibody; Sigma Aldrich, USA, catalog number: F-3165

Monoclonal anti V5 antibody; Sigma Aldrich, USA, catalog number: V-8012

NOX4 antibody; a gift from J. Hänze, Klinik für Urologie und Kinderurologie, Marburg

Pan-specific TGF-β1,2,3 neutralizing antibody; R&D Systems, USA, catalog number: MAB1835

PIPK I α (C17) antibody; Santa Cruz Biotechnology, Germany, catalog number: sc-11774

PLD1 antibody; Cell Signaling Technology, USA, catalog number: 3832

Smad 2/3 antibody; Cell Signaling Technology, USA, catalog number: 3102

3.1.9 siRNA

Smad2; Santa Cruz Biotechnology, Germany, catalog number: sc-38374; concentration: 50 nmol/ml cell culture medium, cell harvest: 24 h after transfection

Smad3; Santa Cruz Biotechnology, Germany, catalog number: sc-38376; concentration: 50 nmol/ml cell culture medium, cell harvest: 24 h after transfection

PLD1; Santa Cruz Biotechnology, Germany, catalog number: sc-44000; concentration: 50 nmol/ml cell culture medium, cell harvest: 24 h after transfection

PIPK Iα; Santa Cruz Biotechnology, Germany, catalog number: sc-36232; concentration: 150 nmol/ml cell culture medium, cell harvest: 24 h after transfection

NOX4; custom synthesized by Biomers.net, Germany:
5´-CCU CUU CUU UGU CUU CUAC dTdT-3´ (sense),
5´-GUA GAA GAC AAA GAA GAGG dTdT-3´ (antisense) (67), 250 pmol/well of a six-well plate, cell harvest: 72 h after transfection

Scrambled siRNA; Ambion, USA, catalog number: AM4611; concentration: 50 nmol/ml cell culture medium, cell harvest: 24 h after transfection; when used as a control for NOX4 siRNA: 72 h after transfection

3.2 Methods

3.2.1 Active TGF-β determination and neutralization

Active TGF-β levels in BAL fluids from apparently healthy control human subjects and patients with ARDS were assessed by a human TGF-β1 enzyme-linked immunosorbent assay (ELISA) (R&D Systems; Minneapolis, Minnesota, U.S.A.; DB100B), as per the manufacturer's instructions; or by a dual luciferase reporter bioassay, employing the firefly luciferase-based TGF-β-responsive $p(CAGA)_{12}$ reporter, and a *Renilla* luciferase standardization reporter (79) Transforming growth factor-β was neutralized in cell-culture experiments with a

pan-TGF-β1,2,3 neutralizing antibody, as previously described (80), at a concentration of 10 μg/ml, along with an IgG control antibody also at 10 μg/ml.

3.2.2 The isolated, ventilated and perfused rabbit lung

The model of the isolated, ventilated and perfused rabbit lung allowed for the investigation of fluid transport out of the alveoli in an intact, *ex vivo* organ. The isolated lung serves as a model of edema fluid reabsorption, where a 2 ml fluid challenge applied to the lung by nebulization is absorbed and removed by the perfused vasculature over 60 min. Fluid retention in the lung is indicated by an increase in the net steady-state mass of the lung (compared at the beginning and end of the 60-min period), and by an increased ELF volume.

3.2.3 Isolation of the rabbit lung

Lungs were isolated from adult male rabbits (New Zealand White, Bauer, Neuenstein-Lohe, Germany). Only healthy animals of 3.0 ± 0.5 kg were used. The ear vein of the rabbits was canulated and an initial bolus of anesthetics was administered containing approximately 0.5 - 0.7 ml of a mixture of xylazine and ketamine in a ratio of 3:2. Additionally, 1,000 IU/kg heparin was applied intravenously to prevent coagulation. A further 1 ml of the anesthetics was administered stepwise over three min to achieve deep anesthesia, but still allowing spontaneous breathing. Animals were placed in a supine position and the legs were fixed. Approximately 8-10 ml lidocaine were injected subcutaneously into the ventral center of the neck to achieve local anesthesia, and a median incision from chin to the cranial thorax was performed. Afterwards, the trachea was exposed by blunt dissection and partially transsected, and a tracheal canula with an inner diameter of 3 mm was inserted. Throughout the procedure the animals were artificially ventilated with room air using a Harvard cat/rabbit ventilator. Subsequently, a second median incision was made from the center of the neck to the upper abdomen and a mid-sternal thoracotomy was performed. The xypoid process was clamped and elongated, the diaphragm was dissected and the ribs were spread. Parts of the parietal pleura, the thymus and the bulk of the pericardium were removed to expose the heart, and the apex of the heart was

clamped. A loose thread loop was formed around the ascendent aorta as well as pulmonary trunk, a bolus of 2 ml ketamine/xylazine was administered intravenously and a small incision in the upper right ventricle was done. Through the opening a fluid-filled pulmonary artery catheter of an inner diameter of 3 mm was inserted into the pulmonary artery and fixed with a thread loop immediately after which the left atrium was opened by removing the apex of the heart, and the descendent aorta was ligated. Lungs were perfused through the pulmonary artery catheter with a blood-free buffer, initially at 4 ºC at a perfusion rate of 15 ml/min. Thereafter, the lungs, trachea and heart were excised *en bloc* from the thorax. The mitral valves and the *chordae tendineae* were dissected and a second perfusion catheter with an internal diameter of 4 mm was introduced via the left ventricle into the left atrium. A tobacco pouch suture was used to fix this second catheter at the apex of the left ventricle such that no leakage from the catheterization sites or obstruction of the pulmonary circulation occurred. After perfusing at least 1 l of buffer through the lungs to remove all blood from the system, the perfusion circuit was closed for the recirculation, while the perfusion rate was increased from 15 to 100 ml/h and the temperature was increased to 37 ºC.

3.2.4 Mechanical ventilation

During lung preparation, natural respiration was replaced with artificial respiration with room air. The use of a Harvard cat/rabbit ventilator enabled constant gas exchange under deep anesthesia. After isolation and separation of the lungs, room air was supplemented with 4.5 % CO_2 to maintain the pH of the recirculating buffer between 7.35-7.37. Ventilation parameters were set at 30 breaths/min, a plateau pressure of 7.5 mmHg (0 mmHg was referenced at the hilum of the organ), and a ratio between inspiration and expiration of 1:1 to maintain uniform ventilation. To prevent atelectasis, a positive end-expiratory pressure (PEEP) was set to 2 mmHg, resulting in a tidal volume of approximately 6 ml/kg body mass, which is considered protective (81).

3.2.5 Lung perfusion

Krebs-Henseleit buffer containing 120 mM NaCl, 4.3 mM KCl, 1.1 mM Ka_2PO_4, 2.4 mM $CaCl_2$, 1.3 mM magnesium phosphate, 0.24 % (m/v) glucose, and 5% (m/v) hydroxyethylamylopectin (for plasma expansion) was used for perfusion through a tubing system. Approximately 25 ml $NaHCO_3$ were added to maintain a pH of 7.35-7.37. Two independent reservoirs, allowing a perfusate change from one reservoir to the other without interrupting the circulation, were installed in the system. The perfusate was pumped into the circulation at a flow rate of 100 ml/min. After passage through the pulmonary artery and perfusing the lungs, the perfusate left the lung through a catheter placed in the left atrium to the "venous" part of the perfusion. Left atrial pressure (LAP) was adjusted by placing a catheter in the venous tubing system above the hilum. The temperature of the perfusate was maintained at 37 ºC by using a thermostat-controlled water bath and a tube coil dipped into a 37 ºC water bath. A pressure sensor was placed into the pulmonary artery to measure the pulmonary arterial pressure (PAP) and another pressure sensor into the left atrium to measure LAP. Immediately after the fluid-filled arterial catheter was placed into the pulmonary artery and throughout the rest of the preparation, lungs were perfused at a 15 ml/min flow rate and at a temperature of 4 ºC. After the lungs and heart had been isolated and removed *en block* from the thoracic cavity, the flow was increased step-wise to 100 ml/min and the temperature to 37 ºC over approximately 10 min. During this time the lungs were perfused with at least 1 l non-recirculating buffer to remove any residual blood cells from the circulation. A filter of 0.2 µm mesh size was also placed into the circulation system to eliminate remaining cells. After perfusion reached the desired 100 ml/min flow rate and the buffer was heated to 37 ºC the filter system was removed and the perfusion buffer was recirculated. The volume of the recirculating buffer in the system was 300 ml. At the end of the preparation and after the lungs were freely suspended from a force transducer LAP was set at 2 mmHg. Throughout the experiment, a bubble trap was present in the perfusion system to prevent any air embolisms in the circulation.

3.2.6 Broncho-alveolar lavage

To measure the amount of fluid that was retained by the lung after fluid instillation, a BAL was performed. To do so, 50 ml of iso-osmolar mannitol solution were instilled into the right lung and gently reaspirated 3× with a syringe to recover lavage fluid while the left lung was ligated. The fluid was centrifuged at 1,000 revolutions per minute (rpm) for 10 min to remove cellular debris. Altogether approximately 75-80 % of the instilled fluid was recovered during the procedure which was always performed in a time period not longer than 30 s and immediately after termination of ventilation and perfusion. The amounts of BAL fluid from TGF-β treated lungs were compared to the amount of fluid retained by vehicle-treated rabbit lungs to assess the ability of the lung to clear the artificial edema.

3.2.7 Weight measurement of the isolated rabbit lung

For every experiment in the isolated lung model, the mass of the lung was measured, and changes in the lung mass were detected continuously by a force transducer. All analog signals were amplified, converted into digital signals and the use of the PlotIT 3.1 software (Scientific Programming Enterprises, SPE, USA) enabled an on-line graphical demonstration of left ventricular pressure (LVP), PAP, ventilation pressure (VP) and weight on a personal computer troughout the experiment.

In order to compare the edema resolution of TGF-β treated and untreated lungs the differences in weight of the lungs 1.5 h after instillation of the fluid were registered and compared.

3.2.8 Measurement of the transepithelial sodium flux in the isolated rabbit lung

After an initial steady-state period after placing the lung in the heated chamber aerolizations were performed with an ultrasonic nebulizer which was connected to the inspiration loop of the ventilator. The tracer contained 1.2 μCi of ^{22}Na in 5 ml of saline. During a 10-min aerosolization period, 1.6-1.8 ml of aerosol were generated, and a fraction (~60%) of this aerosol (~1 ml) reached the lung, the bulk of which was deposited into the alveolar space (82, 83). A schematic representation of the experimental setup of the rabbit lung treatment after isolation is depicted in Figure 4.

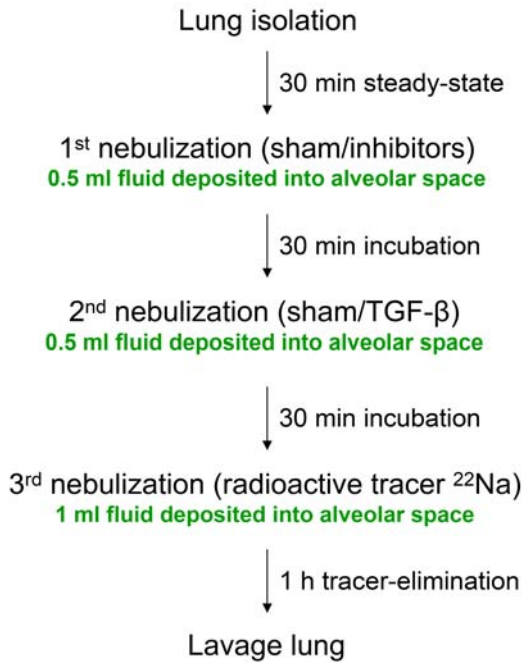

Figure 4. Schematic representation of the experimental setup of the rabbit lung treatment after isolation.

Lungs were isolated and placed freely hanging from a force transducer in a chamber heated to 37 ºC. After an equilibration time of 30 min an artificial edema was produced by nebulizing altogether 2 ml of fluid into the lungs. Nebulization was performed in three steps, each of them followed up by a 30-min incubation time. Broncho-alveolar lavages were performed at the end of the experiments, approximately 2 h after lung isolation.

Gamma detectors were placed around the perfusate reservoir and the lung. Those detectors were connected to an automated high-voltage power supply that was integrated into a computer system, and detected the radiation emitted from the

lung and the perfusate, thereby measured tracer movement and ^{22}Na clearance from the alveolar compartment. Measurements were performed every 30 s.

3.2.9 Culture of *E. coli* bacteria

3.2.9.1 Preparation of agar plates and medium

In order to prepare medium for bacterial cells 25 g of Luria broth base powder (Invitrogen) were dissolved in 1 l of distilled water and subsequently autoclaved. After the liquid had cooled to ~50 ºC ampicillin as selective antibiotic was added to a concentration of 50 mg/ml medium. In order to prepare agar plates for bacterial cells, 25 g of Luria broth base and 7.5 g bacto agar were dissolved in 1 l of distilled water and then autoclaved. After the antibiotic had been added the agar containing medium was quickly poured into sterile Petri dishes (250 ml of medium make approximately 12 10-cm plates). Once the agar had solidified, the plates were stored in the dark at 4 ºC until needed.

3.2.9.2 Preparation of frozen competent cells

Using a sterilized inoculating loop, *E. coli* DH5α from a frozen stock were streaked onto a SOB agar plate without antibiotics and incubated overnight (16 h) at 37 ºC. After 16 h a single colony from the plate was transferred into 5 ml of SOB medium containing 20 mM $MgSO_4$ and incubated for 16 h at 37 ºC with shaking (120 rpm). On the next day, the culture was diluted to 200 ml of SOB medium containing 20 mM $MgSO_4$ and incubated on a shaker (120 rpm) at 37 ºC for 2-3 h. The optical density at 600 nm was monitored every 15 min with a spectrophotometer, and when it reached ~3.5 the cells were aliquoted into 50 ml Falcon tubes on ice and cooled for 10 min. The bacteria were then centrifuged at 4,000 rpm for 10 min at 4 ºC. The medium was aspirated off and the tubes were kept in an inverted position for 1 min to allow the medium to drain off cell pellet. Each pellet was then resuspended in 20 ml of ice-cold frozen storage buffer (FSB) and kept on ice for 10 min. Then the cells were pelleted again at 4,000 rpm for 10 min at 4 ºC. The buffer was aspirated off and the tubes were kept in an inverted

position for 1 min followed by another resuspension step in 4 ml of ice-cold FSB. To each tube containing 4 ml of bacterial suspension, 140 µl of DMSO were added, mixed gently, and incubated on ice for 15 min. Then additional 140 µl of DMSO were added and mixed gently. Finally the cell suspensions were quickly aliquoted into sterile 0.5 ml Eppendorf tubes on ice, snap-frozen in liquid nitrogen and stored at -80 ºC until needed.

3.2.9.3 Plasmid extraction from filter paper

When a DNA construct was received from another laboratory on a filter paper, the plasmid had to be extracted from the paper in order perform a bacterial transformation. Usually the sender had drawn a circle around the spot on the paper with a pencil where the DNA had been applied. The paper was cut carefully around the circle and into thin strips and put into a 1.5-ml Eppendorf tube, on ice. Then, 80-200 µl of sterile water were added, depending on the size of the spot. The tube was vortexed every 5 min for 30 min and finally spun down briefly in order to collect all the liquid on the bottom of the tube. Then, 5 µl of this solution was used to perform bacterial transformation with *E. coli* as described above. The tube containing the paper and the remaining liquid was kept in the freezer for several months.

3.2.9.4 Cryopreservation and resuscitation of frozen bacteria containing DNA plasmids in glycerol

In order to preserve transformed bacteria for longer time-periods, glycerol stocks of transformed bacteria were prepared. To do so, 5 ml of LB-medium containing 50 mg antibiotic per ml were inoculated with one single colony of transformed bacteria from an agar plate and incubated overnight (16 h) shaking at 220 rpm at 37 ºC. To prepare a glycerol stock, 1 ml of the bacterial culture was gently mixed with 500 µl of pure glycerol in a cryotube and immediately frozen at -80 ºC. In order to resuscitate frozen bacteria, glycerol stocks were slowly thawed on ice and bacteria were streaked onto the surface of a fresh ampicillin-containing agar plate

with a sterile metal loop. Afterwards, the plate was incubated upside-down at 37 ºC for 16-24 h.

3.2.9.5 Plasmid transformation of competent cells

In order to transform DNA plasmids into competent bacteria, 10 ng of plasmid were pipetted into Eppendorf tubes on ice. Competent bacteria were slowly thawed on ice and 50 µl of the competent bacteria cell suspension were added to the DNA. After incubation for 30 min on ice, the bacteria were heat-shocked at exactly 42 ºC for 50 s. Thereafter, the reactions were kept on ice for 2 min, after which 900 µl of LB-medium at room temperature (RT) without antibiotics were added, and the bacteria were incubated at 37 ºC shaking at 220 rpm for 1.5 h, after which 100 µl of the bacteria cell suspension were plated on an agar plate containing the required antibiotic, until the agar had absorbed all the liquid. The plate was kept upside-down in the incubator to allow bacterial growth at 37 ºC overnight.

3.2.10 Plasmid extraction from bacterial cultures

3.2.10.1 Mini-preparation of DNA

Five milliliters of LB-medium were inoculated with one colony of bacteria and were incubated overnight at 37 ºC, with shaking at 220 rpm. Small-scale isolations of plasmid DNA were performed using the QIAprep Spin Miniprep kit (Qiagen) using a microcentrifuge, according to the manufacturer`s protocol.

3.2.10.2 Midi-preparation of DNA

In order to obtain larger amounts of plasmid DNA, 5 ml of LB-medium were inoculated with one colony of bacteria and were incubated for 8 h at 37 ºC with shaking at 220 rpm. This preparation was then transferred into 250 ml of LB-medium in an autoclaved Erlenmeyer flask and incubated for 16 h at 37 ºC on the shaker. Large-scale DNA preparation was performed using the PureYield™

Plasmid Midiprep System (Promega) according to the manufacturer`s instructions, using the protocol “DNA purification by centrifugation”.

3.2.10.3 Site-directed mutagenesis of plasmid DNA

Site-directed mutagenesis was performed on the human *SCNN1B* and mouse *scnn1b* genes, encoding hβENaC and mβENaC, respectively, using the QuikChange II site-directed mutagenesis kit (Stratagene, Germany). In a V5-tagged mβENaC-expressing construct, all five cysteines in the cytosolic domains were mutated to serine: Cys^{10}, Cys^{30}, Cys^{43}, Cys^{557} and Cys^{595}. In hβENaC, Cys^{30} and Cys^{43} are the only two intracellular cysteine residues, which were also converted to serine. The primers employed are listed in Table 2 on page 22. Thermal cycling was performed using *PfuUltra* HF DNA polymerase which was provided in the kit. After digestion of the parental DNA by adding 1 µl of *Dpn* I restriction enzyme to each reaction tube, the DNA was transformed into competent bacteria as described previously. After transformation single bacterial colonies were picked and transferred into 5 ml of LB-medium containing ampicillin. After 16 to 24 h of incubation at 37 ºC with shaking at 220 rpm, minipreps were prepared and sequenced in order to confirm the successful mutagenesis, and to check for strand displacement.

3.2.11 Culture of mammalian cell lines

The A549 and MLE-12 cells were purchased from American Type Culture Collection (ATCC-LGC, Wesel, Germany). The cells were cultured in monolayers in cell culture flasks in D-MEM containing 20 mM HEPES and 10% fetal calf serum (FCS) for A549 cells and 2% FCS for MLE-12 cells. For MLE-12 cells the following additives were filter-sterilized and added to the medium: Insulin-Transferrin-Selenium supplement (gibco/Invitrogen), 10 ml/l medium, β-estradiol (Sigma-Aldrich, Germany) to a final concentration of 10 nM and hydrocortisone (Sigma-Aldrich, Germany) at 10 nM. The medium was changed every two to three days. The cells were kept in an incubator in a humidified atmosphere with 5% CO_2 and 21% O_2 at 37 ºC.

3.2.12 Subculture of mammalian cells

When the cells had reached a confluency of 70-90% the cells were detached from the flask using Trypsin-EDTA solution (PAA, Austria), diluted in medium and subcultured in new flasks. The medium was aspirated from the culture flasks using an aspirator and a sterile glass Pasteur pipette. The cells were then rinsed once with PBS without Ca^{2+} and Mg^{2+} (PAA) to remove any remaining FCS-containing medium. Subsequently, the cells were incubated with 2 ml of Trypsin-EDTA solution (PAA) for 3-5 min in the incubator at 37 ºC. The state of detachment from the surface of the cell culture flask was monitored by observing the cells under a microscope. The reaction of trypsin was stopped by adding cell culture medium containing 10% FCS. In order to obtain a single-cell suspension the cells were gently repeat pipetted and then aliquoted into new flasks or cell culture dishes.

3.2.13 Transient transfection of A549 and MLE-12 cells

The A549 or MLE-12 cells were transiently transfected with plasmid cDNA using Lipofectamine™ 2000 transfection reagent (Invitrogen, Karlsruhe). To transfect cells in a 60-mm dish, cells were plated the day before transfection to attain approximately 70% confluency at the time of transfection. Two sterile bacterial culture tubes were prepared per cDNA sample. Then, 0.5 ml of Opti-MEM® transfection medium was pipetted into each of the tubes. To one of the tubes 2.4 µl of Lipofectamine™ 2000 transfection reagent were added. To the other tube 2.4 µg of the respective cDNA were added and mixed gently. After 5 min incubation at room temperature (RT), the DNA-containing medium and the Lipofectamine™ 2000-containing medium were combined and incubated for another 20 min at RT to form liposome-like complexes. The complexes were then gently pipetted drop-wise onto the plated cells and the plate was gently rocked back and forth in order to evenly spread the DNA. After 5 h the medium was exchanged. The cells were then incubated at 37 ºC for 16-19 h prior to further treatment.

3.2.14 Short interfering RNAs transfection of mammalian cells

The A549 cells were transiently tranfected with siRNA using Lipofectamine™ 2000 transfection reagent (Invitrogen). To transfect A549 cells in a 60-mm dish cells were plated the day before transfection so they were approximately 50% confluent at the time of transfection. To transfect the cells, two sterile bacterial culture tubes were prepared per sample. Then, 100 µl of Opti-MEM® transfection medium was pipetted into each of the tubes. To one of them 5 µl of Lipofectamine™ 2000 transfection reagent was added and mixed gently. After 15 min incubation at RT the respective siRNA was added to the other medium-containing tube and mixed by repeat pipetting. The siRNA-containing medium and the Lipofectamine™ 2000-containing medium were then combined and incubated for another 15 min at RT. The mixture was then gently pipetted drop-wise onto the plated cells and the plate was gently rocked back-and-forth in order to evenly spread the siRNA. After 5 h the medium was exchanged. The cells were then incubated at 37 ºC for 48 h. For every set of siRNA treated cells one sample with scrambled siRNA was prepared as a negative control.

3.2.15 Stimulation of A549 or MLE-12 cells

Cells were stimulated with recombinant TGF-β at a concentration of 10 ng/ml cell culture medium. Before stimulation the growth medium was aspirated from the cells using a sterile Pasteur glass pipette and an aspirator. The cells were then rinsed twice with prewarmed sterile PBS without Ca^{2+} and Mg^{2+}. To stimulate cells on a 60-mm cell culture dish, 3 µl of a TGF-β stock solution (concentration: 10 µg/µl) were diluted in 10 ml of prewarmed D-MEM cell culture medium containing 10% FCS, mixed well and then pipetted onto the cells. The cells were then incubated at 37 ºC for different time periods. Furthermore, the cells were stimulated with: Brefeldin A (BFA) at 10 µg/ml; the phospholipase A2 inhibitor, *N*-(*p*-amylcinnamoyl)anthranilic acid at 25 µM; the Ca^{2+}-chelator, BAPTA-AM at 25 mM; the protein kinase C inhibitor, bisindolylmaleimide I at 1 and 10 µM; the Ca^{2+}/calmodulin-dependent protein kinase kinase inhibitor, STO-609 at 20 µg/ml; the phosphoinositide-3-kinase inhibitor, wortmannin at 100 nM; the

phospholipase A inhibitor, isotetrandrine at 1 μg/ml; and the c-jun N-terminal kinase inhibitor II at 50 μM.

3.2.16 Quantitative real-time RT PCR

Primary mouse ATII cells were isolated and kindly provided by our technical assistant, Miriam Schmidt. Total RNA was isolated from cultured cells using a Qiagen RNeasy kit (Qiagen, Hilden, Germany), followed by DNase treatment to remove any contaminating genomic DNA. Quantitative changes in mRNA expression of genes were assessed by quantitative realtime PCR using a Platinum® SYBR® Green qPCR SuperMix UDG kit (Invitrogen), and a Sequence Detection System StepOnePlus (Applied Biosystems, Foster City, CA) and the intron-spanning primer pairs indicated in Table 1 (custom synthesized by Eurofins MWG Opereron, Germany). The ubiquitously expressed, pseudogene-free hprt gene was used as reference. Cycling conditions were 50 ºC for 2 min, 95 ºC for 5 min, followed by 40 cycles of 95 ºC for 5 s, 59 ºC for 5 s, and 72 ºC for 30 s. The exclusive amplification of the expected PCR product was confirmed by melting curve analysis and gel electrophoresis.

3.2.17 Surface biotinylation of A549 or MLE-12 cells

After stimulation with TGF-β cells were washed 3× with ice-cold PBS containing Ca^{2+} and Mg^{2+}. Then, 3 ml of ice-cold PBS with Ca^{2+} and Mg^{2+} containing 1 mg EZ-Link Sulfo-NHS-LC-Biotin (Thermo Fisher Scientific Inc., USA) per ml were added to each 60-mm plate. The cells were incubated with biotin for 20 min on ice.

After incubation the biotin-PBS solution was removed from the cells and the cells were washed 3×10 min each with 10 ml of ice-cold PBS with Ca^{2+} and Mg^{2+} containing 100 mM of glycine to quench any unbound biotin. Afterwards, the cells were washed 1×10 min with ice-cold PBS with Ca^{2+} and Mg^{2+} without glycine.

3.2.18 Protein isolation from biotinylated A549 or MLE-12 cells

Proteins were extracted from the biotinylated cells using NP-40 cell lysis buffer with Complete™ Protease inhibitor (Roche) and vanadate added shortly before use. After mixing, 100 µl of lysis buffer were dispersed on each 60-mm dish. Cells were scraped thoroughly from the culture plate using a cell scraper and the lysate was pipetted into a 1.5 ml Eppendorf tube on ice. After a 20-min incubation on ice with intermittent vortexing, cell debris and insoluble proteins were removed by centrifuging the cell lysate for 20 min at 10,000 rpm at 4 ºC. The supernatant was then transferred into a new 1.5 ml Eppendorf tube on ice.

3.2.19 Measurement of protein concentration

Each protein solution was diluted 1:30 with water. For each sample plus a buffer blank, two wells of a 96 well plate were prepared by pipetting 200 µl of Biorad Quickstart® Bradford solution into each well. Then, 10 µl of the diluted protein sample or the buffer (same dilution) were added (in duplicates). After 15 min incubation the absorption was read in a plate reader at 570 nm. The concentration of protein in each sample was calculated employing a previously-prepared protein standard curve.

3.2.20 Pull-down of biotinylated proteins

To pull down biotinylated proteins from the lysate, 250 µg of protein of each sample were incubated with 60 µl streptavidin beads. First, 100 µl of beads were washed in 100 µl NP-40 cell lysis buffer. After centrifugation, the supernatant was aspirated and the beads were resuspended in 80 µl of lysis buffer. From this mixture, 60 µl were used for the pull-down of each sample. After adding the protein, the volume of each sample was brought to 300 µl by adding lysis buffer. The tubes were incubated overnight on a rotor at 4 ºC rotating at low speed. On the next day, the beads were washed with four different solutions (see buffers at the end of this chapter). The beads were washed once with solution A, twice with solution B and 3× with solution C. For a final wash, Tris pH 6.8 was used. Then, 20 µl of protein loading buffer containing 20 mM DTT were added to each tube and the samples were boiled at 95 ºC for 10 min on a heating block to remove the

biotinylated proteins from the streptavidin beads. When phospholipase D (PLD)1 was the object of investigation, the samples were heated at 70 ºC for 10 min. Then the content of the tubes was spun in a microcentrifuge for 3 min to collect the sample at the bottom of the tube, and to pellet the beads. The supernatants were then subjected to sodium dodecyl sulfate polyacrylamide gel electrophoresis (SDS-PAGE) on a 10% SDS-PAGE gel. From each original protein sample, 5 µg of protein were loaded on the same gel as an input loading control.

3.2.21 Protein separation by SDS-PAGE

The SDS-PAGE gels were prepared the day before use. First, the ingredients for the resolving gel were mixed in a small beaker and poured between two glass plates held in a gel casting device with spacers, tightened by a clamp. The resolving gel was carefully overlaid with a few ml of isopropanol to smoothen the gel surface and to exclude air. After polymerization, the isopropanol was removed and the ingredients for the stacking gel were mixed and poured on top of the resolving gel. Afterwards the comb to form the wells for loading was inserted into the stacking gel and the gel was allowed to polymerize completely.

Composition of a 10% SDS-Polyacrylamide gel, 40 ml:

Resolving gel:

Water (distilled)	19.5 ml
30% acrylamide	13.3 ml
Tris-Cl, 1.5 M, pH 8.8	10 ml
SDS, 10% (w/v)	400 µl
APS, 10% (w/v)	400 µl
TEMED	16 µl

Stacking gel, 20 ml:

Water (distilled)	13.6 ml
30% acrylamide	3.4 ml
Tris-Cl, 1.5 M, pH 6.8	2.5 ml

SDS, 10% (w/v)	200 µl
APS, 10% (w/v)	200 µl
TEMED	20 µl

3.2.22 Western blot

After running the gel for 2 h at 110 mV, or until the bromophenol blue marker band had reached the bottom of the gel, the proteins were blotted onto a nitrocellulose membrane. To do so 1× blotting buffer was prepared by diluting 800 ml of 10× blotting buffer with distilled water and 200 ml methanol. After pouring the buffer into a glass tank, western blot sponges and three filter papers were pre-wet and the "blotting sandwich" was assembled in the following order: black plastic part of the sandwich cassette, sponge, two filter papers, gel, membrane, one filter paper, sponge, clear part of the sandwich cassette. Before the cassette was closed firmly, air bubbles were removed carefully with a rolling pin. The cassette was locked and placed in the voltage module such that the black part of the cassette was facing the black part of the module. An ice box was used to keep the blot cool during protein transfer, which was performed for 1 h at 115 mV. After a 1-min wash of the membrane with phosphate-buffered saline + Tween® 20 (PBST) to remove gel residues, the blot was incubated in blocking buffer (5% (w/v) non-fat dry milk powder or 5% (w/v) bovine serum albumin (BSA) in PBST, depending on the requirements for the respective primary antibody) for 1 h at RT. After blocking, the primary antibody (diluted in blocking buffer, depending on the requirements for the respective antibody) was added and incubated overnight at 4 ºC. On the following day, the blot was washed 3× for 10 min with PBST. Then, the blot was incubated in the respective horseradish peroxidase-bound secondary antibody for 1 h at RT. After 5×10-min washes in PBST, the blot was incubated for 5 min with enhanced chemiluminescence reagent (Amersham). The protein bands were then visualized on a film (Agfa Gevaert) or a hypersensitive film (ECL™ Hyperfilm™, Amersham).

3.2.23 Fluorescence-based reactive oxygen species detection

The compound 2′,7′-dichlorodihydrofluorescein diacetate (**H_2**DCFDA) is the chemically reduced and acetylated form of 2′,7′-dichlorofluorescein. It permeates the cell membrane and diffuses into the cell where the acetate groups are removed by intracellular deesterification. The product of this reaction is a charged molecule which is much less likely to diffuse out of the cell than is the acetylated form and which is converted to the fluorescent 5-chloromethyl-2′-7′-dichlorofluorescein (DCF) upon oxidation. Oxidation of H_2DCFDA in response to TGF-β in A549 cells was detected by monitoring the change in fluorescence with a microplate reader. The A549 cells were grown overnight to 30-50% confluency on a 96-well optical plate. Before loading cells with dye, cells were washed once with prewarmed PBS. Then, 0.005 g of DCFDA were dissolved in 100 µl of DMSO, diluted 1:1,000 in phenol red-free cell culture medium shortly before use, and 100 µl of this solution were pipetted into each well. The cells were incubated in a cell culture incubator (37 ºC) for 30 min. After dye-loading, the cells were incubated with phenol red-free medium containing the relevant pharmacological agent (except for siRNA transfections and EUK-134 application, which were performed 24 h prior to H_2DCFDA preloading). After 30-min incubation, medium was replaced with medium containing TGF-β (or vehicle alone) plus the relevant pharmacological agent (or vehicle alone). After 30 min, cells were washed 1× with PBS, prior to assessment of DCF fluorescence in a microplate spectrofluorimeter at λ_{ex} 485 nm, λ_{ex} 520 nm. Untreated cells loaded with H_2DCFDA only were used as blank.

3.3 Buffers

Protein lysis buffer

20 mM Tris-Cl pH 7.5
150 mM NaCl
1 mM EDTA
1 mM EGTA
0.5% Igepal® CA-630 (NP-40)

1 mM Na_3VO_4 added directly before use

Complete™ 1 tablet per 25 ml of lysis buffer, added directly before use

2× loading buffer

100 mM Tris-Cl pH 6.8

4% SDS

0.2% bromophenol blue

20% glycerol

20 mM DTT (added directly before use)

10× SDS running buffer

250 mM Tris

2.5 M Glycine

1% SDS

Blotting buffer

25 mM Tris

192 mM glycine

20% methanol

Washing buffer PBST

1× PBS

0.1% Tween® 20

Blocking buffer

1× PBS

0.1% Tween® 20

5% non-fat dry milk

FSB Transformation buffer for competent cells

10 mM potassium acetate, pH 7.5
45 mM $MnCl_2 \cdot 4H_2O$
10 mM $CaCl_2 \cdot 2H_2O$
10 mM KCl
100 mM hexamminecobalt chloride
100 ml glycerol
H_2O to 1 l

3.4 Wash solutions for biotinylated proteins on streptavidin beads

Solution A

150 mM NaCl
50 mM Tris pH 7.4
5 mM EDTA

Solution B

500 mM NaCl
50 mM Tris pH 7.4
5 mM EDTA

Solution C

500 mM NaCl
20 mM Tris pH 7.4
0.2% (w/v) BSA

3.5 Statistics

Data are presented as mean ± S.D.. For the animal studies differences between groups were assessed by ANOVA with the Newman-Keuls modification. For cell-based studies, an unpaired Student's *t*-test was employed. *P* values <0.05 were considered significant.

4 Results

Alveolar fluid clearance is an essential mechanism that maintains the amount of ELF constant and thereby prevents pulmonary edema persistence. Pulmonary edema is a hallmark of ARDS, a syndrome of acute respiratory failure caused by alveolar damage. In broncho-alveolar lavage fluids of patients suffering from ARDS, significantly elevated levels of TGF-β have been reported (54), and in these patients, lower TGF-β levels correlate with more ventilator-free and ICU-free days (78). It was hypothesized in this study that TGF-β blocks active fluid reabsorption, thereby contributing to the formation and the persistence of alveolar edema.

4.1 Exogenous TGF-β application blocks fluid reabsorption in isolated, ventilated and perfused rabbit lungs

To delineate the effects of TGF-β on fluid balance in the lung, an isolated, ventilated and perfused rabbit lung was employed. The isolated lung serves as a model of edema fluid reabsorption, where a 2 ml fluid challenge applied to the lung is absorbed and removed by the perfused vasculature over 60 min, post-nebulization. Fluid retention in the lung is indicated by an increase in the net steady-state mass of the lung (compared at the beginning and end of the 60 min-period), and by an increased ELF volume. Vehicle-treated control lungs exhibited a net loss in mass of ~0.2 g (Figure 5A), while lungs maintained at 8 ºC (where active transport processes are shut down) exhibited a net gain of 1.51 ± 0.25 g, comparable with that observed to TGF-β application (10 ng/ml, final concentration in the ELF), and TGF-β combined with low temperature (Figure 5A). Application of SB431542 (10 μM final concentration in the ELF), an inhibitor of TGF-β signaling via the type I TGF-β receptor Tgfbr1 that acts as a competitive adenosine triphosphate (ATP) binding-site inhibitor, had no effect on net lung mass, however, preapplication of SB431542 abrogated the effects of TGF-β on net lung mass (Figure 5A). Amiloride increased net lung mass to 1.0 ± 0.03 g, although TGF-β applied together with amiloride had no additive effect over that of TGF-β applied alone, suggesting that TGF-β and amiloride may

share the same targets. Since ENaC function can be regulated by actin-dependent trafficking events (84, 85), phalloidin oleate (PO), a cell membrane-permeable inhibitor of F→G actin conversion was employed (at 1 μM final concentration in the ELF). Application of PO had no impact on the net mass of vehicle treated control lungs, however, preapplication of PO abrogated the effects of TGF-β on net lung mass (Figure 5A), indicating a role for F→G actin conversion in mediating the effect of TGF-β on lung fluid dynamics.

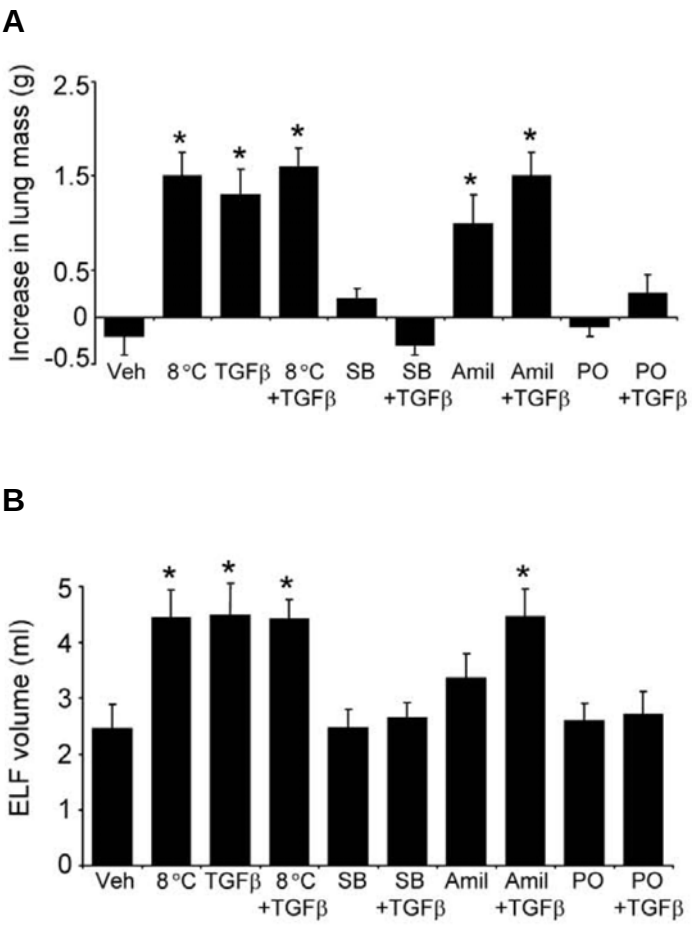

Figure 5. Exogenous TGF-β application blocks fluid reabsorption in isolated, ventilated and perfused rabbit lungs.

(**A**) Epithelial lining fluid (ELF) volumes were assessed in isolated, ventilated and perfused rabbit lungs treated with vehicle (Veh), low temperature (8 ºC), TGF-β (TGFβ), SB431542 (SB), amiloride (Amil), phalloidin oleate (PO), or combinations thereof, 60 min after a 2 ml fluid challenge. (n = 8, per group). (**B**) The increase in ELF volume of isolated lungs described in (**A**) was also assessed. Data represent mean ± S.D. *, $P < 0.05$.

Trends in changes in the ELF volume of the isolated, ventilated, and perfused rabbit lungs (Figure 5B) paralleled the observations made on net lung mass (Figure 5A). Application of low temperature (8 ºC) and/or TGF-β resulted in a two-fold increase in ELF volume of 2 ml, which approximates the volume of the fluid applied to the lung in the 2 ml fluid challenge. This increase in ELF volume was prevented by preapplication of SB431542 or PO, although neither agent alone had any effect on net lung mass (Figure 5B). Taken together, data generated in the isolated, ventilated and perfused rabbit lung indicate that TGF-β applied to the alveolar airspaces blocked alveolar fluid reabsorption, as was evident by the inability of the lung to clear a fluid challenge.

4.2 Exogenous TGF-β application blocks active $^{22}Na^{+}$ efflux from the alveolar airspaces in isolated, ventilated and perfused rabbit lungs

Transepithelial Na^{+} transport out of the alveolar airspaces drives AFC (6). Since fluid clearance from the lung was blocked by TGF-β administration to the alveolar airspaces, the effects of TGF-β application on active transepithelial Na^{+} transport from the alveolar airspaces into the vasculature were assessed in an isolated, ventilated, and perfused rabbit lung. Application of TGF-β (10 ng/ml final concentration in the ELF) caused an 80% reduction in the active component of $^{22}Na^{+}$ efflux from the alveolar airspaces (Figure 6A and 6B). The effects of TGF-β were blocked by preapplication of SB431542 (Figure 6A and 6B) or PO (Figure 6C and 6D). Amiloride application resulted in a 60% reduction in the active component of $^{22}Na^{+}$ efflux from the alveolar airspaces (Figure 6C and 6D), however, the effects of the administration of amiloride and TGF-β together (Figure 6C and 6D) were not additive over the effects of TGF-β applied alone (Figure 6A and 6B), suggesting that TGF-β and amiloride share the same targets. Taken together, these data demonstrate that TGF-β blocks active $^{22}Na^{+}$ efflux from the alveolar airspaces in isolated, ventilated and perfused rabbit lungs.

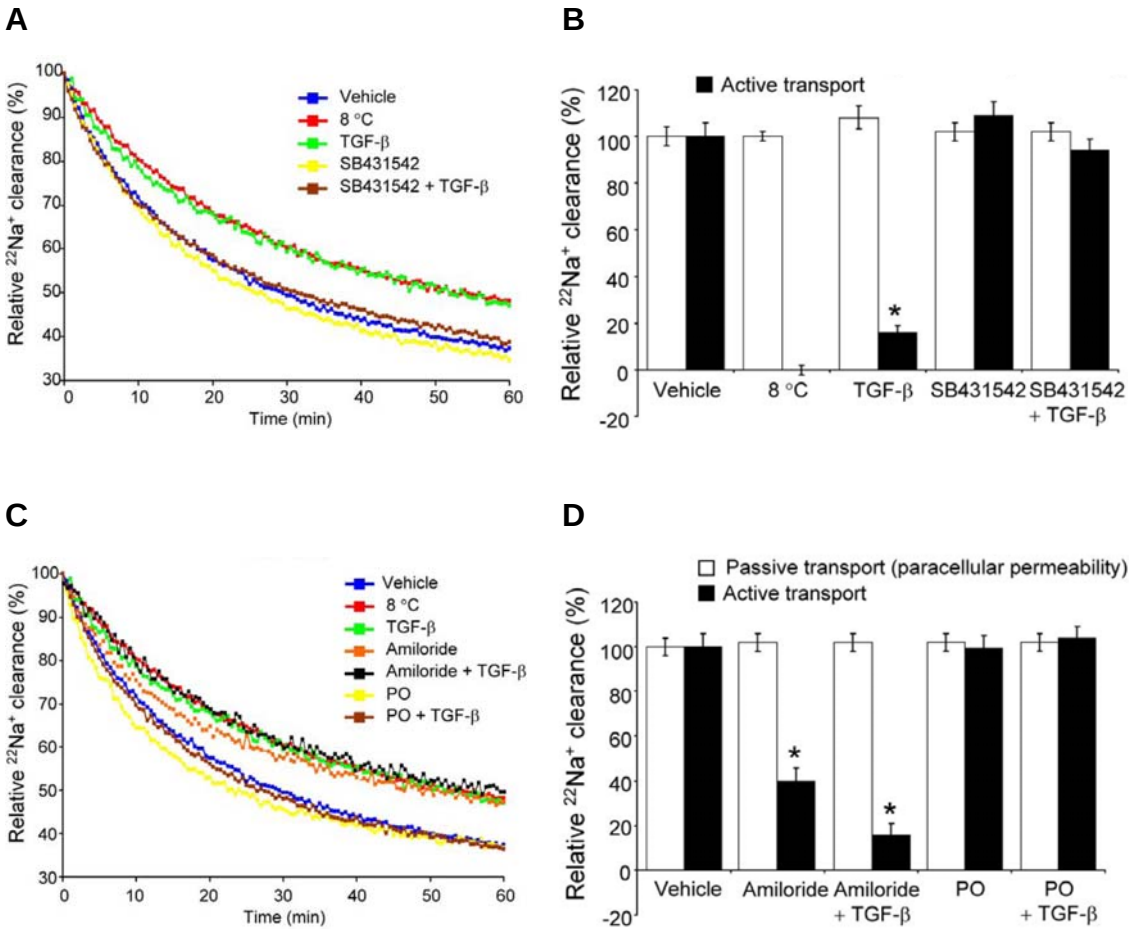

Figure 6. TGF-β signaling blocks $^{22}Na^+$ clearance from alveolar airspaces and alveolar fluid reabsorption.

(**A**) Representative original recording of $^{22}Na^+$ clearance from an isolated, ventilated, and perfused rabbit lung, treated with vehicle, illustrating baseline clearance over 1 h (blue), or low temperature (8 ºC; red), TGF-β [10 ng/ml in epithelial lining fluid (ELF); green], SB431542 (10 μM in ELF; yellow), and TGF-β after SB431542 preapplication (brown). (**B**) Data quantified from multiple experiments (n = 8, per group) illustrated in (**A**), for passive transport, determined from [^{3}H]mannitol flux, and the active component of $^{22}Na^+$ clearance. (**C**) Representative original recording of $^{22}Na^+$ clearance from an isolated, ventilated, and perfused rabbit lung, illustrating the effects of amiloride (10 μM in ELF; orange) and phalloidin oleate (PO; 1 μM in the ELF; yellow) in the absence of TGF-β. Both amiloride (black) and PO (brown) were also applied 30 min after TGF-β application. (**D**) Data quantified from multiple experiments (n = 8; per group) illustrated in (**C**), for passive transport, determined from [^{3}H]mannitol flux, and the active component of the $^{22}Na^+$ clearance. Data represent mean ± S.D. *, $P < 0.05$.

4.3 TGF-β does not acutely influence ENaC gene expression in lung epithelial cells

To verify that ENaC was indeed targeted by TGF-β, both the expression and cell surface distribution of the three classical ENaC subunits, αENaC (encoded by the *SCNN1A* gene), βENaC (encoded by the *SCNN1B* gene) and γENaC (encoded by the *SCNN1G* gene) were studied in lung epithelial cells 30 min and 150 min after TGF-β (10 ng/ml) application. Stimulation with TGF-β for 150 min did not alter steady-state mRNA levels of the *SCNN1A*, *SCNN1B*, or *SCNN1G* genes in A549 cells (Figure 7A), or of the *scnn1a*, *scnn1b*, or *scnn1g* genes in primary mouse alveolar type II (ATII) cells (Figure 7B).

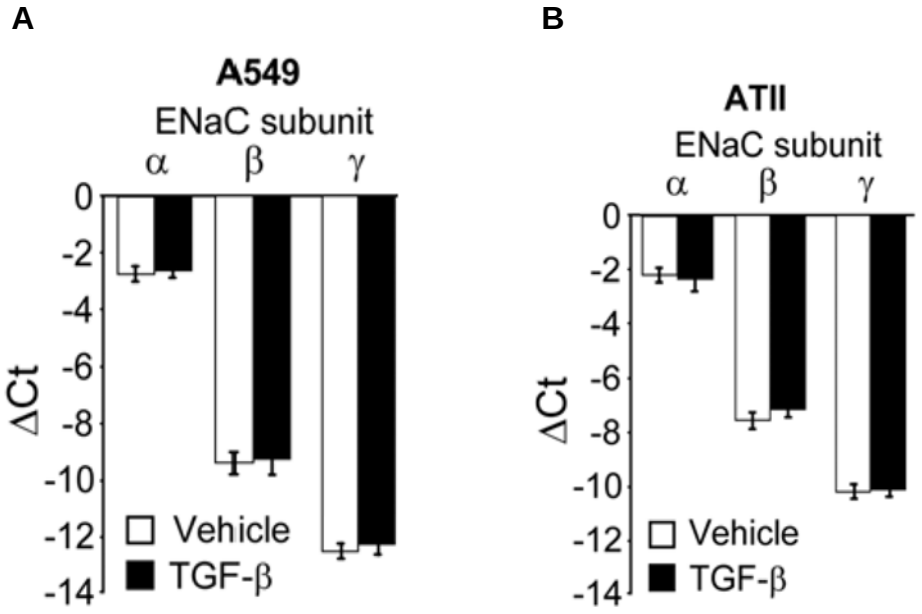

Figure 7. TGF-β does not acutely influence gene expression of ENaC in lung epithelial cells.

Levels of mRNA transcripts encoding αENaC (*scnn1a*), βENaC (*scnn1b*) and γENaC (*scnn1g*) assessed by real-time RT-PCR in A549 (**A**) and mouse alveolar type II (ATII) cells (**B**) after TGF-β (10 ng/ml) exposure ($n = 3$, per group). *, $P < 0.05$.

4.4 TGF-β drives endocytosis of human ENaC in lung epithelial cells

Since the effect of TGF-β appeared to be independent of gene expression, the surface abundance of ENaC subunits was assessed. Given the very low surface

expression levels of ENaC complexes on primary ATII cells and lung epithelial cell lines, human (A549) and mouse (MLE-12) cells were transfected with human and mouse epitope-tagged ENaC subunits, respectively, to study the effects of TGF-β on ENaC surface abundance (Figure 8).

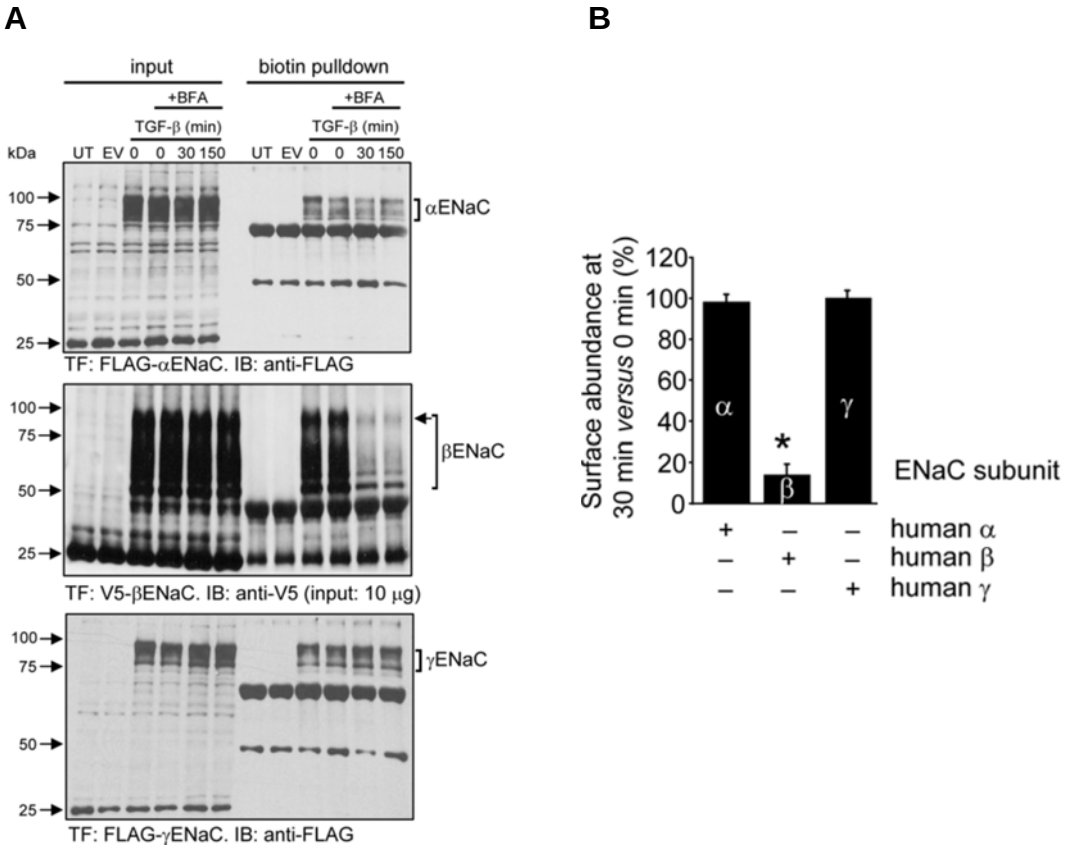

Figure 8. TGF-β drives endocytosis of human ENaC in lung epithelial cells.

(**A**) A549 cells expressing FLAG-tagged human αENaC or γENaC or V5-tagged human βENaC. Total cellular levels are evident in input lanes, while cell surface abundance was assessed by cell surface biotinylation, pull-down, and immunoblot (IB) on the same membrane. Cells were pretreated (or not) with brefeldin A (BFA; 10 μg/ml), and were untransfected (UT), transfected with empty vector (EV), or transfected (TF) with constructs expressing the epitope-tagged ENaC subunits. (**B**) Data from multiple experiments were quantified by densitometric analysis of immunoblot bands. Data represent mean ± S.D. (n = 3-8, per group). *, $P < 0.05$.

In these studies, cells were pretreated with brefeldin A (BFA), to prevent retrograde trafficking of ENaC to the cell surface after endocytosis (86). Several cross-reacting bands were evident when A549 cell extracts were probed with anti-FLAG or anti-V5 antibodies. These cross-reacting bands conveniently served

as loading controls (see untransfected (UT) and empty vector-transfected (EV) lanes). The A549 cells transfected with plasmids expressing FLAG-tagged human αENaC or γENaC demonstrated a typical multi-band smear for the cell surface ENaC fraction (Figure 8A), due to proteolytic processing of these ENaC subunits at the cell surface (87). The application of TGF-β (10 ng/ml) for 30 min or 150 min had no effect on cell surface abundance of either subunit (Figure 8A, quantified in Figure 8B). For V5-tagged human βENaC, gels loaded with 10 μg input also revealed a multi-band smear for βENaC. Treatment of transfected A549 cells with TGF-β caused a rapid (within 30 min) and dramatic (>80%) reduction in the cell surface abundance of V5-tagged human βENaC (Figure 8A, quantified in Figure 8B).

4.5 TGF-β drives endocytosis of mouse ENaC in lung epithelial cells

A similar study as for human βENaC was performed for mouse βENaC, where TGF-β caused a rapid loss of surface abundance of V5-tagged mouse βENaC transfected into mouse MLE-12 cells (Figure 9).

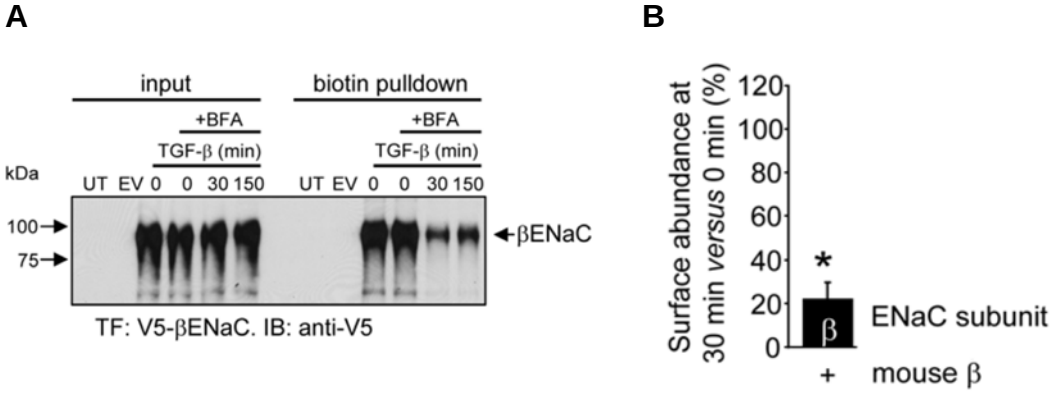

Figure 9. TGF-β drives endocytosis of mouse ENaC in lung epithelial cells.

(**A**) Mouse lung epithelial MLE-12 cells were transfected (TF) with V5-tagged mouse βENaC, and the effect of TGF-β on cell surface abundance of V5-tagged βENaC assessed by cell surface biotinylation, pull-down, and immunoblot (IB) on the same membrane. Cells were pretreated (or not) with brefeldin A (BFA; 10 μg/ml), and were untransfected (UT), transfected with empty vector (EV), or transfected (TF) with constructs expressing the V5-tagged βENaC subunit. (**B**) Data from multiple experiments were quantified by densitometric analysis of immunoblot bands. Data represent mean ± S.D. (n = 3-8, per group). *, $P < 0.05$.

Thus, the ability of TGF-β to promote loss of βENaC from the lung epithelial cell surface was conserved between mouse and human. When all three epitope-tagged ENaC subunits were expressed together, TGF-β treatment was able to reduce the surface abundance of the βENaC subunit, as well as the FLAG-tagged αENaC and γENaC subunits (Figure 10A, quantified in Figure 10B). Taken together, these data demonstrate that TGF-β can rapidly promote loss of ENaC complexes from the surface of lung epithelial cells.

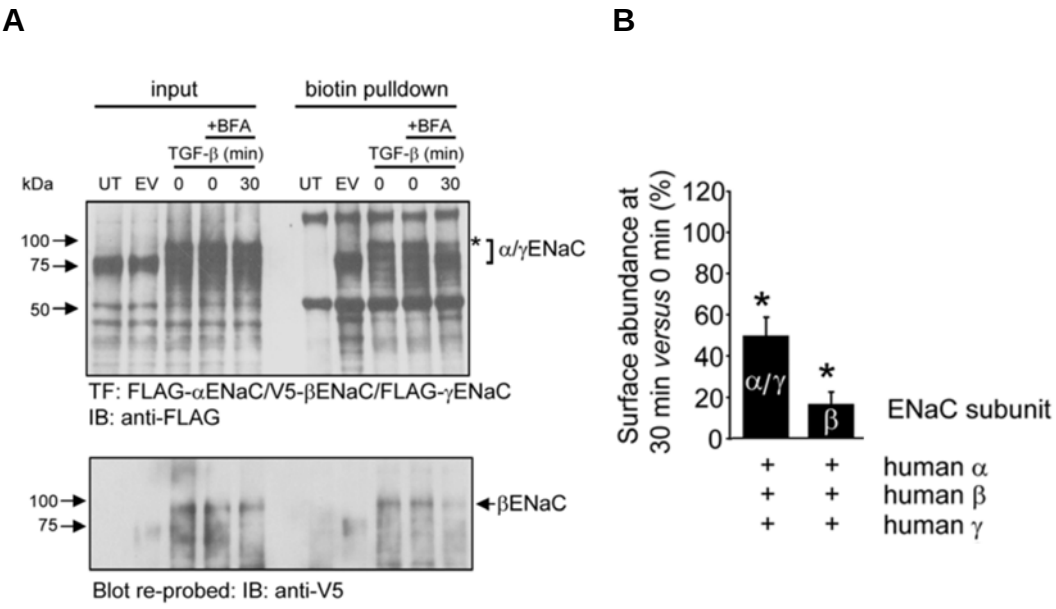

Figure 10. The βENaC subunit is the target for the TGF-β-induced withdrawal of ENaC complexes from the cell surface.

(**A**) A549 cells were transfected with all three tagged ENaC subunits simultaneously, and the effects of TGF-β on surface abundance of FLAG-tagged αENaC and γENaC assessed. Total cellular levels are evident in input lanes, while cell surface abundance was assessed by cell surface biotinylation, pull-down, and immunoblot (IB) on the same membrane. Cells were pretreated (or not) with brefeldin A (BFA; 10 μg/ml), and were untransfected (UT), transfected with empty vector (EV), or transfected (TF) with constructs expressing the epitope-tagged ENaC subunits. Given similar molecular masses, it was not possible to differentiate between αENaC and γENaC, however, a clear reduction in the intensity of the band marked by an asterisk (*) is evident. The same immunoblot was reprobed with an anti-V5 antibody to reveal surface abundance of the βENaC. (**B**) Data from multiple experiments were quantified by densitometric analysis of immunoblot bands. Data represent mean ± S.D. (n = 3-8, per group). *, $P < 0.05$.

4.6 An intact TGF-β/Tgfbr1/Smad2/3 axis is required for TGF-β-induced effects on ENaC cell surface abundance

Transforming growth factor-β may signal through a variety of receptors and second messengers, therefore, a combination of pharmacological inhibitors and genetic approaches was employed to delineate the proximal signaling pathway underlying the effects of TGF-β on ENaC cell surface abundance. Application of SB431542 (10 μM), an inhibitor of TGF-β signaling via the type I TGF-β receptor Tgfbr1 blocked the ability of TGF-β to reduce cell surface abundance of βENaC (Figure 11A, quantified in Figure 11C).

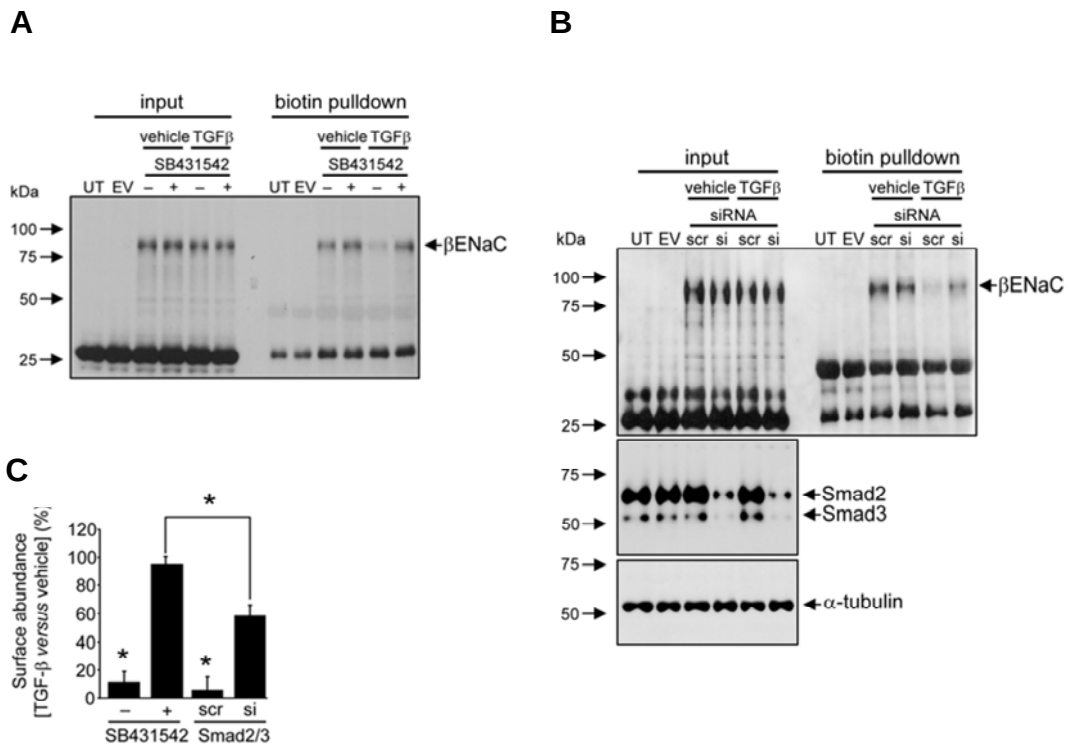

Figure 11. TGF-β drives ENaC endocytosis in a Tgfbr1/Smad2/3-dependent pathway.
Effects of (**A**) the TGF-β receptor (Tgfbr)1 inhibitor SB431542 (10 μM) and (**B**) Smad2/3 knockdown by small interfering (si)RNA, on the endocytosis of V5-tagged βENaC by A549 cells stimulated by TGF-β (10 ng/ml). Scrambled (scr) siRNA sequences served as tranfection controls (**C**). Data from multiple experiments were quantified by densitometry (n = 3, per group). Data represent mean ± S.D. *, $P < 0.05$; UT, untransfected; EV, empty vector-transfected.

Simultaneous genetic ablation of Smad2 and Smad3 by small interfering (si)RNA also blocked the ability of TGF-β to reduce cell surface abundance of βENaC (Figure 11B, quantified in Figure 11C). Together, these data indicate that TGF-β signaling was mediated by Tgfbr1 and Smad2/3.

4.7 Actin mobility is required for TGF-β-induced effects on ENaC cell surface abundance

Phalloidin oleate (PO), a cell membrane-permeable inhibitor of F→G actin conversion (1 μM) blocked the ability of TGF-β to reduce cell surface abundance of βENaC (Figure 12). These data indicate that ENaC was endocytosed in an actin-dependent manner in response to TGF-β stimulation.

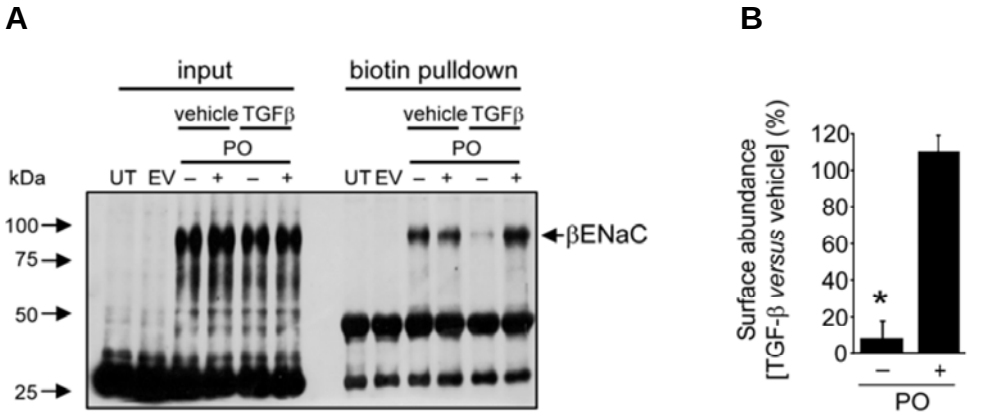

Figure 12. Actin mobility is required for TGF-β-induced effects on ENaC cell surface abundance.

(**A**) The effect of phalloidin oleate (PO), an endocytic inhibitor, on the endocytosis of V5-tagged βENaC by A549 cells stimulated by TGF-β (10 ng/ml). (**B**) Data from multiple experiments were quantified by densitometry (n = 3, per group). Data represent mean ± S.D. *, $P < 0.05$; UT, untransfected; EV, empty vector-transfected.

4.8 TGF-β is the active principle in the lung fluids of ARDS patients that promotes loss of ENaC from the lung epithelial cell surface

When BAL fluids from ARDS patients were applied to A549 cells transfected with V5-tagged human βENaC, a rapid (within 30 min) loss of βENaC from the

cell surface was observed, in comparison with transfected cells treated with BAL fluids from control patients (Figure 13A). This effect of BAL fluids from ARDS patients could be abrogated when BAL fluids were preincubated with a pan-TGF-β1,2,3 nAB (Figure 13B and D) or when transfected A549 cells were pretreated with SB431542 (Figure 13C and D). These data indicate that TGF-β is the active principle in BAL fluid from ARDS patients that can induce endocytosis of βENaC.

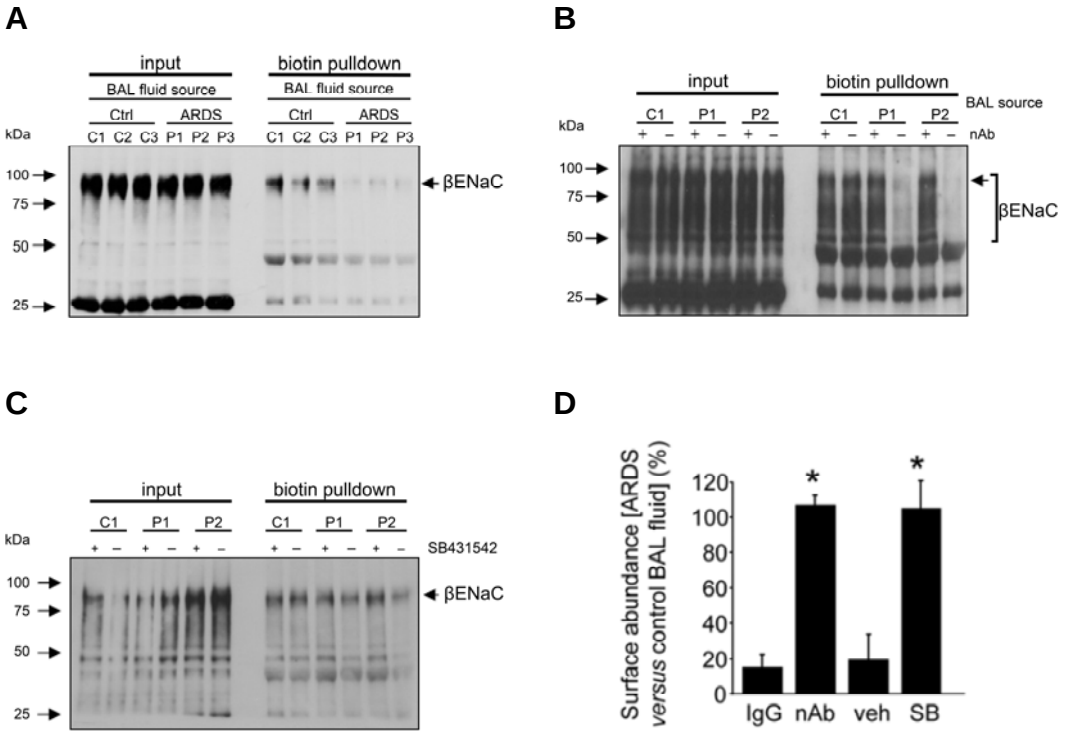

Figure 13. TGF-β is the active principle in the lung fluids of ARDS patients that promotes loss of ENaC from the lung epithelial cell surface.

(**A**) Effects of BAL fluid from three control patients (designated C1, C2, and C3) and three ARDS patients (designated P1, P2, and P3) on βENaC endocytosis in A549 cells. (**B**) Ability of a TGF-β1,2,3 neutralizing antibody (nAb) to block BAL fluid-induced βENaC endocytosis in A549 cells [in control lanes (-), the nAb (10 μg/ml) was replaced by a non-specific IgG (IgG)], and (**C**) the ability of SB431542 to block BAL fluid-induced βENaC endocytosis by A549 cells. In control lanes (-), the SB431542 was replaced by vehicle alone [0.1% (v/v) dimethyl sulfoxide]. (**D**) Data from multiple experiments were quantified by densitometry (n = 3, per group). Data represent mean ± S.D. *, $P < 0.05$. veh, vehicle; UT, untransfected; EV, empty vector-transfected.

4.9 TGF-β effects on ENaC cell surface stability are dependent upon PLD1

Efforts were then made to identify more distal parts of the TGF-β pathway that promoted ENaC endocytosis. An initial broad screen of candidate signaling molecules ruled out several key cell signaling pathways. The following inhibitors did not inhibit TGF-β-stimulated endocytosis of βENaC in a biotin pull-down assay: The phospholipase A2 inhibitor, *N*-(*p*-amylcinnamoyl)anthranilic acid (25 μM) (Figure 14A); the Ca^{2+}-chelator, BAPTA-AM (25 mM) (Figure 14B); the protein kinase C inhibitor, bisindolylmaleimide I (1 and 10 μM) (Figure 14C and 14D); the Ca^{2+}/calmodulin-dependent protein kinase kinase inhibitor, STO-609 (20 μg/ml) (Figure 14E); the phosphoinositide-3-kinase inhibitor, wortmannin (100 nM) (Figure 14F); the phospholipase A inhibitor, isotetrandrine (1 μg/ml) (Figure 14G); and c-jun N-terminal kinase inhibitor II (50 μM) (Figure 14H). In contrast, preincubation of A549 cells with 0.1% (v) *n*-butanol blocked the ability of TGF-β (10 ng/ml) to stimulate V5-tagged βENaC endocytosis, thus implicating PLD (Figure 15A). In the presence of *n*-butanol PLD converts phosphatidylcholine by transphosphorylation into phosphatidylbutanol (PBut) rather than into phosphatidic acid (PA), a natural reaction product of PLD activity, and therefore it is commonly used as an antagonist of PLD-induced PA generation. In contrast, *t*-butanol [also at 0.1 % (v/v)], which is not a substrate for transphosphatidylation by PLD, was employed as a control, and did not impact the effects of TGF-β (Figure 15A).

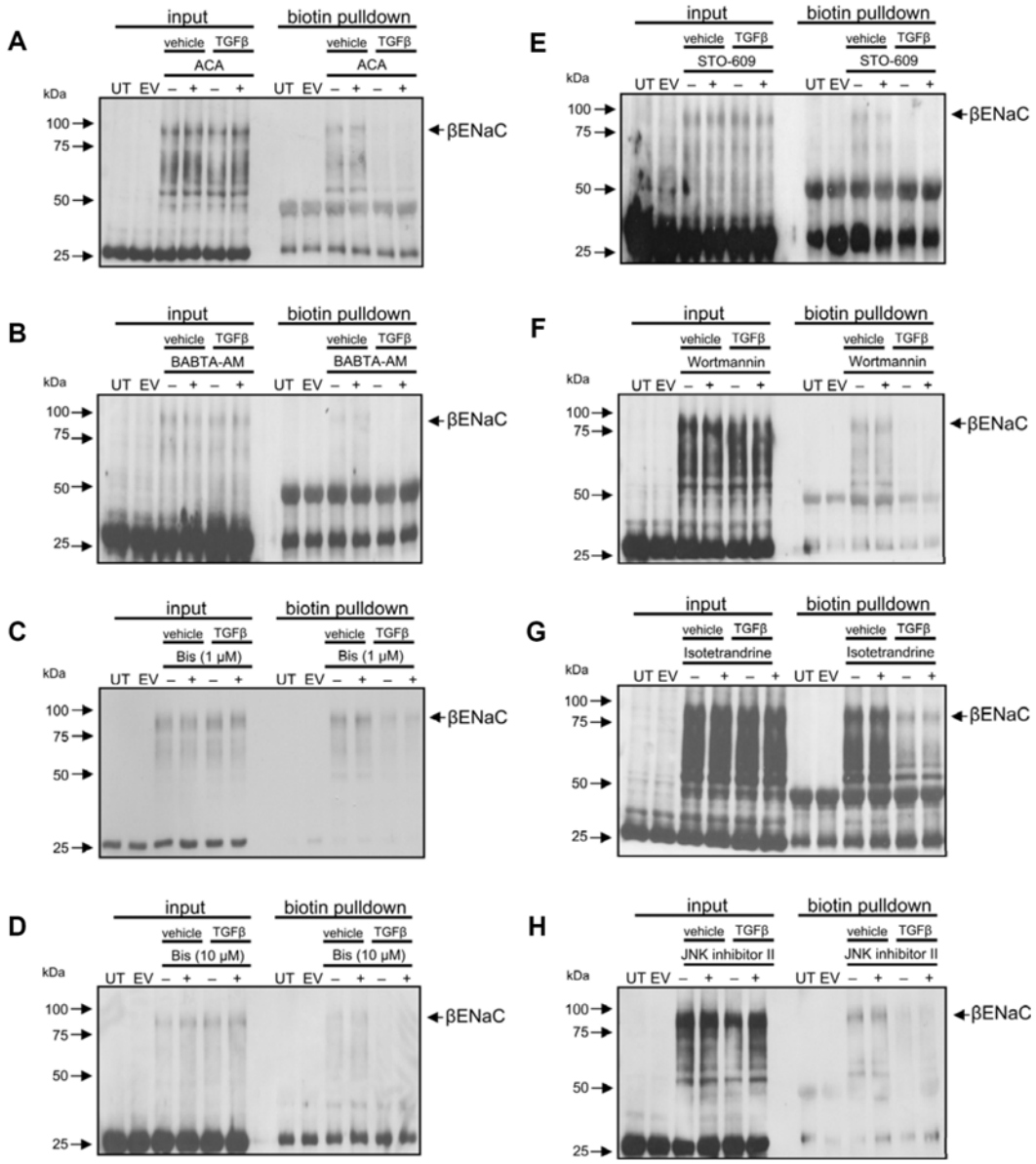

Figure 14. Screening pathway inhibitors for impact on TGF-β-induced ENaC endocytosis.

The A549 cells expressing V5-tagged human βENaC were treated with a spectrum of signaling pathway inhibitors prior to treatment with TGF-β (TGFβ; 10 ng/ml): (**A**) the phospholipase A2 inhibitor, *N*-(*p*-amylcinnamoyl)anthranilic acid (ACA) (25 μM), (**B**) the membrane-permeable intracellular Ca^{2+}-chelator BAPTA-AM (25 mM), (**C**) the protein kinase C inhibitor, bisindolylmaleimide I (BIS) (1 μM), (**D**) the protein kinase C inhibitor, bisindolylmaleimide I (10 μM), (**E**) the Ca^{2+}/calmodulin-dependent protein kinase kinase inhibitor, STO-609 (20 μg/ml), (**F**) the phosphoinositide-3-kinase inhibitor, wortmannin (100 nM), (**G**) the phospholipase A inhibitor, isotetrandrine (1 μg/ml), and (**H**) the c-jun N-terminal kinase (JNK) inhibitor II (50 μM). Total cellular levels are evident in input lanes, while cell surface abundance was assessed by cell surface biotinylation, pull-down, and immunoblot on the same membrane. Cells were pretreated with brefeldin A (10 μg/ml), and were untransfected (UT), transfected with empty vector (EV), or transfected with a construct expressing V5-tagged human βENaC.

TGF-β (10 ng/ml) stimulated the production of PA by A549 cells (Figure 15B), further supporting a role for PLD. The measurements of the production of PA were conducted by a group from the University of Essen, not by the author, and are included to facilitate the flow of arguments.

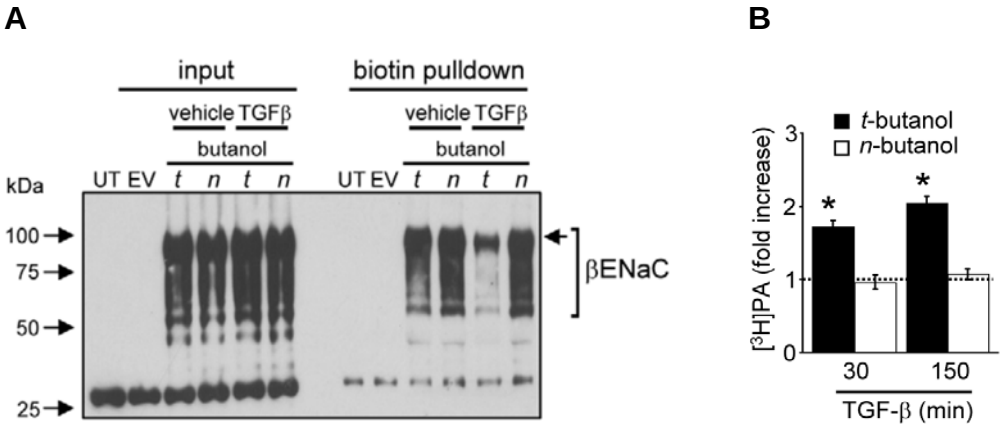

Figure 15. TGF-β activation of phospholipase D1 is required for βENaC endocytosis.
(**A**) The impact of *n*-butanol [*n*; 0.1 % (v/v); a PLD inhibitor] or *t*-butanol [*t*; 0.1 % (v/v); which is not a substrate for transphosphatidylation, and was employed as a control] on βENaC endocytosis by A549 cells in response to TGF-β (10 ng/ml) was assessed by biotin pull-down. An arrow indicates the primary βENaC band, while a bracket indicates the βENaC smear. (**B**) The production of [^{3}H]phosphatidic acid (PA) was assessed in A549 cells after stimulation with TGF-β (10 ng/ml) (n = 3, per group) after pretreatment of A549 cells with *n*- or *t*-butanol [0.1 % (v/v)]. Data in panel (**B**) were generated by a group from the University of Essen, not by the author, and were included to facilitate the flow of arguments. Data represent mean ± S.D. *, $P < 0.05$; UT, untransfected; EV, empty vector-transfected.

Also, genetic ablation of PLD1 by siRNA knockdown blocked the ability of TGF-β to stimulate βENaC endocytosis (Figure 16).

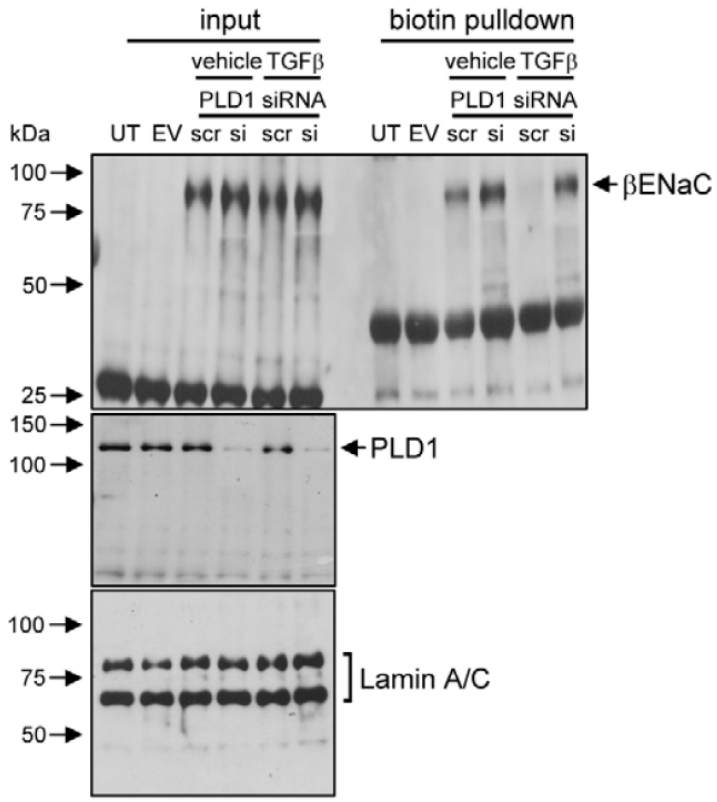

Figure 16. TGF-β activation of phospholipase D1 is required for βENaC endocytosis.
The impact of *PLD1* gene ablation by small interfering (si)RNA knockdown on βENaC endocytosis by A549 cells in response to TGF-β was assessed by biotin pull-down. A scrambled (scr) siRNA sequence served as a transfection control; UT, untransfected; EV, empty vector-transfected.

In further support of a role for PLD1, expression of a dominant-negative PLD1 variant in A549 cells markedly reduced the ability of TGF-β to drive βENaC endocytosis (Figure 17).

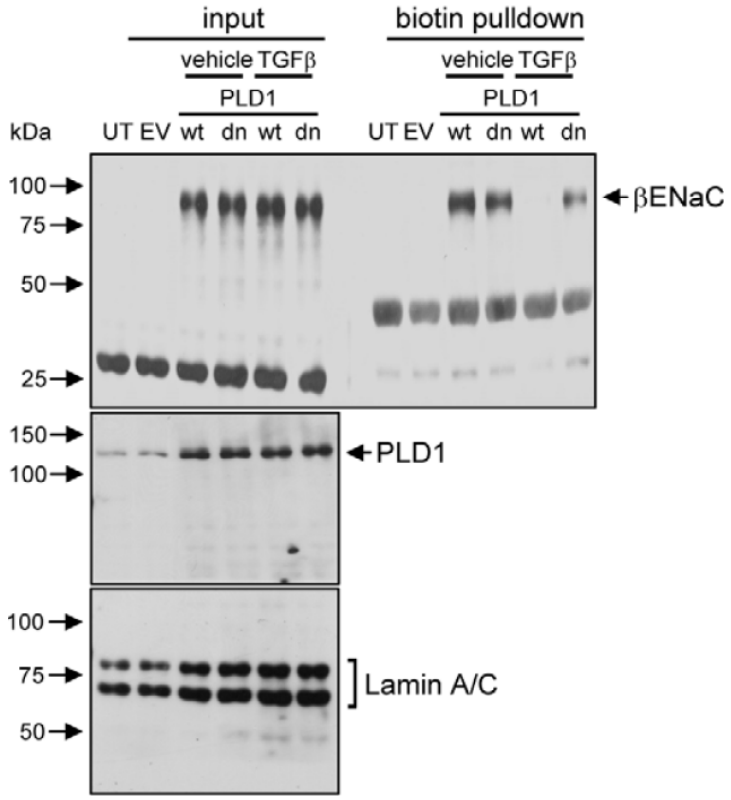

Figure 17. TGF-β activation of phospholipase D1 is required for βENaC endocytosis.
The impact of overexpression of wild-type (wt) or a dominant-negative (dn) variant of PLD1 on βENaC endocytosis by A549 cells in response to TGF-β was assessed by biotin pull-down; UT, untransfected; EV, empty vector-transfected.

Stimulation of untransfected A549 cells with TGF-β (10 ng/ml) drove production of phosphatidylbutanol (PBut), which is diagnostic for PLD activity (Figure 18). Genetic ablation of Smad2/3 blocked TGF-β-induced PBut formation placing PLD activity downstream of Tgfbr1-induced Smad2/3 phosphorylation in this pathway (Figure 18). These experiments were conducted by a group from the University of Essen, not by the author, and are included to facilitate the flow of arguments. These data thus implicate PLD1 in the signaling cascade that connects TGF-β signaling with βENaC endocytosis in lung epithelial cells.

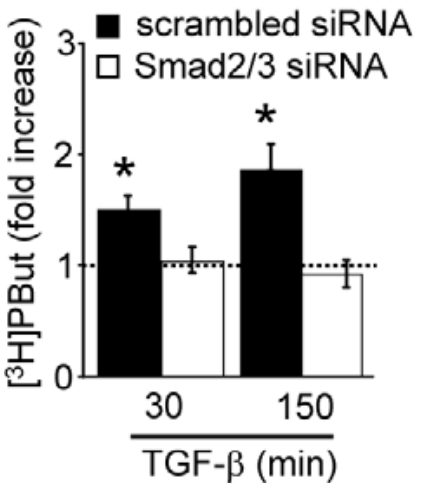

Figure 18. TGF-β drives production of phosphatidylbutanol (PBut).

The production of [^{3}H]Phosphatidylbutanol (PBut) was assessed in A549 cells after stimulation with TGF-β (10 ng/ml) (n = 3, per group) after pretreatment of A549 cells with scrambled siRNA or siRNA targeting Smad2/3. Data represent mean ± S.D. *, $P < 0.05$. These data were generated by a group from the University of Essen, not by the author, and are included to facilitate the flow of arguments.

4.10 TGF-β effects on ENaC cell surface stability are dependent upon phosphatidylinositol-4-phosphate 5-kinase 1α

The PA generated by PLD1 is an important regulator of phosphoinositide signaling (88), being a key regulator of phosphatidylinositol-4-phosphate 5-kinase 1α (PIP5K1α) which generates phosphatidylinositol (4,5)-bisphosphate [PtdIns(4,5)P_2], a phosphoinositide that has been implicated in the positive (89) and negative (90) regulation of ENaC activity. No specific inhibitor of PIP5K1α exists, therefore, a gene ablation approach using siRNA was employed. Knockdown of PIP5K1α expression in A549 cells abrogated the effects of TGF-β, preventing TGF-β-induced endocytosis of βENaC (Figure 19A). However, knockdown of PIP5K1α expression did not impact the ability of TGF-β to drive PA production (Figure 19B), indicating that the role of of PIP5K1α in the TGF-β/βENaC endocytosis pathway was downstream of PLD1.

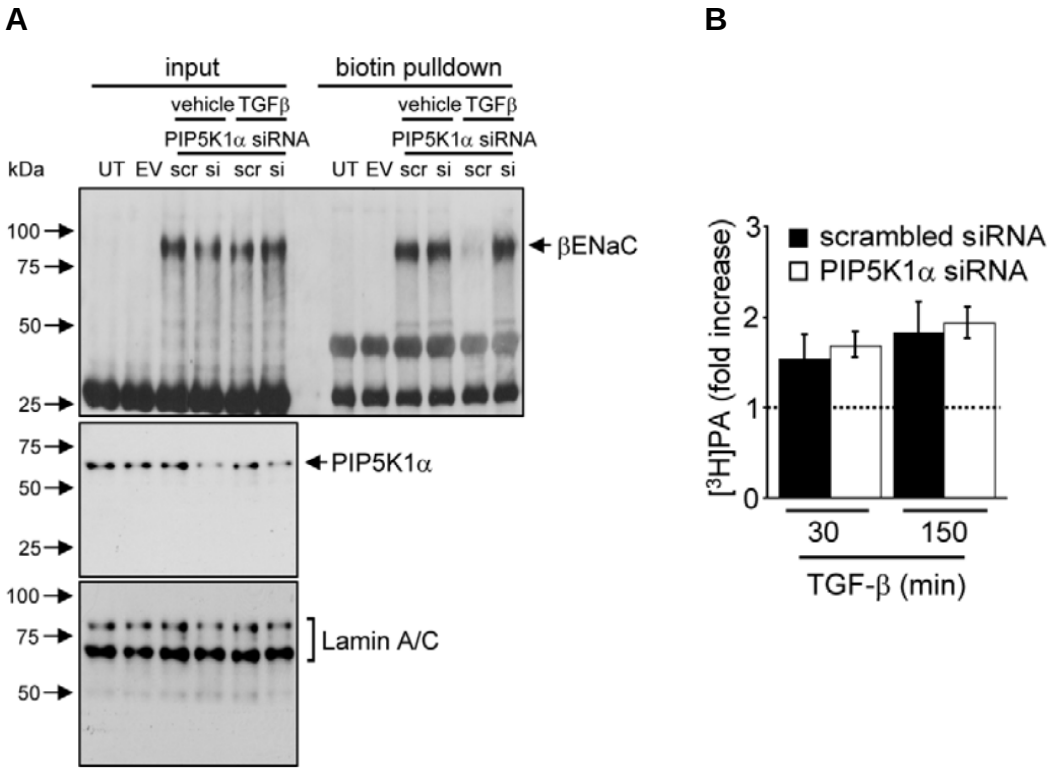

Figure 19. TGF-β activation of phosphatidylinositol-4-phosphate 5-kinase 1α is required for βENaC endocytosis.

(**A**) The impact of *PIP5K1A* gene ablation by small interfering (si)RNA knockdown on βENaC endocytosis by A549 cells in response to TGF-β (10 ng/ml) was assessed by biotin pull-down. Scrambled (scr) siRNA sequences served as a transfection controls. (**B**) The impact of *PIP5K1A* gene ablation by small interfering (si)RNA knockdown on the production of [^{3}H]phosphatidic acid (PA) by A549 cells stimulated by TGF-β. Data represent mean ± S.D. *, $P < 0.05$. UT, untransfected; EV, empty vector-transfected.

The siRNA knockdown data were confirmed by expression of a dominant-negative of PIP5K1α in A549 cells, which also prevented βENaC endocytosis in response to TGF-β stimulation of A549 cells (Figure 20).

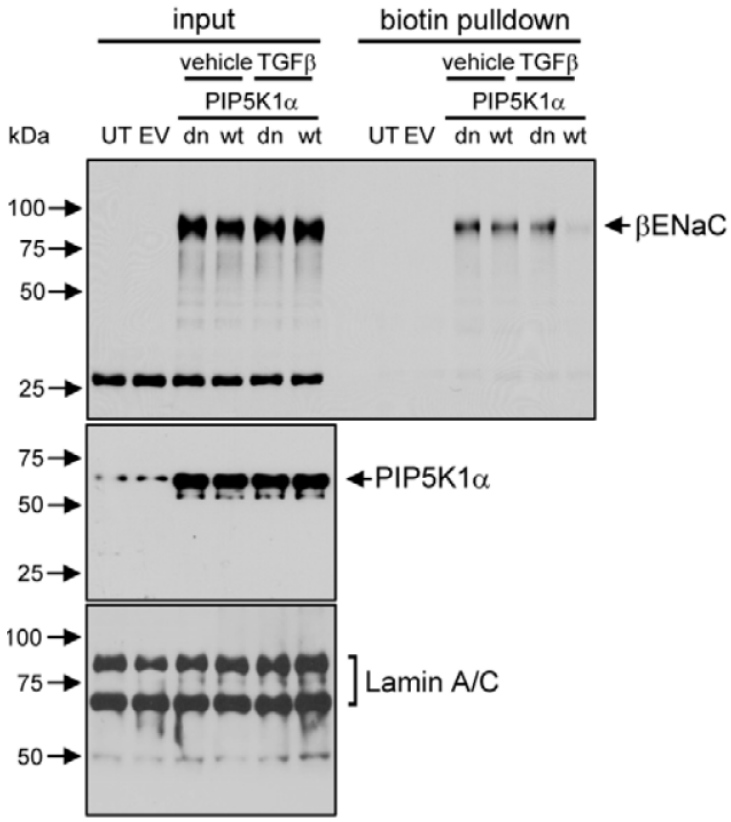

Figure 20. TGF-β activation of phosphatidylinositol-4-phosphate 5-kinase 1α is required for βENaC endocytosis.

The impact of overexpression of wild-type (wt) or a dominant-negative (dn) variant of *PIP5K1A* on βENaC endocytosis by A549 cells in response to TGF-β was assessed by biotin pull-down. UT, untransfected; EV, empty vector-transfected.

4.11 TGF-β effects on ENaC plasma membrane stability are dependent upon reactive oxygen species

The role of reactive oxygen species (ROS) as well as reactive nitrogen derivatives in the modulation of AFC (91), and ENaC activity in particular (92), has been widely explored. During a preliminary pathway screen, two cell-permeable and non-specific quenchers of ROS, EUK-134 (Figure 21A) and polyethylene glycol (PEG)-complexed superoxide dismutase (SOD; Figure 21B) blocked the ability of TGF-β to drive βENaC endocytosis.

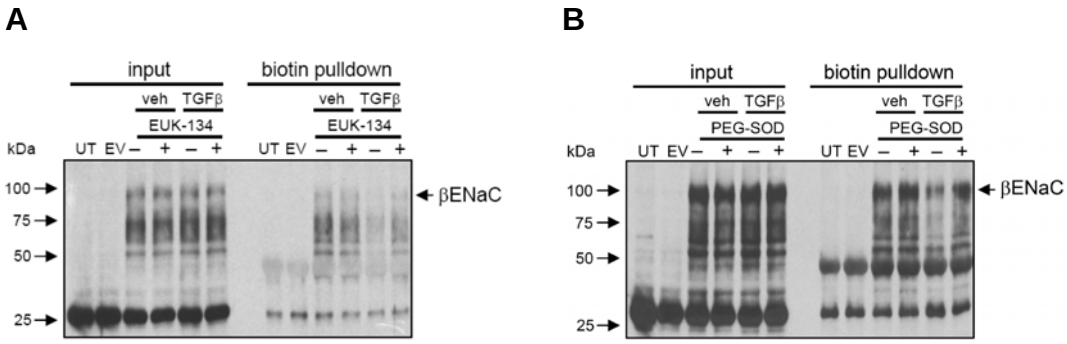

Figure 21. Effects of reactive oxygen species (ROS) scavengers on TGF-β-driven βENaC endocytosis by A549 cells.

Effects of the ROS scavengers EUK-134 (**A**) and polyethylene glycol (PEG)-complexed superoxide dismutase (SOD) (**B**) on TGF-β-driven βENaC endocytosis by A549 cells. veh, vehicle; TGFβ, TGF-β; UT, untransfected; EV, empty vector-transfected.

In contrast, L-NAME (100 mM; an inhibitor of NO generation by nitric oxide synthases) was without effect (Figure 22).

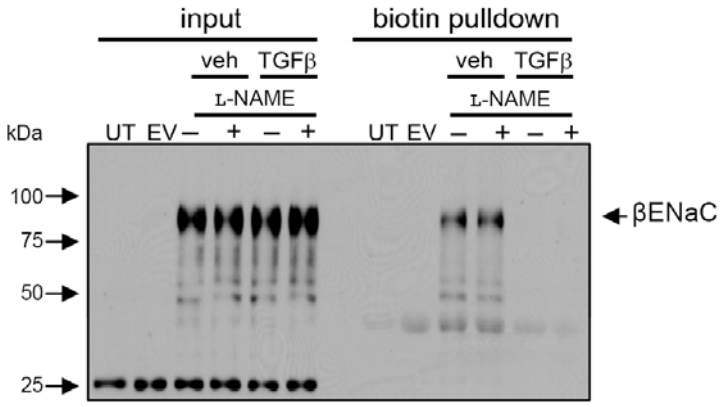

Figure 22. Effect of nitric oxide synthase inhibition on TGF-β-induced ENaC endocytosis.

The A549 cells expressing V5-tagged human βENaC were treated with L-NAME (100mM) prior to treatement with TGF-β (TGFβ; 10 ng/ml). Total cellular levels of V5-ENaC are evident in input lanes, while surface-abundance was assessed by cell surface biotinylation, pull-down and immunoblot on the same membrane. Cells were pretreated with brefeldin A (10 μg/ml) and were untransfected (UT), transfected with empty vector (EV), or transfected with a construct expressing V5-tagged human βENaC.

Using a fluorescence-based assay for ROS production, based on the measurement of H_2O_2, it was demonstrated that TGF-β could drive ROS production in A549 cells (Figure 23A). This effect was blocked by pretreatment of A549 cells with

SB431542, and by knockdown of Smad2 and Smad3 expression (Figure 23B), implicating the Tbfbr1/Smad2/3 axis in TGF-β-induced ROS production.

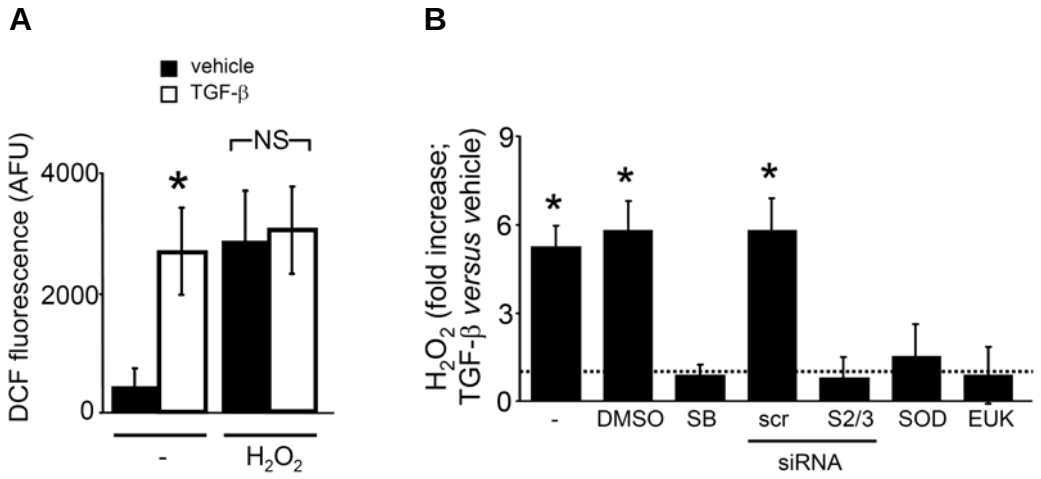

Figure 23. TGF-β drives reactive oxygen species (ROS) production in A549 cells.

(**A**) illustrates the arbitrary fluorescence units (AFU) obtained with untreated or TGF-β-treated naïve cells, without (-) or with addition of 100 μM H_2O_2 as a positive control. (**B**) TGF-β pathway inhibitors and ROS scavengers were assessed for effects on TGF-β-induced ROS production (measured as H_2O_2 production) by A549 cells, which were untreated (-), or treated with dimethylsulfoxide [DMSO; 0.1% (v/v)]; SB431542 (SB; 10 μM); scrambled small interfering (si)RNA (scr), siRNA targeting Smad2 and Smad3 (S2/3); PEG-complexed SOD (SOD; 150 U/ml); or EUK-134 (EUK; 20 μM). (n = 3, per group). Data represent mean ± S.D. *, $P < 0.05$.

None of the inhibitors of complexes I-III of the mitochondrial electron transport chain could block TGF-β-induced ROS production, including 3-nitroproprionic acid (complex II), thenoyltrifluoroacetone (complex II), antimycin A (complex III), and rotenone (complex I) (Figure 24). However, NaN_3, an inhibitor of complex IV and NADPH oxidases, was able to do so (Figure 24), suggesting a role for either complex IV or NADPH oxidases in TGF-β-induced ROS production by A549 cells.

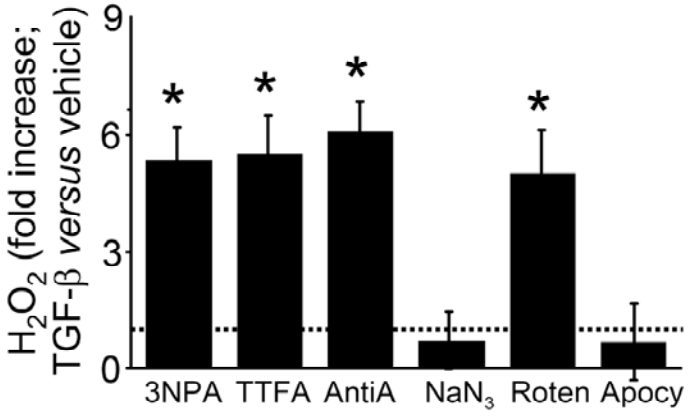

Figure 24. TGF-β-induced ROS is dependent on either complex IV of the respiratory chain or NAPDH oxidases.

Inhibitors of the electron transport chain and NADPH oxidases were assessed for effects on TGF-β-induced ROS production by A549 cells: 3-nitroproprionic acid (3NPA; 5 mM), thenoyltrifluoroacetone (TTFA; 10 μM), antimycin A (AntiA; 3 μg/ml), rotenone (Roten; 100 μM), NaN_3 (1 mM), and apocynin (100 μM; Apocy) (n = 5, per group). Data represent mean ± S.D. *, $P < 0.05$.

4.12 TGF-β effects on ENaC plasma membrane stability are dependent upon reactive oxygen species generated by NOX4

Sodium azide, an inhibitor of complex IV and NADPH (nicotinamide adenine dinucleotide phosphate) oxidases, was able to block TGF-β-induced ROS production (Figure 24), suggesting a role for either complex IV or NADPH oxidases in TGF-β-induced ROS production by A549 cells. To test this idea further, A549 cells were pretreated with apocynin, an inhibitor of NADPH oxidases, which also blocked both the ability of TGF-β to drive ROS production in A549 cells (Figure 24), and the ability of TGF-β to promote βENaC endocytosis (Figure 25). These data confirmed a role for NADPH oxidases in the TGF-β/βENaC endocytosis pathway.

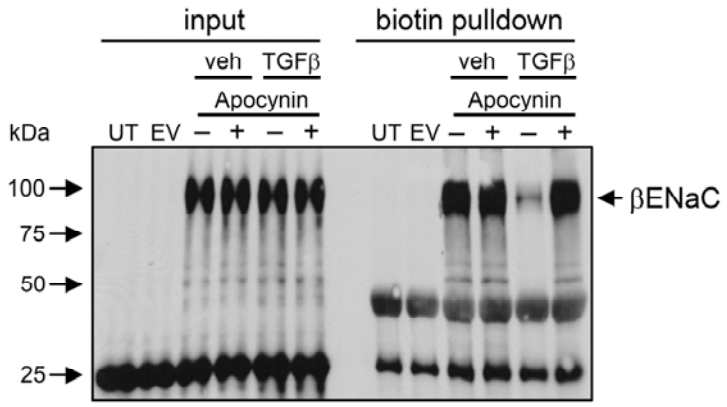

Figure 25. TGF-β effects on ENaC plasma membrane stability are dependent upon reactive oxygen species generated by NADPH oxidases.

The effect of apocynin, an inhibitor of NADPH oxidases (300 μM) on TGF-β-driven βENaC endocytosis by A549 cells. veh, vehicle; UT; untransfected; EV, empty vector-transfected.

Genetic ablation of NOX (NADPH oxidase) 4 by siRNA both completely blocked TGF-β-stimulated ROS production in A549 cells (Figure 26A), and prevented the TGF-β-induced endocytosis of βENaC by A549 cells (Figure 27). These data confirm NOX4 as the source of TGF-β-induced ROS in A549 cells.

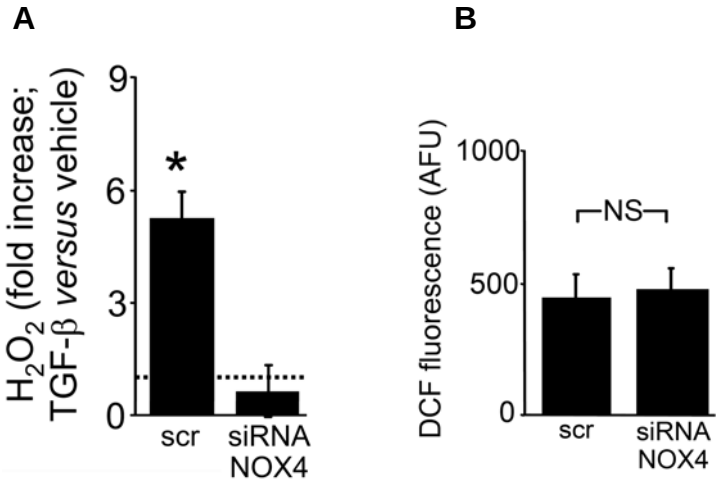

Figure 26. The effects of genetic ablation of *NOX4* on TGF-β-induced ROS production by A549 cells.

(**A**)The impact of *NOX4* gene ablation by small interfering (si)RNA knockdown on βENaC endocytosis by A549 cells in response to TGF-β (n = 3, per group). (**B**) The effect of *NOX4* knockdown on baseline ROS levels (n = 3, per group). Data represent mean ± S.D. *, $P < 0.05$.

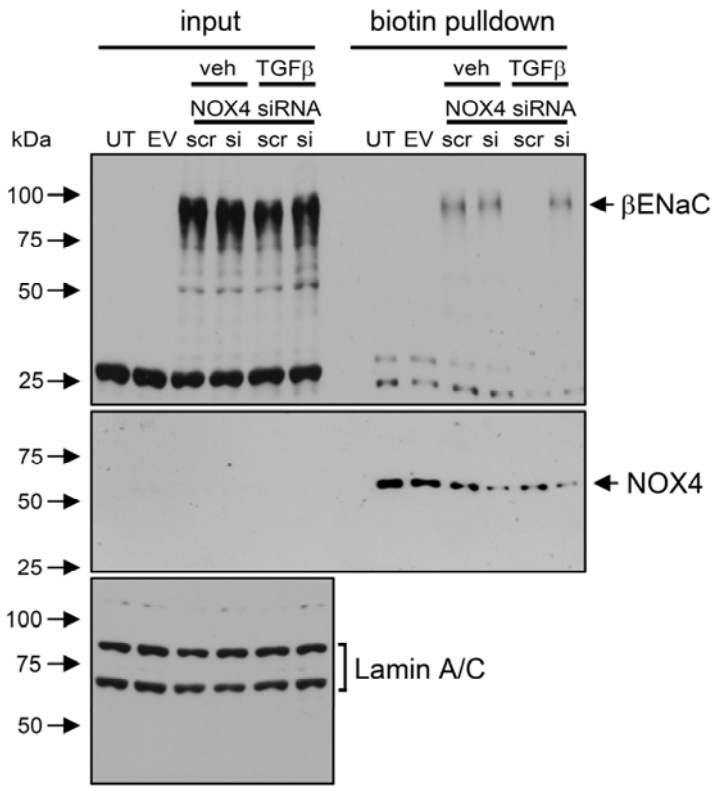

Figure 27. TGF-β effects on ENaC plasma membrane stability are dependent upon reactive oxygen species generated by NOX4.

The impact of *NOX4* gene ablation by small interfering (si)RNA knockdown on βENaC endocytosis by A549 cells in response to TGF-β. A scrambled (scr) siRNA sequence served as a transfection control. veh, vehicle; UT; untransfected; EV, empty vector-transfected.

Genetic ablation of both PLD1 and PIP5K1α in A549 cells prevented TGF-β-stimulated ROS production, suggesting that NOX4-generated ROS in the TGF-β/βENaC endocytosis pathway was downstream of both PLD1 and PIP5K1α (Figure 28).

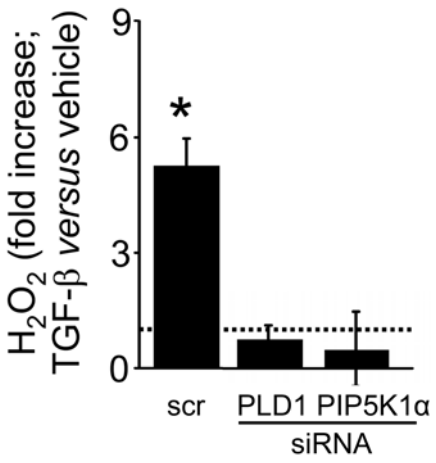

Figure 28. The effects of genetic ablation of *PLD1* and *PIP5K1A* on TGF-β-induced ROS production by A549 cells.

Scrambled small-interfering (si)RNA (scr), siRNA targeting phospholipase D1 (PLD1) and phosphatidylinositol-4-phosphate 5-kinase 1α (PIP5K1α; n = 3, per group). Data represent mean ± S.D. *, $P < 0.05$.

4.13 TGF-β signaling targets Cys^{43} of βENaC in human and mouse cells

Hydrogen peroxide is emerging as an important second messenger in intracellular signaling. Although H_2O_2 is a relatively mild oxidant, its signaling activity has been attributed to chemoselective oxidation of cysteine residues (93, 94). Therefore, all cysteine residues in the cytosolic domains of βENaC (being the region proximal to the M1 transmembrane domain, and the region distal to the M2 transmembrane domain; (Figure 29) were converted by site-directed mutagenesis of the human *SCNN1B* and mouse *scnn1b* genes, to serine or alanine residues. A schematic illustration of the cytosolic domains of human and mouse βENaC is depicted in figure 29.

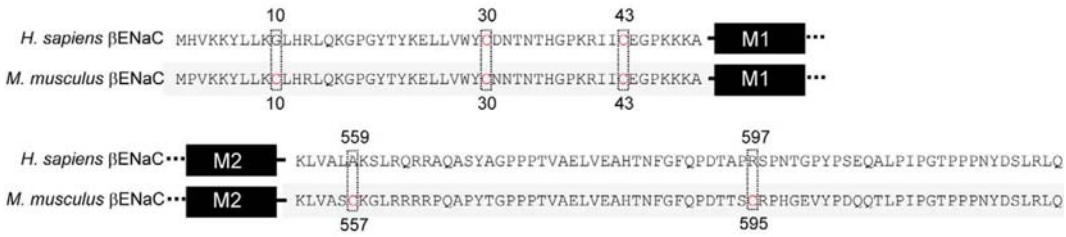

Figure 29. TGF-β signaling targets Cys[43] of βENaC in human and mouse cells.

Schematic illustration of the cytosolic domains of human and mouse βENaC. The amino acid sequences of the regions proximal to the first transmembrane (M1) domain and distal to the second transmembrane domain (M2) are illustrated. All cysteine residues are indicated.

Conversion of Cys[10], Cys[30], Cys[557] and Cys[595] mouse βENaC to a serine residue had no effect on the ability of TGF-β to promote V5-tagged mouse βENaC endocytosis by MLE-12 cells (Figure 30). However, conversion of Cys[43] to a serine residue completely blocked the ability of TGF-β to promote V5-tagged mouse βENaC endocytosis by MLE-12 cells (Figure 30).

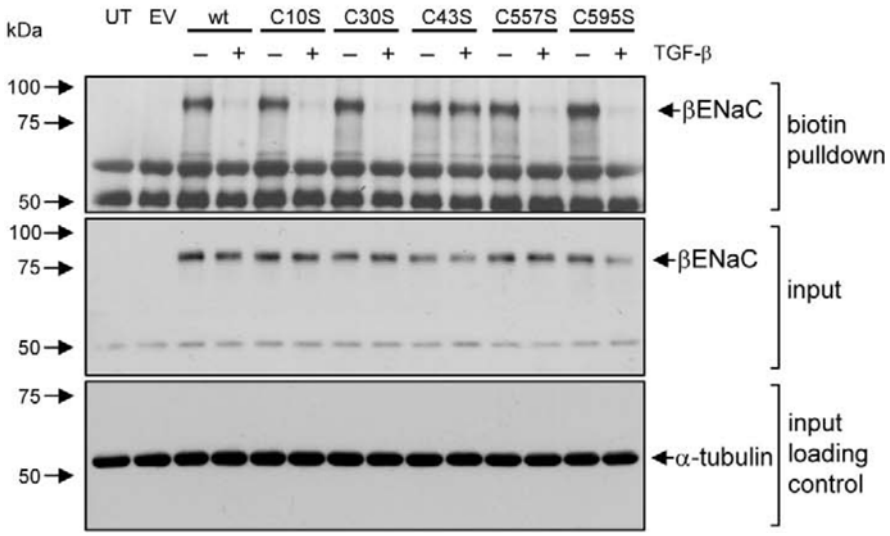

Figure 30. The impact of cysteine residue replacements on mouse βENaC endocytosis by MLE-12 cells in response to TGF-β.

The impact of cysteine residue replacements on mouse βENaC endocytosis by MLE-12 cells in response to TGF-β (10 ng/ml; 30 min) was assessed by biotin pull-down. As the biotin pull-down and input fractions were resolved on separate gels, an α-tubulin input loading control was also prepared. UT, untransfected; EV, empty vector-transfected.

Identical trends were observed when using human βENaC, where conversion of Cys^{43} to a serine residue (Figure 31A) also completely blocked the ability of TGF-β to promote V5-tagged human βENaC endocytosis by A549 cells, while conversion of Cys^{30} to a serine residue was without any effect (Figure 31B).

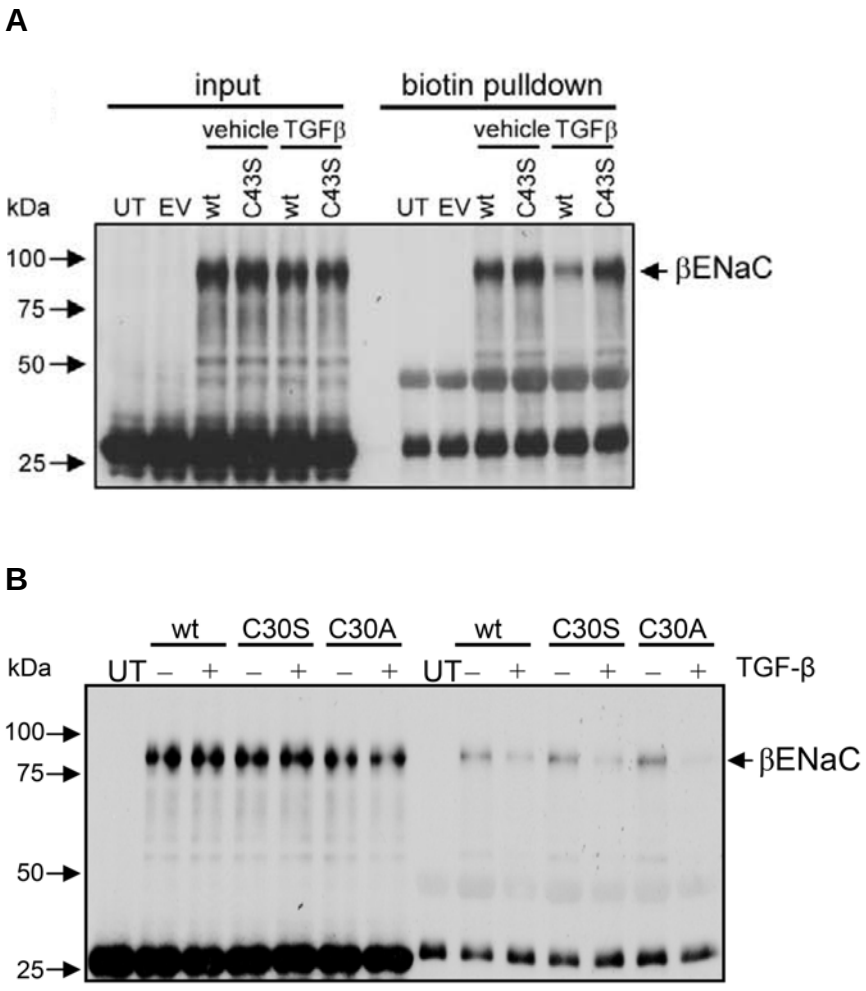

Figure 31. The impact of Cys^{43} and Cys^{30} replacement on human βENaC endocytosis by A549 cells in response to TGF-β.

(**A**) The impact of Cys^{43} replacement with serine on human βENaC endocytosis by A549 cells in response to TGF-β (30 min) was assessed by biotin pull-down. (**B**) The impact of Cys^{30} replacement with alanine or serine on human βENaC endocytosis by A549 cells in response to TGF-β (30 min) was assessed by biotin pull-down. wt, wild-type; UT, untransfected; EV, empty vector-transfected.

Interestingly, Cys^{30} and Cys^{43} are the only two intracellular cysteine residues in human βENaC, and their positions are exactly conserved comparing mouse and

human ENaC. Thus, the conserved Cys^{43} appears to represent a direct or indirect target of TGF-β-induced ROS, generated by NOX4.

The preceding data, therefore, establish the sequence of this novel TGF-β signaling pathway as

TGF-β→Tgfbr1→Smad2/3→PLD1→PIP5K1α→NOX4→ROS→βENaC(Cys^{43}).

5 Discussion

The data presented here demonstrate that TGF-β plays a key role in the acute regulation of ENaC activity, and hence, can impact alveolar ion and fluid transport. These observations are relevant to pathological conditions characterized by a failure of fluid reabsorption, with such a condition being exemplified by alveolar edema in patients with ALI/ARDS. Transforming growth factor-β has already been implicated as an important mediator of ALI, however, to date, all proposed roles for TGF-β in ARDS have been ascribed to long-term effects dependent upon gene regulation. For example, TGF-β is activated locally by integrin $\alpha_v\beta_6$ (95), which, in the case of mechanical ventilation, acts in cooperation with PAR-1 (96), to increase epithelial and endothelial permeability, and promote alveolar flooding. The mechanisms underlying this effect are unclear, but have been attributed to the depletion of reduced glutathione, and increased oxidized glutathione which results from downregulation of γ-glutamylcysteine synthetase gene expression by TGF-β. Similarly, TGF-β (10 ng/ml) downregulated *SCNN1A* (encoding αENaC) gene expression in alveolar epithelial cells, which would also impair transepithelial alveolar ion and fluid transport (97), which was consistent with the observation made in that study that 24 h after intratracheal instillation of TGF-β into live rats (250 ng/rat), a reduction in distal airspace fluid clearance was observed (97).

In addition to local integrin-mediated activation, other studies have demonstrated that TGF-β may be activated and released from the lung extracellular matrix by proteases such as elastase (98), leading to elevated active TGF-β levels in BAL fluids of patients with ARDS. The authors of two reports have demonstrated increased abundance of both TGF-β mRNA and protein in lung tissue from ARDS patients (54) and increased active TGF-β1 levels (7-14 ng/ml ELF) in BAL fluids from patients with ARDS (54, 78). Notably, lower BAL fluid TGF-β levels in ARDS patients were correlated with more ventilator-free and ICU-free days (78), correlating TGF-β levels with the severity of ARDS. This concentration of TGF-β is approximately double that of circulating TGF-β levels in the plasma of healthy subjects [4.1 ± 2.0 ng/ml normal human plasma (99)], although it was substantially lower than TGF-β levels in the pleural fluid during thoracic

empyema [40 ng/ml (100)]. Irrespective of whether TGF-β is locally activated at the epithelial cell surface, or whether increased free, active TGF-β levels are generated in the lung, as long as TGF-β can access Tgfbr1, the same downstream pathway, described in this study, is likely to be activated, culminating in impaired alveolar ion and fluid transport.

In the present study, it was shown that when TGF-β was applied to isolated, ventilated, and perfused rabbit lungs, a rapid and pronounced block in alveolar fluid reabsorption was evident. Subsequent investigations revealed that active Na^+ transport out of the alveolar airspaces was impaired, leading to perturbed AFC. This suggested that the sodium transport machinery was most likely targeted by TGF-β, the two leading candidates being the Na,K-ATPase and ENaC, which together drive transepithelial alveolar sodium transport (15, 101). Further investigations using the ENaC inhibitor amiloride in the isolated, ventilated and perfused rabbit lung suggested that amiloride-sensitive sodium channels such as ENaC were the target of TGF-β.

The activity of ENaC may be regulated chronically (at the gene transcription level), and defects in ENaC gene regulation have been associated with disease. For example, transcription of the *SCNN1G* gene (encoding γENaC) is impaired by tumor necrosis factor-α in Crohn's disease, a chronic inflammatory bowel disease (102), leading to impaired sodium transport across the colon epithelium (103). Directly related to this study, TGF-β can downregulate the *SCNN1A* gene (encoding αENaC) in alveolar epithelial cells, after a 96-h exposure to 10 ng/ml TGF-β (97). In this study, however, TGF-β did not impact mRNA levels of genes encoding the α β, and γ ENaC subunits over the short (30 min-2 h) experimental time-course, ruling out gene regulatory effects.

The primary mechanisms regulating ENaC activity are acute, allowing the cell to rapidly respond to fast-changing needs in sodium absorption. These mechanisms target channel open probablity (P_o), or membrane trafficking, which alters channel cell surface abundance (104). Phosphoinositides can bind βENaC and γENaC, rapidly increasing ENaC P_o, and hence, channel activity (105). Additionally, both membrane-bound serine peptidases (87, 106) and laminar shear stress can activate ENaC by increasing P_o (107). Membrane trafficking also represents a means of acute regulation of ENaC activity (108), since only a small fraction of ENaC

channels reside on the plasma membrane, the rest being located in sub-apical compartments that are rapidly delivered to the plasma membrane by the appropriate stimulus, to increase ENaC cell surface abundance, and drive sodium absorption (104). The activity of ENaC is negatively regulated by endocytosis of channel complexes into clathrin-coated pits (108), but the pathways directing ENaC endocytosis are unclear (108). To date, ubiquitination mediated by the E3 ubiquitin ligase NEDD4-2 represents a convergence point for the regulation of ENaC surface density by several pathways, including the aldosterone/serum and glucocorticoid kinase pathway, the extracellular regulated kinase pathway, and the vasopressin/cAMP pathway (108). In the present study, using transfected human and mouse lung epithelial cell lines expressing epitope-tagged ENaC subunits, the β subunit of ENaC was identified as a target for TGF-β-driven endocytosis. Appropriately, the β subunit of ENaC is the regulatory subunit responsible for stabilizing ENaC complexes in the plasma membrane (101). This represents a hitherto undescribed ENaC regulatory pathway that relies on ENaC trafficking.

Disturbances to ENaC trafficking which lead to abnormal cell surface stability of the αβγENaC complex cause severe disease, an example being Liddle's Syndrome, characterized by severe hypertension, hypokalemia, and hypoaldosteronism. In affected patients, mutations in the *SCNN1B* and *SCNN1G* genes generate βENaC and γENaC variants which are truncated at the C-terminus (109), leading to loss of a critical PY (proline/tyrosine) domain that serves as a docking motif for NEDD4-2 (110). In the absence of NEDD4-2 docking, the βENaC and γENaC Liddle variants are not ubiquitinated (110), and hence, are not endocytosed, leading to increased cell surface stability and thus, hyperabsorption of sodium in the renal tubule.

In the present study, a new ENaC trafficking defect is described, where TGF-β promotes excessive endocytosis of βENaC, leading to a pronounced reduction in αβγENaC complexes at the lung epithelial cell surface, and hence, reduced sodium and fluid reabsorption. Importantly, BAL fluids from healthy volunteers did not drive ENaC endocytosis, while BAL fluids from ARDS patients did. Thus, BAL fluids from ARDS patients contain a factor which drove ENaC endocytosis in alveolar epithelial cells. The acute respiratory distress syndrome is characterized by protein-rich edema fluid in lungs of affected patients. Therefore,

BAL fluids from ARDS patients contain a multitude of growth factors, cytokines and other molecules, which could contribute to disease pathogenesis. In this study, using neutralizing antibodies or a TGF-β signaling pathway inhibitor (SB431542), TGF-β was identified as being the factor in ARDS patient BAL fluids that was exclusively responsible for driving ENaC endocytosis by alveolar epithelial cells. This observation makes a strong case for a role for TGF-β in the impaired alveolar fluid reabsorption observed in ARDS patients, thereby contributing to the rapid onset and dangerous persistence of alveolar edema in these patients. In the longer term, these effects would be exacerbated by the chronic effects of TGF-β on the transcriptional regulation of ion transporting machinery described by other investigators (95, 97, 111). Seven steps of an entirely novel TGF-β signaling pathway (Figure 32) that underlie this ENaC trafficking defect are being clarified in the present study. Unique for TGF-β signaling – which generally affects gene regulation – this pathway drives a rapid (within 30 min) and dramatic (>80%) reduction in the cell surface abundance of ENaC on lung epithelial cells. This new signaling pathway is activated by TGF-β acting through Tgfbr1, a type I TGF-β receptor. Activation of Tgfbr1 (acting in concert with Tgfbr2) will drive Smad2 and Smad3 phosphorylation. This represents the proximal arm of the classical TGF-β signaling pathway, which normally proceeds by driving complex formation between phosphoSmad2/3 and Smad4, and translocation of the Smad2/3/4 complex into the nucleus, where Smad complexes bind to target promoters and then recruit additional coactivators or corepressors, which regulate the expression of a multitude of TGF-β-responsive genes. This novel pathway diverges from the classical gene regulatory pathway at the point of Smad2/3 phosphorylation, which within minutes activated PLD1, a phospholipid phosphohydrolase which catalyzes the hydrolysis of phosphatidylcholine and other membrane phospholipids to PA and choline. PA may also be generated intracellularly by the phosphorylation of 1,2-diacylgylcerol by diacylglycerol kinase (88), however, since siRNA-mediated knockdown of PLD1 completely blocked the ability of TGF-β to drive ENaC endocytosis in A549 cells, a role for diacylglycerol kinase was not considered further.

The PA generated by PLD1 is an important regulator of phosphoinositide signaling (88), given the ability of PA to activate PIP5K1α (112). This suggested

that PIP5K1α might play a part in the TGF-β/βENaC endocytic pathway. Indeed, siRNA knockdown or overexpression of a dominant-negative PIP5K1α blocked the ability of TGF-β to drive βENaC endocytosis, confirming a key role for PIP5K1α in this pathway. This study highlights a role for PIP5K1α-derived phosphoinositides in ENaC regulation by TGF-β, contributing to a growing and complex discussion about how phosphoinositides regulate ENaC activity (105). PIP5K1α generates PtdIns(4,5)P_2, a phosphoinositide that has been implicated in both positive (89) and negative (90) regulation of ENaC. PtdIns(4,5)P_2 increased ENaC P_o in excised inside-out patches (113), and resting levels of PtdIns(4,5)P_2 set basal ENaC activity (114), suggesting PtdIns(4,5)P_2 as a positive regulator of ENaC. However, PIP5K1α also decreases the cell surface abundance of ENaC in cortical collecting duct cells (90), in a pathway believed to rely on PtdIns(4,5)P_2-mediated recruitment of epsin to the plasma membrane, which drives the formation of clathrin-coated vesicles. In this study, a new role for phosphoinositides in acute, negative regulation of ENaC activity that is related to ROS production has been identified. How PIP5K1α-generated PtdIns(4,5)P_2 both negatively and positively regulate ENaC remains a matter of discussion. It is proposed that the precise subcellular location of PtdIns(4,5)P_2 generation (and breakdown) defines phosphoinositide effects on ENaC.

Data presented here indicate that siRNA knockdown of PIP5K1α prevented ROS formation in response to TGF-β stimulation of A549 cells. Thus, PIP5K1α was located upstream of the ROS-producing oxidase. A combination of inhibitor and gene ablation studies revealed that oxidase to be NADPH oxidase 4 (NOX4) [reviewed in (115)], and it is speculated here that PtdIns(4,5)P_2 generated by PIP5K1α activated NOX4 (Figure 32). The possibility of a bridging molecule between PIP5K1α and NOX4 has also not been ruled out. Knockdown of NOX4 did not impact baseline (unstimulated) ROS levels, thus, a knock-on effect of reduced baseline ROS levels on the expression of ROS-sensitive NADPH oxidases and associated subunits such as NOX1, NOX2, and $p22^{phox}$ (116), was ruled out. The activation of NADPH oxidases (although not NOX4) by PIP5K1α enzymatic products is not without precedent, since PtdIns(4,5)P_2 can regulate the subcellular distribution and ROS production of NOX5 (117). The proper cellular localization of NADPH oxidases is critical for NADPH oxidase function (115),

therefore, PtdIns(4,5)P_2 might directly activate NOX4, or might recruit or position NOX4 to drive βENaC endocytosis. Interestingly, TGF-β is known to upregulate gene expression of NOX4 in lung vascular smooth muscle cells (118). However, the rapid effect of TGF-β on ENaC endocytosis reported here precludes a role for NOX4 gene expression. Thus, this is the first report of the ability of TGF-β to activate NOX4, and drive ROS production by NOX4, in the absence of transcriptional regulation of the NOX4 gene. These data add to a growing body of evidence which highlights NOX4 as an important player in a diverse range of lung pathologies, including pulmonary arterial hypertension (119) and fibrotic lung disease (120).

The findings presented here which document the acute negative regulation of ENaC activity by ROS are interesting considering that neutralization of ROS in animal models of ARDS, for example, by application of the membrane-permeable aminothiol N-acetylcysteine in an acute pancreatitis rat model (121), or application of the ROS quencher EUK-8 in a porcine LPS model (122), both attenuated alveolar edema. It is tempting to speculate that that might have been due, in part, to neutralization of NOX4-generated ROS which would drive ENaC endocytosis.

Both ROS, RNS and H_2O_2 are emerging as important second messengers in intracellular signaling, particularly in the context of ENaC regulation (123), where both ROS and NO regulate channel activity (123). It is demonstrated here that NOS-generated NO did not impact TGF-β induced endocytosis of βENaC, in contrast to NOX4-generated ROS (measured as H_2O_2), which mediated this process. Although H_2O_2 is a relatively mild oxidant, its signaling activity has been attributed to chemoselective oxidation of cysteine residues (124). Therefore, all cysteine residues in the cytosolic domains of βENaC (being the region proximal to the M1 transmembrane domain, and the region distal to the M2 transmembrane domain; Figure 29) were converted by site-directed mutagenesis of the human *SCNN1B* and mouse *scnn1b* genes, to serine residues. A critical role for a conserved cysteine residue, Cys^{43}, in both mouse and human ENaC was demonstrated using this approach. This suggests that the TGF-β/ENaC endocytic pathway is a conserved means of ENaC regulation across many species [Cys^{43} is

also conserved in rabbits (GenBank™ accession number NP001076197) and dogs (GenBank™ accession number XP534912), for example].

The βENaC Cys^{43} residue might be oxidized by NOX4-generated ROS, which in itself could serve as a trigger for βENaC endocytosis. The Cys^{43} residue appears to be an excellent candidate as a target for reaction with ROS, RNS or H_2O_2 due to the adjacent acidic residue (Glu), which confers special reactivity conducive to oxidative modification (124). Interestingly, of all cysteine residues, only Cys^{43} was conserved between human and mouse βENaC in that an adjacent acidic residue was present (Figure 29). Alternatively, NOX4-generated ROS might target an intermediate signaling molecule which recognizes Cys^{43} in βENaC and promotes βENaC endocytosis. These questions form the basis of projects that will be built on these studies. This pathway is schematically illustrated in Figure 32, in the background of what is already known about TGF-β and AFC.

In summary, an entirely novel TGF-β signaling pathway is described here, which acutely regulates the activity of ENaC in the alveolar epithelium. Elucidation of this pathway is particularly exciting, since TGF-β is generally accredited with long-term (chronic) effects that rely on changes to gene expression. This regulatory pathway appears to be conserved across several species, including mouse, rabbit and humans, and may also represent a normal ENaC regulatory mechanism in healthy tissues. Given the pathological roles played by TGF-β in conditions associated with a failure of fluid reabsorption, such as the persistence of pulmonary edema in ARDS, this pathway represents a candidate pathomechanism at play in affected lungs. This possibility is underscored by the demonstration here that TGF-β in lung fluids from patients with ARDS was able to drive ENaC endocytosis in alveolar epithelial cells. Delineation of this signaling pathway revealed several candidate enzyme systems which might be targeted in an attempt to normalize AFC in affected patients, including targeting phosphoinositide metabolism and ROS. Additionally, this pathway may also be operative under physiological and pathological conditions in other organs where ENaC plays an important role, including the collecting tubules of the kidney, and the colon.

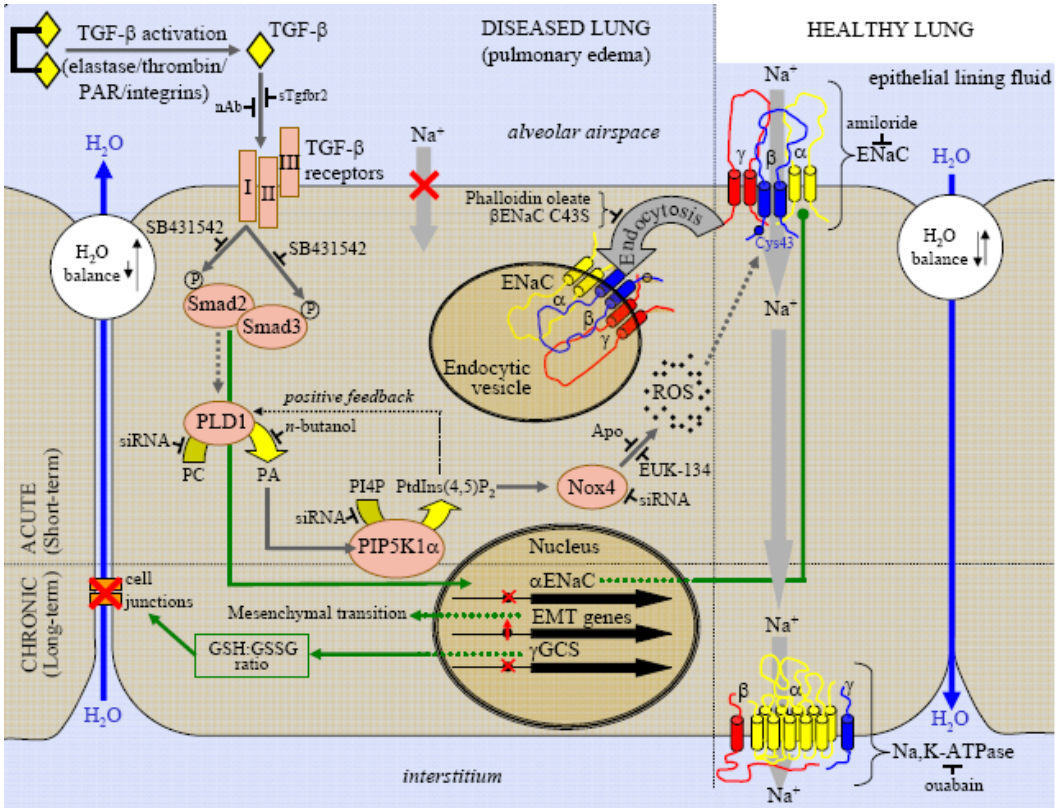

Figure 32. Schematic illustration of the TGF-β/ENaC pathway described in this study.

In healthy lungs, latent TGF-β is inactive, and the Na,K-ATPase and epithelial sodium channel (ENaC) drive Na^+ absorption by epithelial cells, maintaining fluid influx and reabsorption in equilibrium, and epithelial lining fluid volume at an appropriate level. Activation of latent TGF-β by elastase (98), integrin-dependent (1) or protease-activated receptor (PAR)-dependent mechanisms (125) in acute lung injury has been described. TGF-β is implicated in chronic (gene regulatory) effects (green arrows), including loss of cell-cell junctions (1), downregulation of *SCNN1A* (encoding αENaC) (53), and epithelial-to-mesenchymal transition (EMT) (126), leading to barrier failure. Application of a TGF-β neutralizing antibody (nAb) or a soluble type II receptor (sTgfbr2) dampened the deleterious effects of TGF-β (1). In this report, an acute effect of TGF-β on alveolar fluid reabsorption is described. In the novel signaling pathway delineated (dark gray arrows), TGF-β, acting through the type I TGF-β receptor, induces Smad2/3 phosphorylation, which in turn activates phospholipase D1 (PLD1). The PLD1 generates phosphatidic acid (PA) from phosphatidylcholine (PC). PA is an activator of phosphatidylinositol-4-phosphate 5-kinase 1α (PIP5K1α), which drives NOX4 activation, perhaps by phosphatidylinositol (4,5)-bisphosphate [PtdIns(4,5)P_2] formation from phosphatidylinositol 4′-monophosphate (PI4P). Activated NOX4 generates reactive oxygen species (ROS) which either directly or indirectly promote βENaC endocytosis in a manner dependent on Cys^{43}. This leads to loss of Na^+-absorbing capacity of the epithelial cell and alveolar flooding, promoting the formation or persistence of alveolar edema. The targets of reagents employed in this study are also illustrated.

6 Summary

TGF-β is a pathogenic factor in patients with acute respiratory distress syndrome (ARDS), a devastating condition characterized by alveolar edema. In the present study, a novel TGF-β signaling pathway is described, which rapidly and dramatically promotes endocytosis of the epithelial sodium channel (ENaC) from the surface of alveolar epithelial cells. Elevated TGF-β levels were demonstrated in bronchoalveolar lavage fluids from ARDS patients, where TGF-β was identified as the principle in lung fluid of ARDS patients that promoted ENaC endocytosis. Administration of TGF-β to the alveolar airspaces of isolated rabbit lungs caused pronounced fluid retention and impaired sodium transport. The same effect could be observed in the presence of amiloride, an inhibitor of the epithelial sodium channel, and was abrogated after treatment with SB431542, an inhibitor of TGF-β signaling via the type I TGF-β receptor, suggesting ENaC as the target of TGF-β. Moreover, preapplication of PO abrogated the effects of TGF-β on net lung mass, indicating a role for F→G actin conversion in mediating the effect of TGF-β on lung fluid dynamics.

TGF-β rapidly activated phospholipase D1, which activated phosphatidylinositol-4-phosphate 5-kinase 1α, which drove NADPH oxidase 4 activation, generating reactive oxygen species which promoted βENaC endocytosis in a manner dependent on Cys^{43} of βENaC. This led to loss of sodium-absorbing capacity of the epithelial cells, and alveolar flooding, promoting the formation or persistence of alveolar edema. These data describe a novel TGF-β-dependent mechanism that regulates ion and fluid transport in the lung that is relevant to pathological mechanisms at play in ARDS patients.

7 Zusammenfassung

TGF-β ist ein pathogener Faktor in Patienten mit einem akuten respiratorischen Syndrom (ARDS). Das akute respiratorische Syndrom ist eine schwerwiegende Erkrankung, welche durch ein alveoläres Ödem gekennzeichnet ist. In der vorliegenden Studie wird ein neuer TGF-β Signaltransduktionsweg beschrieben, der schnell und gravierend eine Endozytose des epithelialen Natriumkanals (ENaC) von der Oberfläche von alveolären Epithelzellen verursacht. In bronchiolo-alveolärer Lavage-Flüssigkeit von ARDS Patienten wurden erhöhte TGF-β-Konzentrationen gemessen, wobei TGF-β als der Faktor, der für die Endozytose von ENaC verantwortlich ist, identifiziert wurde. Vernebelung von TGF-β in die Alveolen von isolierten Kaninchenlungen führte zu einem ausgeprägten Aufstau von Flüssigkeit und vermindertem Natriumtransport in den Lungen. Derselbe Effekt wurde in der Gegenwart von Amilorid, einem ENaC Inhibitoren, beobachtet, und war aufgehoben, wenn vorher SB431542, ein TGF-β-Signaltransduktionsweg-Inhibitor, gegeben wurde. Daraus ließ sich schließen, dass TGF-β ENaC beeinflusst. Des Weiteren konnte durch Verabreichung von Phalloidin Oleat der durch TGF-β ausgelöste Effekt auf den Flüssigkeitstransport in der Lunge verhindert werden, was darauf hindeutet, dass die Umwandlung von F- zu G-Aktin an dem beobachteten von TGF-β-induzierten Effekt beteiligt ist.

TGF-β aktivierte innerhalb kurzer Zeit Phospholipase D1, welche wiederum Phosphatidylinositol-4-phosphat 5-Kinase 1α aktivierte, was anschließend zur Aktivierung der NADPH Oxidase 4 führte, die reaktive Sauerstoffspezies produzierte, welche die Endozytose von ENaC verusachten. Dieser letzte Schritt war durch eine Veränderung am Cystein 43 der βENaC Untereinheit bedingt. Die Fähigkeit der Epithelzellen, Natrium zu absorbieren, war dadurch stark reduziert, was einen Flüssigkeitsstau in den Alveolen und damit die Entwicklung oder Persistenz eines alveolären Ödems fördert. Die Daten der vorliegenden Studie dokumentieren einen bisher unbekannten TGF-β-abhängigen Mechanismus, welcher den Ionen- und Flüssigkeitstransport in der Lunge reguliert, und der daher während der Pathogenese eines akuten respiratorischen Syndroms von großer Bedeutung ist.

8 Literature

1. Pittet, J.F., Griffiths, M.J., Geiser, T., Kaminski, N., Dalton, S.L., Huang, X., Brown, L.A., Gotwals, P.J., Koteliansky, V.E., Matthay, M.A., and Sheppard, D. 2001. TGF-beta is a critical mediator of acute lung injury. *J Clin Invest* 107:1537-1544.
2. Rubenfeld, G.D., Caldwell, E., Peabody, E., Weaver, J., Martin, D.P., Neff, M., Stern, E.J., and Hudson, L.D. 2005. Incidence and outcomes of acute lung injury. *N Engl J Med* 353:1685-1693.
3. 1971. Adult respiratory distress syndrome. *Am J Med* 50:521-529. (no authors listed)
4. Ashbaugh, D.G., Bigelow, D.B., Petty, T.L., and Levine, B.E. 1967. Acute respiratory distress in adults. *Lancet* 2:319-323.
5. Bernard, G.R., Artigas, A., Brigham, K.L., Carlet, J., Falke, K., Hudson, L., Lamy, M., LeGall, J.R., Morris, A., and Spragg, R. 1994. Report of the American-European Consensus conference on acute respiratory distress syndrome: definitions, mechanisms, relevant outcomes, and clinical trial coordination. Consensus Committee. *J Crit Care* 9:72-81.
6. Matthay, M.A., Folkesson, H.G., and Clerici, C. 2002. Lung epithelial fluid transport and the resolution of pulmonary edema. *Physiol Rev* 82:569-600.
7. Albertine, K.H., Soulier, M.F., Wang, Z., Ishizaka, A., Hashimoto, S., Zimmerman, G.A., Matthay, M.A., and Ware, L.B. 2002. Fas and fas ligand are up-regulated in pulmonary edema fluid and lung tissue of patients with acute lung injury and the acute respiratory distress syndrome. *Am J Pathol* 161:1783-1796.
8. Sznajder, J.I. 2001. Alveolar edema must be cleared for the acute respiratory distress syndrome patient to survive. *Am J Respir Crit Care Med* 163:1293-1294.
9. Ware, L.B., and Matthay, M.A. 2000. The acute respiratory distress syndrome. *N Engl J Med* 342:1334-1349.
10. Bland, R.D., and Nielson, D.W. 1992. Developmental changes in lung epithelial ion transport and liquid movement. *Annu Rev Physiol* 54:373-394.
11. Attiyeh, E.F., London, W.B., Mosse, Y.P., Wang, Q., Winter, C., Khazi, D., McGrady, P.W., Seeger, R.C., Look, A.T., Shimada, H., Brodeur, G.M., Cohn, S.L., Matthay, K.K., and Maris, J.M. 2005. Chromosome 1p and 11q deletions and outcome in neuroblastoma. *N Engl J Med* 353:2243-2253.

12. Guidot, D.M., Folkesson, H.G., Jain, L., Sznajder, J.I., Pittet, J.F., and Matthay, M.A. 2006. Integrating acute lung injury and regulation of alveolar fluid clearance. *Am J Physiol Lung Cell Mol Physiol* 291:L301-306.
13. Johnson, M.D. 2007. Ion transport in alveolar type I cells. *Mol Biosyst* 3:178-186.
14. Matthay, M.A., Robriquet, L., and Fang, X. 2005. Alveolar epithelium: role in lung fluid balance and acute lung injury. *Proc Am Thorac Soc* 2:206-213.
15. Matalon, S., and O'Brodovich, H. 1999. Sodium channels in alveolar epithelial cells: molecular characterization, biophysical properties, and physiological significance. *Annu Rev Physiol* 61:627-661.
16. Morty, R.E., Eickelberg, O., and Seeger, W. 2007. Alveolar fluid clearance in acute lung injury: what have we learned from animal models and clinical studies? *Intensive Care Med* 33:1229-1240.
17. Li, T., Koshy, S., and Folkesson, H.G. 2007. Involvement of αENaC and Nedd4-2 in the conversion from lung fluid secretion to fluid absorption at birth in the rat as assayed by RNA interference analysis. *Am J Physiol Lung Cell Mol Physiol* 293:L1069-1078.
18. Hummler, E., Barker, P., Gatzy, J., Beermann, F., Verdumo, C., Schmidt, A., Boucher, R., and Rossier, B.C. 1996. Early death due to defective neonatal lung liquid clearance in alpha-ENaC-deficient mice. *Nat Genet* 12:325-328.
19. Kellenberger, S., and Schild, L. 2002. Epithelial sodium channel/degenerin family of ion channels: a variety of functions for a shared structure. *Physiol Rev* 82:735-767.
20. Schild, L. 2004. The epithelial sodium channel: from molecule to disease. *Rev Physiol Biochem Pharmacol* 151:93-107.
21. Palmer, L.G., and Frindt, G. 1986. Amiloride-sensitive Na channels from the apical membrane of the rat cortical collecting tubule. *Proc Natl Acad Sci U S A* 83:2767-2770.
22. Canessa, C.M., Horisberger, J.D., and Rossier, B.C. 1993. Epithelial sodium channel related to proteins involved in neurodegeneration. *Nature* 361:467-470.
23. Lingueglia, E., Voilley, N., Waldmann, R., Lazdunski, M., and Barbry, P. 1993. Expression cloning of an epithelial amiloride-sensitive Na^+ channel. A new channel type with homologies to Caenorhabditis elegans degenerins. *FEBS Lett* 318:95-99.

24. Canessa, C.M., Schild, L., Buell, G., Thorens, B., Gautschi, I., Horisberger, J.D., and Rossier, B.C. 1994. Amiloride-sensitive epithelial Na^+ channel is made of three homologous subunits. *Nature* 367:463-467.

25. Waldmann, R., Champigny, G., Bassilana, F., Voilley, N., and Lazdunski, M. 1995. Molecular cloning and functional expression of a novel amiloride-sensitive Na^+ channel. *J Biol Chem* 270:27411-27414.

26. Babini, E., Geisler, H.S., Siba, M., and Grunder, S. 2003. A new subunit of the epithelial Na^+ channel identifies regions involved in Na^+ self-inhibition. *J Biol Chem* 278:28418-28426.

27. Snyder, P.M., McDonald, F.J., Stokes, J.B., and Welsh, M.J. 1994. Membrane topology of the amiloride-sensitive epithelial sodium channel. *J Biol Chem* 269:24379-24383.

28. Kosari, F., Sheng, S., Li, J., Mak, D.O., Foskett, J.K., and Kleyman, T.R. 1998. Subunit stoichiometry of the epithelial sodium channel. *J Biol Chem* 273:13469-13474.

29. Cheng, C., Prince, L.S., Snyder, P.M., and Welsh, M.J. 1998. Assembly of the epithelial Na^+ channel evaluated using sucrose gradient sedimentation analysis. *J Biol Chem* 273:22693-22700.

30. Snyder, P.M., Cheng, C., Prince, L.S., Rogers, J.C., and Welsh, M.J. 1998. Electrophysiological and biochemical evidence that DEG/ENaC cation channels are composed of nine subunits. *J Biol Chem* 273:681-684.

31. Eskandari, S., Snyder, P.M., Kreman, M., Zampighi, G.A., Welsh, M.J., and Wright, E.M. 1999. Number of subunits comprising the epithelial sodium channel. *J Biol Chem* 274:27281-27286.

32. Garty, H. 1994. Molecular properties of epithelial, amiloride-blockable Na^+ channels. *FASEB J* 8:522-528.

33. Flahaut, M., Rossier, B.C., and Firsov, D. 2002. Respective roles of calcitonin receptor-like receptor (CRLR) and receptor activity-modifying proteins (RAMP) in cell surface expression of CRLR/RAMP heterodimeric receptors. *J Biol Chem* 277:14731-14737.

34. Ochs, M., Nyengaard, J.R., Jung, A., Knudsen, L., Voigt, M., Wahlers, T., Richter, J., and Gundersen, H.J. 2004. The number of alveoli in the human lung. *Am J Respir Crit Care Med* 169:120-124.

35. Weibel, E.R. 2009. What makes a good lung? *Swiss Med Wkly* 139:375-386.
36. Johnson, M.D., Widdicombe, J.H., Allen, L., Barbry, P., and Dobbs, L.G. 2002. Alveolar epithelial type I cells contain transport proteins and transport sodium, supporting an active role for type I cells in regulation of lung liquid homeostasis. *Proc Natl Acad Sci U S A* 99:1966-1971.
37. Johnson, M.D., Bao, H.F., Helms, M.N., Chen, X.J., Tigue, Z., Jain, L., Dobbs, L.G., and Eaton, D.C. 2006. Functional ion channels in pulmonary alveolar type I cells support a role for type I cells in lung ion transport. *Proc Natl Acad Sci U S A* 103:4964-4969.
38. Herzog, E.L., Brody, A.R., Colby, T.V., Mason, R., and Williams, M.C. 2008. Knowns and unknowns of the alveolus. *Proc Am Thorac Soc* 5:778-782.
39. Fehrenbach, H. 2001. Alveolar epithelial type II cell: defender of the alveolus revisited. *Respir Res* 2:33-46.
40. Christy, N.P. 1993. Grant W. Liddle. *Trans Am Clin Climatol Assoc* 104:xliii-xlv.
41. Schild, L., Canessa, C.M., Shimkets, R.A., Gautschi, I., Lifton, R.P., and Rossier, B.C. 1995. A mutation in the epithelial sodium channel causing Liddle disease increases channel activity in the Xenopus laevis oocyte expression system. *Proc Natl Acad Sci U S A* 92:5699-5703.
42. Azad, A.K., Rauh, R., Vermeulen, F., Jaspers, M., Korbmacher, J., Boissier, B., Bassinet, L., Fichou, Y., des Georges, M., Stanke, F., De Boeck, K., Dupont, L., Balascakova, M., Hjelte, L., Lebecque, P., Radojkovic, D., Castellani, C., Schwartz, M., Stuhrmann, M., Schwarz, M., Skalicka, V., de Monestrol, I., Girodon, E., Ferec, C., Claustres, M., Tummler, B., Cassiman, J.J., Korbmacher, C., and Cuppens, H. 2009. Mutations in the amiloride-sensitive epithelial sodium channel in patients with cystic fibrosis-like disease. *Hum Mutat* 30:1093-1103.
43. Sheridan, M.B., Fong, P., Groman, J.D., Conrad, C., Flume, P., Diaz, R., Harris, C., Knowles, M., and Cutting, G.R. 2005. Mutations in the beta-subunit of the epithelial Na^+ channel in patients with a cystic fibrosis-like syndrome. *Hum Mol Genet* 14:3493-3498.
44. O'Brodovich, H., Hannam, V., Seear, M., and Mullen, J.B. 1990. Amiloride impairs lung water clearance in newborn guinea pigs. *J Appl Physiol* 68:1758-1762.

45. Egli, M., Duplain, H., Lepori, M., Cook, S., Nicod, P., Hummler, E., Sartori, C., and Scherrer, U. 2004. Defective respiratory amiloride-sensitive sodium transport predisposes to pulmonary oedema and delays its resolution in mice. *J Physiol* 560:857-865.

46. Mall, M., Grubb, B.R., Harkema, J.R., O'Neal, W.K., and Boucher, R.C. 2004. Increased airway epithelial Na^+ absorption produces cystic fibrosis-like lung disease in mice. *Nat Med* 10:487-493.

47. Pittet, J.F., Wiener-Kronish, J.P., McElroy, M.C., Folkesson, H.G., and Matthay, M.A. 1994. Stimulation of lung epithelial liquid clearance by endogenous release of catecholamines in septic shock in anesthetized rats. *J Clin Invest* 94:663-671.

48. Hickman-Davis, J.M., McNicholas-Bevensee, C., Davis, I.C., Ma, H.P., Davis, G.C., Bosworth, C.A., and Matalon, S. 2006. Reactive species mediate inhibition of alveolar type II sodium transport during mycoplasma infection. *Am J Respir Crit Care Med* 173:334-344.

49. Otulakowski, G., Rafii, B., Harris, M., and O'Brodovich, H. 2006. Oxygen and glucocorticoids modulate alphaENaC mRNA translation in fetal distal lung epithelium. *Am J Respir Cell Mol Biol* 34:204-212.

50. Baxendale-Cox, L.M. 1999. Terbutaline increases open channel density of epithelial sodium channel (ENaC) in distal lung. *Respir Physiol* 116:1-8.

51. Minakata, Y., Suzuki, S., Grygorczyk, C., Dagenais, A., and Berthiaume, Y. 1998. Impact of beta-adrenergic agonist on Na^+ channel and Na^+-K^+-ATPase expression in alveolar type II cells. *Am J Physiol* 275:L414-422.

52. Saldias, F.J., Lecuona, E., Comellas, A.P., Ridge, K.M., Rutschman, D.H., and Sznajder, J.I. 2000. beta-adrenergic stimulation restores rat lung ability to clear edema in ventilator-associated lung injury. *Am J Respir Crit Care Med* 162:282-287.

53. Frank, J., Roux, J., Kawakatsu, H., Su, G., Dagenais, A., Berthiaume, Y., Howard, M., Canessa, C.M., Fang, X., Sheppard, D., Matthay, M.A., and Pittet, J.F. 2003. Transforming growth factor-beta1 decreases expression of the epithelial sodium channel alphaENaC and alveolar epithelial vectorial sodium and fluid transport via an ERK1/2-dependent mechanism. *J Biol Chem* 278:43939-43950.

54. Fahy, R.J., Lichtenberger, F., McKeegan, C.B., Nuovo, G.J., Marsh, C.B., and Wewers, M.D. 2003. The acute respiratory distress syndrome: a role for transforming growth factor-beta 1. *Am J Respir Cell Mol Biol* 28:499-503.

55. Wesselkamper, S.C., Case, L.M., Henning, L.N., Borchers, M.T., Tichelaar, J.W., Mason, J.M., Dragin, N., Medvedovic, M., Sartor, M.A., Tomlinson, C.R., and Leikauf, G.D. 2005. Gene expression changes during the development of acute lung injury: role of transforming growth factor beta. *Am J Respir Crit Care Med* 172:1399-1411.

56. Kaminski, N., Allard, J.D., Pittet, J.F., Zuo, F., Griffiths, M.J., Morris, D., Huang, X., Sheppard, D., and Heller, R.A. 2000. Global analysis of gene expression in pulmonary fibrosis reveals distinct programs regulating lung inflammation and fibrosis. *Proc Natl Acad Sci U S A* 97:1778-1783.

57. Assoian, R.K., Komoriya, A., Meyers, C.A., Miller, D.M., and Sporn, M.B. 1983. Transforming growth factor-beta in human platelets. Identification of a major storage site, purification, and characterization. *J Biol Chem* 258:7155-7160.

58. Feng, X.H., and Derynck, R. 2005. Specificity and versatility in tgf-beta signaling through Smads. *Annu Rev Cell Dev Biol* 21:659-693.

59. Shi, Y., and Massague, J. 2003. Mechanisms of TGF-beta signaling from cell membrane to the nucleus. *Cell* 113:685-700.

60. Eickelberg, O. 2001. Endless healing: TGF-beta, SMADs, and fibrosis. *FEBS Lett* 506:11-14.

61. Aubert, J.D., Dalal, B.I., Bai, T.R., Roberts, C.R., Hayashi, S., and Hogg, J.C. 1994. Transforming growth factor beta 1 gene expression in human airways. *Thorax* 49:225-232.

62. Coker, R.K., Laurent, G.J., Shahzeidi, S., Hernandez-Rodriguez, N.A., Pantelidis, P., du Bois, R.M., Jeffery, P.K., and McAnulty, R.J. 1996. Diverse cellular TGF-beta 1 and TGF-beta 3 gene expression in normal human and murine lung. *Eur Respir J* 9:2501-2507.

63. Miyazono, K., Olofsson, A., Colosetti, P., and Heldin, C.H. 1991. A role of the latent TGF-beta 1-binding protein in the assembly and secretion of TGF-beta 1. *EMBO J* 10:1091-1101.

64. Vehvilainen, P., Hyytiainen, M., and Keski-Oja, J. 2009. Matrix association of latent TGF-beta binding protein-2 (LTBP-2) is dependent on fibrillin-1. *J Cell Physiol* 221:586-593.
65. Kusakabe, M., Cheong, P.L., Nikfar, R., McLennan, I.S., and Koishi, K. 2008. The structure of the TGF-beta latency associated peptide region determines the ability of the proprotein convertase furin to cleave TGF-betas. *J Cell Biochem* 103:311-320.
66. Blobe, G.C., Liu, X., Fang, S.J., How, T., and Lodish, H.F. 2001. A novel mechanism for regulating transforming growth factor beta (TGF-beta) signaling. Functional modulation of type III TGF-beta receptor expression through interaction with the PDZ domain protein, GIPC. *J Biol Chem* 276:39608-39617.
67. Itoh, S., Itoh, F., Goumans, M.J., and Ten Dijke, P. 2000. Signaling of transforming growth factor-beta family members through Smad proteins. *Eur J Biochem* 267:6954-6967.
68. Wiater, E., Harrison, C.A., Lewis, K.A., Gray, P.C., and Vale, W.W. 2006. Identification of distinct inhibin and transforming growth factor beta-binding sites on betaglycan: functional separation of betaglycan co-receptor actions. *J Biol Chem* 281:17011-17022.
69. Wrana, J.L., Attisano, L., Carcamo, J., Zentella, A., Doody, J., Laiho, M., Wang, X.F., and Massague, J. 1992. TGF beta signals through a heteromeric protein kinase receptor complex. *Cell* 71:1003-1014.
70. Letamendia, A., Lastres, P., Almendro, N., Raab, U., Buhring, H.J., Kumar, S., and Bernabeu, C. 1998. Endoglin, a component of the TGF-beta receptor system, is a differentiation marker of human choriocarcinoma cells. *Int J Cancer* 76:541-546.
71. Blobe, G.C., Schiemann, W.P., Pepin, M.C., Beauchemin, M., Moustakas, A., Lodish, H.F., and O'Connor-McCourt, M.D. 2001. Functional roles for the cytoplasmic domain of the type III transforming growth factor beta receptor in regulating transforming growth factor beta signaling. *J Biol Chem* 276:24627-24637.
72. Derynck, R., and Zhang, Y.E. 2003. Smad-dependent and Smad-independent pathways in TGF-beta family signalling. *Nature* 425:577-584.
73. Massague, J. 1998. TGF-beta signal transduction. *Annu Rev Biochem* 67:753-791.

74. Massague, J. 2000. How cells read TGF-beta signals. *Nat Rev Mol Cell Biol* 1:169-178.

75. ten Dijke, P., and Hill, C.S. 2004. New insights into TGF-beta-Smad signalling. *Trends Biochem Sci* 29:265-273.

76. Koinuma, D., Tsutsumi, S., Kamimura, N., Imamura, T., Aburatani, H., and Miyazono, K. 2009. Promoter-wide analysis of Smad4 binding sites in human epithelial cells. *Cancer Sci* 100:2133-2142.

77. ten Dijke, P., and Arthur, H.M. 2007. Extracellular control of TGFbeta signalling in vascular development and disease. *Nat Rev Mol Cell Biol* 8:857-869.

78. Budinger, G.R., Chandel, N.S., Donnelly, H.K., Eisenbart, J., Oberoi, M., and Jain, M. 2005. Active transforming growth factor-beta1 activates the procollagen I promoter in patients with acute lung injury. *Intensive Care Med* 31:121-128.

79. Alejandre-Alcázar, M.A., Kwapiszewska, G., Reiss, I., Amarie, O.V., Marsh, L.M., Sevilla-Pérez, J., Wygrecka, M., Eul, B., Köbrich, S., Hesse, M., Schermuly, R.T., Seeger, W., Eickelberg, O., and Morty, R.E. 2007. Hyperoxia modulates TGF-β/BMP signaling in a mouse model of bronchopulmonary dysplasia. *Am J Physiol Lung Cell Mol Physiol* 292:L537-549.

80. Kumarasamy, A., Schmitt, I., Nave, A.H., Reiss, I., van der Horst, I., Dony, E., Roberts, J.D., Jr., de Krijger, R.R., Tibboel, D., Seeger, W., Schermuly, R.T., Eickelberg, O., and Morty, R.E. 2009. Lysyl oxidase activity is dysregulated during impaired alveolarization of mouse and human lungs. *Am J Respir Crit Care Med* 180:1239-1252.

81. ARDSNet. 2000. Ventilation with lower tidal volumes as compared with traditional tidal volumes for acute lung injury and the acute respiratory distress syndrome. *N Engl J Med* 342:1301-1308.

82. Vadasz, I., Morty, R.E., Kohstall, M.G., Olschewski, A., Grimminger, F., Seeger, W., and Ghofrani, H.A. 2005. Oleic acid inhibits alveolar fluid reabsorption: a role in acute respiratory distress syndrome? *Am J Respir Crit Care Med* 171:469-479.

83. Vadasz, I., Morty, R.E., Olschewski, A., Konigshoff, M., Kohstall, M.G., Ghofrani, H.A., Grimminger, F., and Seeger, W. 2005. Thrombin impairs alveolar fluid clearance by promoting endocytosis of Na^+,K^+-ATPase. *Am J Respir Cell Mol Biol* 33:343-354.

84. Cantiello, H.F., Stow, J.L., Prat, A.G., and Ausiello, D.A. 1991. Actin filaments regulate epithelial Na^+ channel activity. *Am J Physiol* 261:C882-888.

85. Mazzochi, C., Bubien, J.K., Smith, P.R., and Benos, D.J. 2006. The carboxyl terminus of the alpha-subunit of the amiloride-sensitive epithelial sodium channel binds to F-actin. *J Biol Chem* 281:6528-6538.

86. Althaus, M., Fronius, M., Buchäckert, Y., Vadász, I., Clauss, W.G., Seeger, W., Motterlini, R., and Morty, R.E. 2009. Carbon monoxide rapidly impairs alveolar fluid clearance by inhibiting epithelial sodium channels. *Am J Respir Cell Mol Biol* 41:639-650.

87. Kleyman, T.R., Carattino, M.D., and Hughey, R.P. 2009. ENaC at the cutting edge: regulation of epithelial sodium channels by proteases. *J Biol Chem* 284:20447-20451.

88. van den Bout, I., and Divecha, N. 2009. PIP5K-driven PtdIns(4,5)*P*2 synthesis: regulation and cellular functions. *J Cell Sci* 122:3837-3850.

89. Ma, H.P., Chou, C.F., Wei, S.P., and Eaton, D.C. 2007. Regulation of the epithelial sodium channel by phosphatidylinositides: experiments, implications, and speculations. *Pflugers Arch* 455:169-180.

90. Weixel, K.M., Edinger, R.S., Kester, L., Guerriero, C.J., Wang, H., Fang, L., Kleyman, T.R., Welling, P.A., Weisz, O.A., and Johnson, J.P. 2007. Phosphatidylinositol 4-phosphate 5-kinase reduces cell surface expression of the epithelial sodium channel (ENaC) in cultured collecting duct cells. *J Biol Chem* 282:36534-36542.

91. Song, W., and Matalon, S. 2007. Modulation of alveolar fluid clearance by reactive oxygen-nitrogen intermediates. *Am J Physiol Lung Cell Mol Physiol* 293:L855-858.

92. Matalon, S., Hardiman, K.M., Jain, L., Eaton, D.C., Kotlikoff, M., Eu, J.P., Sun, J., Meissner, G., and Stamler, J.S. 2003. Regulation of ion channel structure and function by reactive oxygen-nitrogen species. *Am J Physiol Lung Cell Mol Physiol* 285:L1184-1189.

93. Poole, L.B., and Nelson, K.J. 2008. Discovering mechanisms of signaling-mediated cysteine oxidation. *Curr Opin Chem Biol* 12:18-24.

94. Cross, J.V., and Templeton, D.J. 2006. Regulation of signal transduction through protein cysteine oxidation. *Antioxid Redox Signal* 8:1819-1827.

95. Pittet, J.F., Griffiths, M.J., Geiser, T., Kaminski, N., Dalton, S.L., Huang, X., Brown, L.A., Gotwals, P.J., Koteliansky, V.E., Matthay, M.A., and Sheppard, D. 2001. TGF-β is a critical mediator of acute lung injury. *J Clin Invest* 107:1537-1544.

96. Jenkins, R.G., Su, X., Su, G., Scotton, C.J., Camerer, E., Laurent, G.J., Davis, G.E., Chambers, R.C., Matthay, M.A., and Sheppard, D. 2006. Ligation of protease-activated receptor 1 enhances $\alpha_v\beta_6$ integrin-dependent TGF-β activation and promotes acute lung injury. *J Clin Invest* 116:1606-1614.

97. Frank, J., Roux, J., Kawakatsu, H., Su, G., Dagenais, A., Berthiaume, Y., Howard, M., Canessa, C.M., Fang, X., Sheppard, D., Matthay, M.A., and Pittet, J.F. 2003. Transforming growth factor-β1 decreases expression of the epithelial sodium channel αENaC and alveolar epithelial vectorial sodium and fluid transport via an ERK1/2-dependent mechanism. *J Biol Chem* 278:43939-43950.

98. Buczek-Thomas, J.A., Lucey, E.C., Stone, P.J., Chu, C.L., Rich, C.B., Carreras, I., Goldstein, R.H., Foster, J.A., and Nugent, M.A. 2004. Elastase mediates the release of growth factors from lung in vivo. *Am J Respir Cell Mol Biol* 31:344-350.

99. Wakefield, L.M., Letterio, J.J., Chen, T., Danielpour, D., Allison, R.S., Pai, L.H., Denicoff, A.M., Noone, M.H., Cowan, K.H., O'Shaughnessy, J.A., and et al. 1995. Transforming growth factor-β1 circulates in normal human plasma and is unchanged in advanced metastatic breast cancer. *Clin Cancer Res* 1:129-136.

100. Sasse, S.A., Jadus, M.R., and Kukes, G.D. 2003. Pleural fluid transforming growth factor-beta1 correlates with pleural fibrosis in experimental empyema. *Am J Respir Crit Care Med* 168:700-705.

101. Eaton, D.C., Helms, M.N., Koval, M., Bao, H.F., and Jain, L. 2009. The contribution of epithelial sodium channels to alveolar function in health and disease. *Annu Rev Physiol* 71:403-423.

102. Zeissig, S., Bergann, T., Fromm, A., Bojarski, C., Heller, F., Guenther, U., Zeitz, M., Fromm, M., and Schulzke, J.D. 2008. Altered ENaC expression leads to impaired sodium absorption in the noninflamed intestine in Crohn's disease. *Gastroenterology* 134:1436-1447.

103. Sandle, G.I., Higgs, N., Crowe, P., Marsh, M.N., Venkatesan, S., and Peters, T.J. 1990. Cellular basis for defective electrolyte transport in inflamed human colon. *Gastroenterology* 99:97-105.
104. Bhalla, V., and Hallows, K.R. 2008. Mechanisms of ENaC regulation and clinical implications. *J Am Soc Nephrol* 19:1845-1854.
105. Pochynyuk, O., Bugaj, V., and Stockand, J.D. 2008. Physiologic regulation of the epithelial sodium channel by phosphatidylinositides. *Curr Opin Nephrol Hypertens* 17:533-540.
106. Rossier, B.C., and Stutts, M.J. 2009. Activation of the epithelial sodium channel (ENaC) by serine proteases. *Annu Rev Physiol* 71:361-379.
107. Althaus, M., Bogdan, R., Clauss, W.G., and Fronius, M. 2007. Mechano-sensitivity of epithelial sodium channels (ENaCs): laminar shear stress increases ion channel open probability. *FASEB J* 21:2389-2399.
108. Butterworth, M.B., Edinger, R.S., Frizzell, R.A., and Johnson, J.P. 2009. Regulation of the epithelial sodium channel by membrane trafficking. *Am J Physiol Renal Physiol* 296:F10-24.
109. Tamura, H., Schild, L., Enomoto, N., Matsui, N., Marumo, F., and Rossier, B.C. 1996. Liddle disease caused by a missense mutation of β subunit of the epithelial sodium channel gene. *J Clin Invest* 97:1780-1784.
110. Staub, O., Gautschi, I., Ishikawa, T., Breitschopf, K., Ciechanover, A., Schild, L., and Rotin, D. 1997. Regulation of stability and function of the epithelial Na^+ channel (ENaC) by ubiquitination. *EMBO J* 16:6325-6336.
111. Willis, B.C., Kim, K.J., Li, X., Liebler, J., Crandall, E.D., and Borok, Z. 2003. Modulation of ion conductance and active transport by TGF-β1 in alveolar epithelial cell monolayers. *Am J Physiol Lung Cell Mol Physiol* 285:L1192-1200.
112. Moritz, A., De Graan, P.N., Gispen, W.H., and Wirtz, K.W. 1992. Phosphatidic acid is a specific activator of phosphatidylinositol-4-phosphate kinase. *J Biol Chem* 267:7207-7210.
113. Ma, H.P., Saxena, S., and Warnock, D.G. 2002. Anionic phospholipids regulate native and expressed epithelial sodium channel (ENaC). *J Biol Chem* 277:7641-7644.

114. Pochynyuk, O., Bugaj, V., Vandewalle, A., and Stockand, J.D. 2008. Purinergic control of apical plasma membrane PI(4,5)P_2 levels sets ENaC activity in principal cells. *Am J Physiol Renal Physiol* 294:F38-46.
115. Bedard, K., and Krause, K.H. 2007. The NOX family of ROS-generating NADPH oxidases: physiology and pathophysiology. *Physiol Rev* 87:245-313.
116. Brandes, R.P., and Schröder, K. 2008. Differential vascular functions of Nox family NADPH oxidases. *Curr Opin Lipidol* 19:513-518.
117. Kawahara, T., and Lambeth, J.D. 2008. Phosphatidylinositol (4,5)-bisphosphate modulates Nox5 localization via an N-terminal polybasic region. *Mol Biol Cell* 19:4020-4031.
118. Sturrock, A., Cahill, B., Norman, K., Huecksteadt, T.P., Hill, K., Sanders, K., Karwande, S.V., Stringham, J.C., Bull, D.A., Gleich, M., Kennedy, T.P., and Hoidal, J.R. 2006. Transforming growth factor-beta1 induces Nox4 NAD(P)H oxidase and reactive oxygen species-dependent proliferation in human pulmonary artery smooth muscle cells. *Am J Physiol Lung Cell Mol Physiol* 290:L661-L673.
119. Mittal, M., Roth, M., Konig, P., Hofmann, S., Dony, E., Goyal, P., Selbitz, A.C., Schermuly, R.T., Ghofrani, H.A., Kwapiszewska, G., Kummer, W., Klepetko, W., Hoda, M.A., Fink, L., Hanze, J., Seeger, W., Grimminger, F., Schmidt, H.H., and Weissmann, N. 2007. Hypoxia-dependent regulation of nonphagocytic NADPH oxidase subunit NOX4 in the pulmonary vasculature. *Circ Res* 101:258-267.
120. Hecker, L., Vittal, R., Jones, T., Jagirdar, R., Luckhardt, T.R., Horowitz, J.C., Pennathur, S., Martinez, F.J., and Thannickal, V.J. 2009. NADPH oxidase-4 mediates myofibroblast activation and fibrogenic responses to lung injury. *Nat Med* 15:1077-1081.
121. Leme, A.S., Lichtenstein, A., Arantes-Costa, F.M., Landucci, E.C., and Martins, M.A. 2002. Acute lung injury in experimental pancreatitis in rats: pulmonary protective effects of crotapotin and *N*-acetylcysteine. *Shock* 18:428-433.
122. Gonzalez, P.K., Zhuang, J., Doctrow, S.R., Malfroy, B., Benson, P.F., Menconi, M.J., and Fink, M.P. 1996. Role of oxidant stress in the adult respiratory distress syndrome: evaluation of a novel antioxidant strategy in a porcine model of endotoxin-induced acute lung injury. *Shock* 6 Suppl 1:S23-26.
123. Iles, K.E., Song, W., Miller, D.W., Dickinson, D.A., and Matalon, S. 2009. Reactive species and pulmonary edema. *Expert Rev Respir Med* 3:487-496.

124. Forman, H.J., Fukuto, J.M., and Torres, M. 2004. Redox signaling: thiol chemistry defines which reactive oxygen and nitrogen species can act as second messengers. *Am J Physiol Cell Physiol* 287:C246-256.
125. Jenkins, R.G., Su, X., Su, G., Scotton, C.J., Camerer, E., Laurent, G.J., Davis, G.E., Chambers, R.C., Matthay, M.A., and Sheppard, D. 2006. Ligation of protease-activated receptor 1 enhances alpha(v)beta6 integrin-dependent TGF-beta activation and promotes acute lung injury. *J Clin Invest* 116:1606-1614.
126. Zhou, G., Dada, L.A., Wu, M., Kelly, A., Trejo, H., Zhou, Q., Varga, J., and Sznajder, J.I. 2009. Hypoxia-induced alveolar epithelial-mesenchymal transition requires mitochondrial ROS and hypoxia-inducible factor 1. *Am J Physiol Lung Cell Mol Physiol* 297:L1120-1130.

9 Acknowledgments

I would like to gratefully acknowledge Prof. Werner Seeger and Prof. Oliver Eickelberg for initiating the graduate program Molecular Biology and Medicine of the Lung (MBML), and giving me the chance to participate, and to all the faculty members for their excellent teaching.

Furthermore, I would like to thank Dr. Rory E. Morty for taking over the supervision of my PhD and giving me the chance to start a new project, and also for all the help, the discussions and explanations. Thank you for sharing your infinite knowledge, which never ceases to amaze me.

I would also like to thank all my colleagues in the former laboratory of Oliver Eickelberg for all their help and support, their friendship and collegiality.

Thank you very much also to everyone who has contributed to the soon to be published publication: Dr. István Vadász, Łukasz Wujak, Prof. Andrea Olschewski, Dr. Małgorzata Wygrecka, Dr. Sebastian Rummel, Prof. Ralph P. Brandes, Prof. Andreas Günther and Prof. Siegfried Waldegger.

Thanks also to my current boss, Prof. Norbert Weißmann for giving me the time to finish my thesis; and to my colleagues in his laboratory for their friendliness and great helpfulness, although they hardly ever see me.

Finally I would like to thank my family, my friends and Timo Richter, for their endless support and patience. Thank you for never ceasing to believe in the final completion of this thesis.

Der Lebenslauf wurde aus der elektronischen Version der Arbeit entfernt.

The curriculum vitae was removed from the electronic version of the paper.

10.3 Publications

1. **Peters DM**, Griffin JB, Stanley JS, Beck MM, Zempleni J. Exposure to UV light causes increased biotinylation of histones in Jurkat cells. *Am J Physiol Cell Physiol.* 2002 Sep; 283(3):C878-84

2. Morty RE, Nejman B, Kwapiszewska G, Hecker M, Zakrzewicz A, Kouri FM, **Peters DM**, Dumitrascu R, Seeger W, Knaus P, Schermuly RT, Eickelberg O. Dysregulated bone morphogenetic protein signaling in monocrotaline-induced pulmonary arterial hypertension. *Arterioscler Thromb Vasc Biol.* 2007 May; 27(5):1072-8.

3. Sommer D, Bogdan R, Berger J, **Peters DM**, Morty RE, Clauss WG, Fronius M. CFTR-dependent Cl^--secretion in Xenopus laevis lung epithelium. *Respir Physiol Neurobiol.* 2007 Aug 15; 158(1):97-106.

4. **Peters DM**, Vadász I, Wujak Ł, Olschewski A, Wygrecka M, Rummel S, Brandes RP, Günther A, Waldegger S, Seeger W, Eickelberg O, Morty RE. TGF-β impairs edema resolution in acute respiratory distress syndrome by aberrant epithelial sodium channel trafficking, in preparation

10.4 Qualifications

April 2000 Bachelor of Science
Oct. 2003 Master of Science (Diploma)
Oct. 2004-2007 Graduate school "Molecular Biology and Medicine of the Lung, MBML" and the "PhD Programme of the Faculties of Veterinary Medicine and Medicine of the Justus- Liebig University Gießen"

10.5 Internships

Aug. 2000 Analytical chemical lab, Bio-Data GmbH, Linden
Feb.-April 2001 Marketing agency BMO Beratung für Marketing und Organisation GmbH, Frankfurt am Main, department of promotion

March-July 2002 Nestlé Deutschland AG, Frankfurt am Main, department of nutrition and communication

10.6 Practical courses

Feb. 2005 MBML practical course "Proteomics"
Nov. 2007 MBML practical course "Biostatistics"

10.7 Jobs

May 2007 to date: assistant of Dr. Rory Morty for the organisation of the international graduate program "Molecular Biology and Medicine of the Lung, MBML"
October 2010 to date: tutor in the international graduate program "Molecular Biology and Medicine of the Lung, MBML"

10.8 Posters, oral presentations

Aug. 2004, 2005, 2006 presentations at the annual MBML retreat, Rauischholzhausen, Germany
July 2006 & Oct. 2006 presentations at the biannual meetings of the "PhD Programme of the Faculties of Veterinary Medicine and Medicine of the Justus Liebig University Gießen"
June 2007 presentation and poster: "TGF-β1 verhindert die Reabsorbtion von Flüssigkeit aus den Alveolen: Eine mögliche Rolle bei der Entstehung von ARDS?": Pneumologie Update meeting, Innsbruck, Austria
March 2009 Poster: "TGF-β1 inhibits alveolar fluid reabsorbtion – a role in ARDS?", Pneumonet meeting in Innsbruck, Austria
May 2009 Poster "TGF-β1 inhibits alveolar fluid reabsorbtion – a role in ARDS?", annual meeting of the American Thoracic Society, San Diego, USA
April 2011 Poster "Moderate exercise training prevents hypoxia-induced pulmonary hypertension in mice", Deutsche Gesellschaft für Pneumologie Kongress, Dresden
May 2011 Poster "Moderate exercise training prevents hypoxia-induced pulmonary hypertension in mice", Poster "The dual neutral endopeptidase /

endothelin converting enzyme inhibitor SLV338 inhibits experimental pulmonary hypertension in rats", annual meeting of the American Thoracic Society, Denver, USA

10.9 Awards

Oct. 2005 MBML travel award

June 2007 2nd price "PneumoUpdate Preis 2007" for the presentation: "TGF-β1 verhindert die Reabsorbtion von Flüssigkeit aus den Alveolen: Eine mögliche Rolle bei der Entstehung von ARDS? ": Pneumologie Update meeting, Innsbruck, Austria

11 Declaration

I declare that I have completed this dissertation single-handedly without the unauthorized help of a second party and only with the assistance acknowledged therein. I have appropriately acknowledged and referenced all text passages that are derived literally from or are based on the content of published or unpublished work of others, and all information that relates to verbal communications. I have abided by the principles of good scientific conduct laid down in the charter of the Justus Liebig University of Giessen in carrying out the investigations described in the dissertation.